Recombination … electron - ions

Recombination processes in plasma

Binary recombination

α [cm^{3}s^{-1}]

$$H^+ + e \rightarrow H + h\nu$$

RR radiative recombination

$$O_2^+ + e \rightarrow O + O$$

DR dissociative recombination

$$\frac{dn_e}{dt} = \frac{d[O_2^+]}{dt} = -\alpha[O_2^+]n_e = -\alpha n_e^2$$

$$Fe^{7+} + e \rightarrow Fe^{6+}$$

DiR dielectronic recombination

Ternary electron assisted recombination

Recombination processes in plasma

Binary recombination $\alpha\,[\mathrm{cm^3 s^{-1}}]$

$$H^+ + e \rightarrow H + h\nu$$

RR radiative recombination

$$O_2^{\ +} + e \rightarrow O + O$$

DR dissociative recombination

$$\frac{dn_e}{dt} = \frac{d[O_2^{\ +}]}{dt} = -\alpha[O_2^{\ +}]n_e = -\alpha n_e^{\ 2}$$

$$Fe^{7+} + e \rightarrow Fe^{6+}$$

DiR dielectronic recombination

Ternary electron assisted recombination

$$Ar^+ + e + e \rightarrow Ar + e$$

$$\frac{dn_e}{dt} = \frac{d[Ar^+]}{dt} = -K_e[Ar^+]n_e^{\ 2} = -\alpha_{eff}[Ar^+]n_e$$

Collisional Radiative Recombination

CRR

$K_{CRR}\,[\mathrm{cm^6 s^{-1}}]$

$$\alpha_{eff} = K_e n_e$$

Ternary neutral assisted recombination

$$Ar^+ + e + He \rightarrow Ar + He$$

$$\frac{dn_e}{dt} = \frac{d[Ar^+]}{dt} = -K_M[Ar^+]n_e[He] = -\alpha_{eff}[Ar^+]n_e$$

$K_M\,[\mathrm{cm^6 s^{-1}}]$

$$\alpha_{eff} = K_M[He]$$

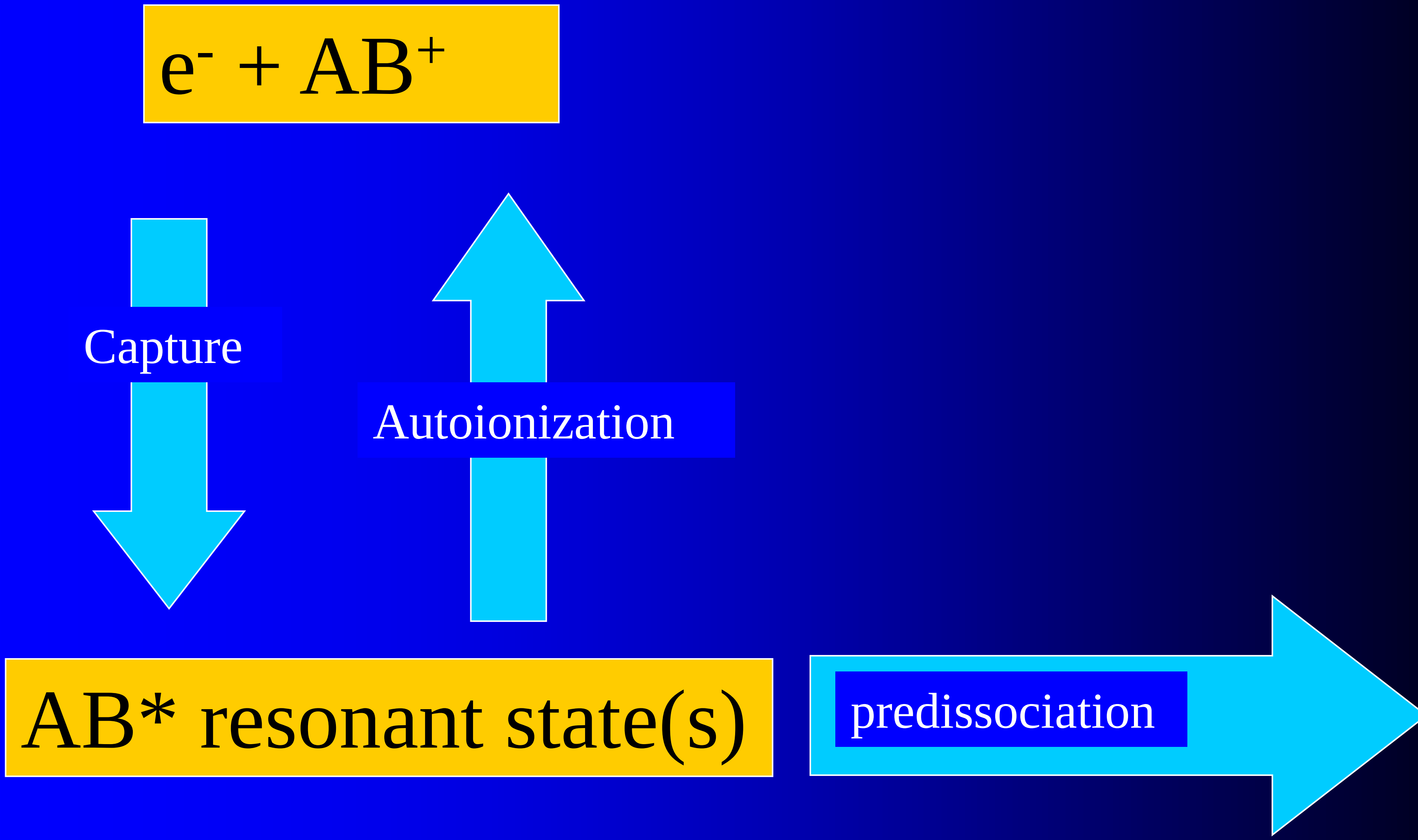

To get high recombination rate, we need

(a) efficient capture

(b) predissociation faster than auto-ionization

Electron-cold molecular ion reaction: Dissociative Recombination

Indirect process

Direct process

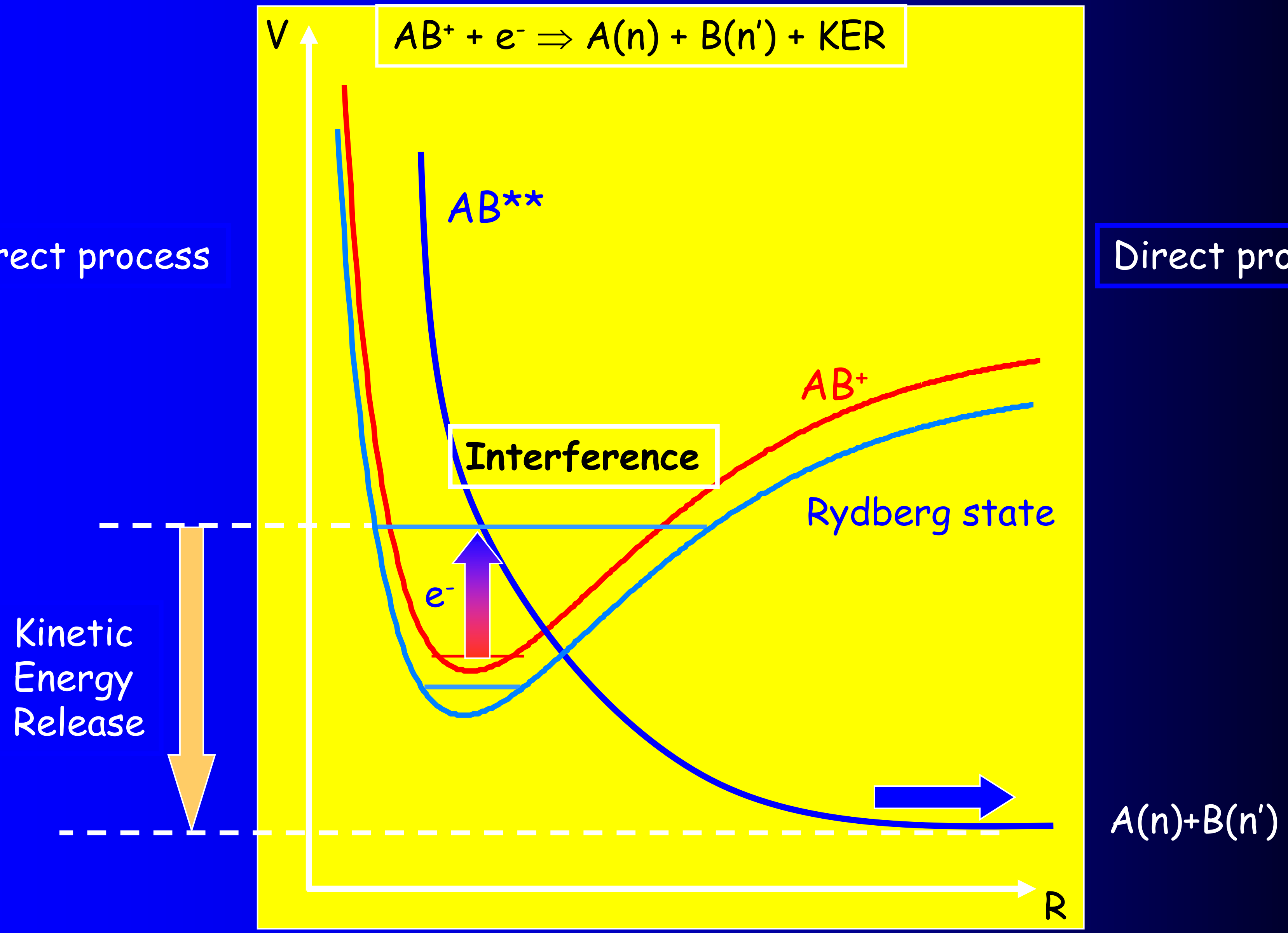

Recombination of H_3^+ : No ion-neutral crossing

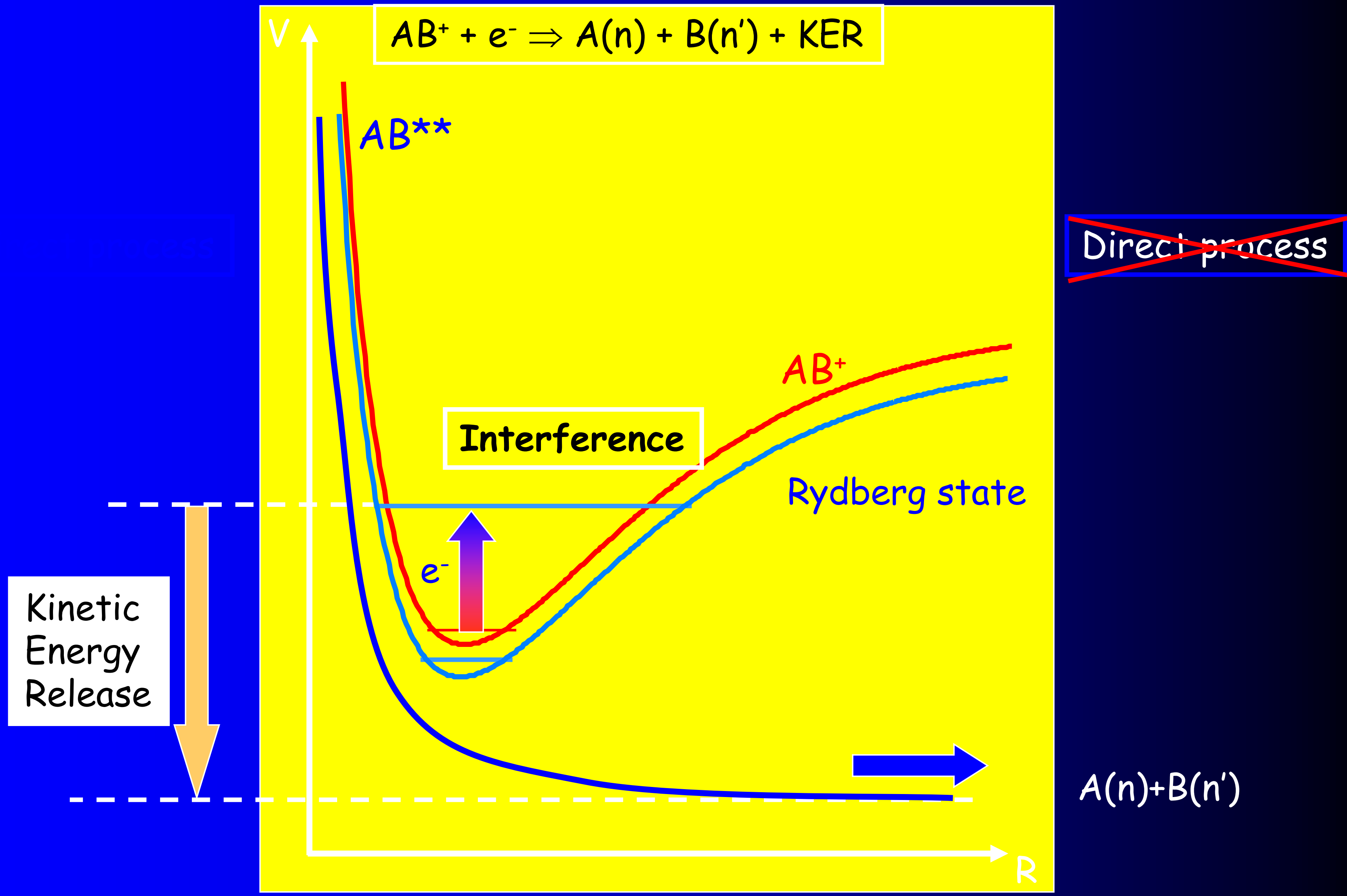

RECOMBINATION

FLOWING AFTERGLOW

FLOWING AFTERGLOW

Ion-molecule reactions

Ion-electron recombination

FA

FA	**E.E.Ferguson, Fehsenfeld, ~1965**
FALP	**J. Hasted, D. Smith, N. Adams, ….**

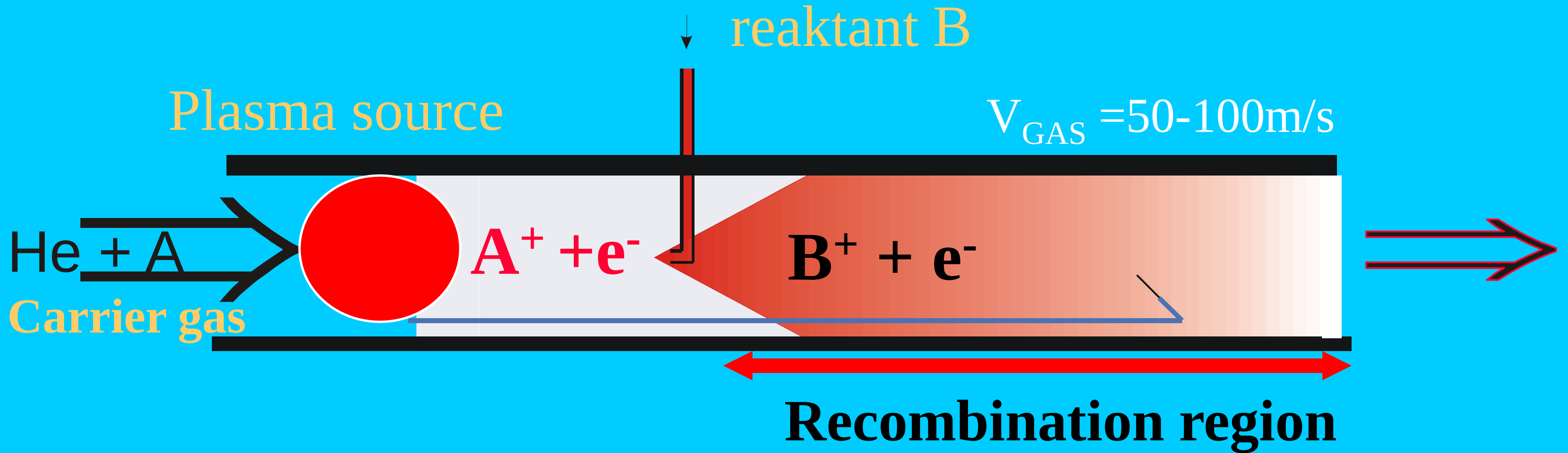

$$A^+ + B \xrightarrow{k} products,$$

$$d[A^+]/dt = -k[B][A^+], \qquad at\ [A^+] << [B]$$

$$[A^+] = [A^+]_0 \exp(-k[B]t) = [A^+]_0 \exp(-k[B]L_0/v)$$

SIFT

D. Smith, N. Adams, ….

Flowing Afterglow Langmuir Probe - FALP

Recombination
Attachment

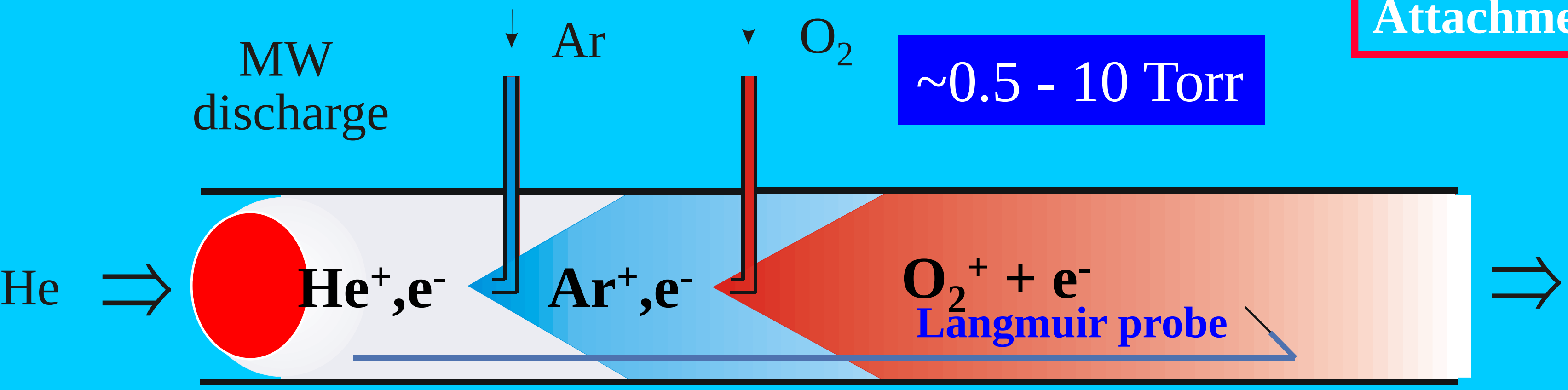

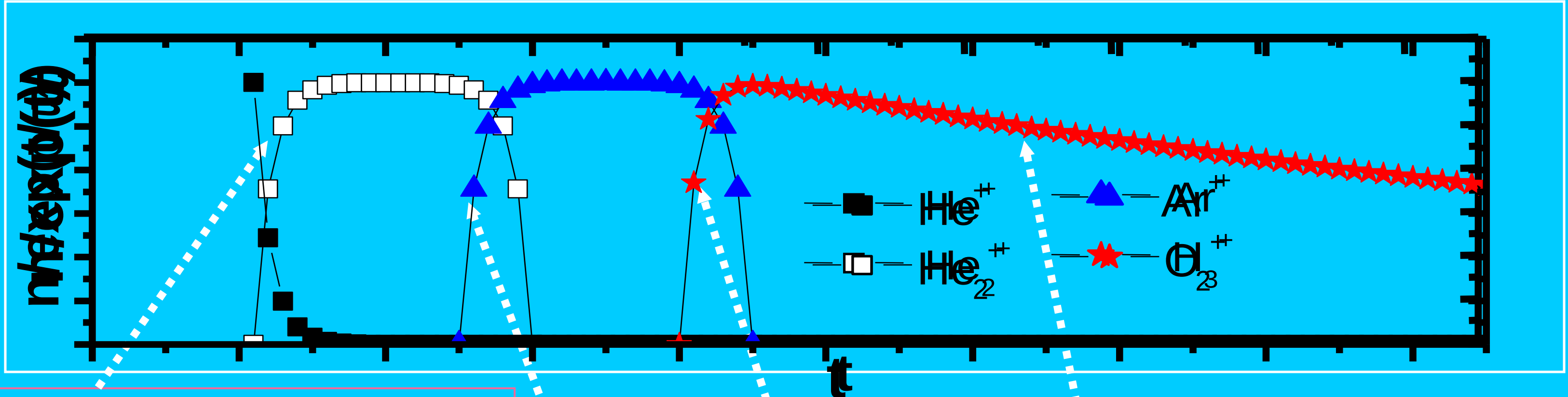

$He^+ + 2He \rightarrow He_2^+ + He$

$He_2^+ + Ar \rightarrow Ar^+ + 2He$

$He^m + Ar \rightarrow Ar^+ + He$

$Ar^+ + O_2 \rightarrow O_2^+ + Ar$

Diffusion, IMR
Recombination

FALP - Formation of H_3^+ in He/Ar/H_2 mixture

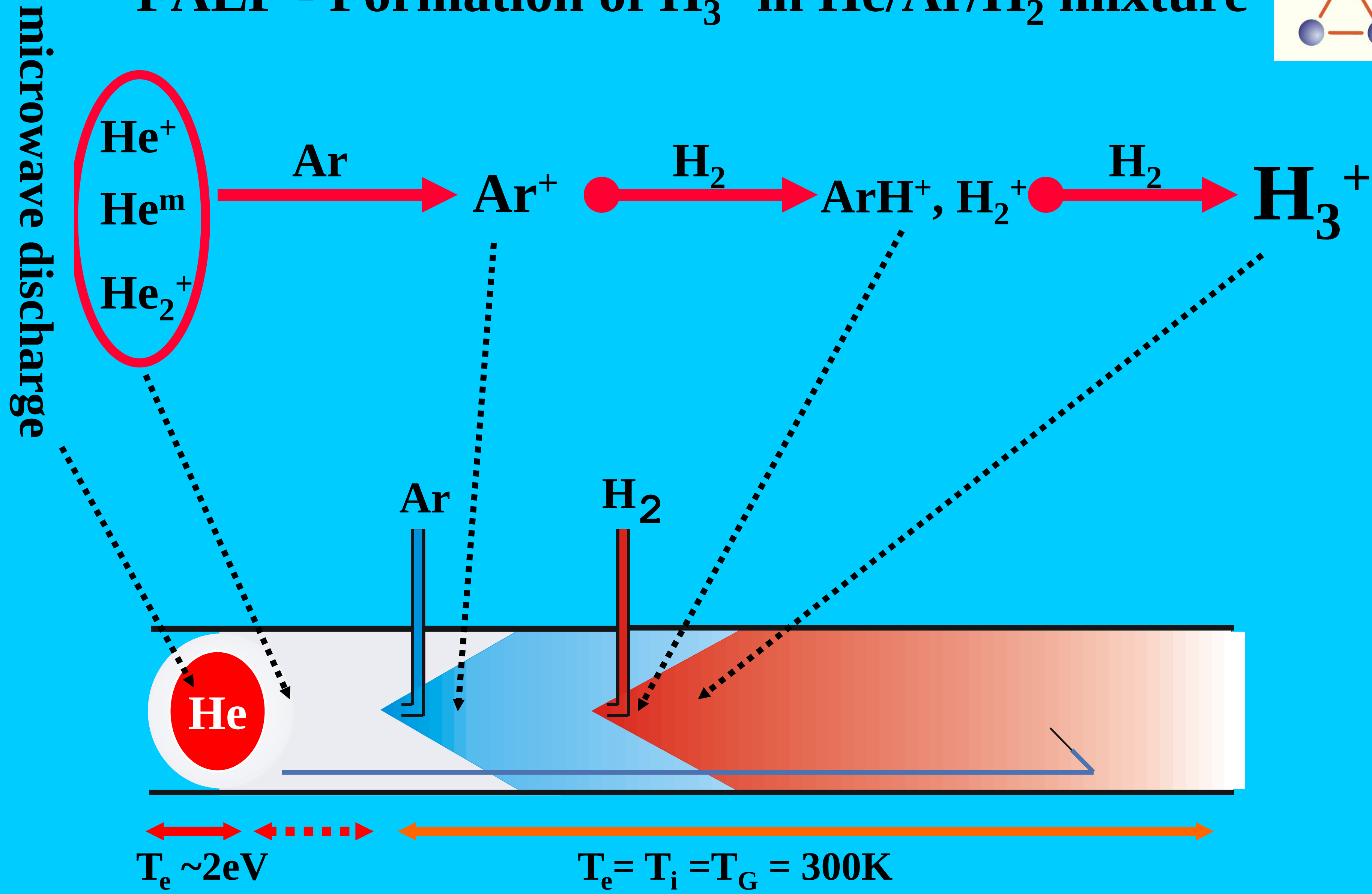

FALP - RECOMBINATION OF H_3

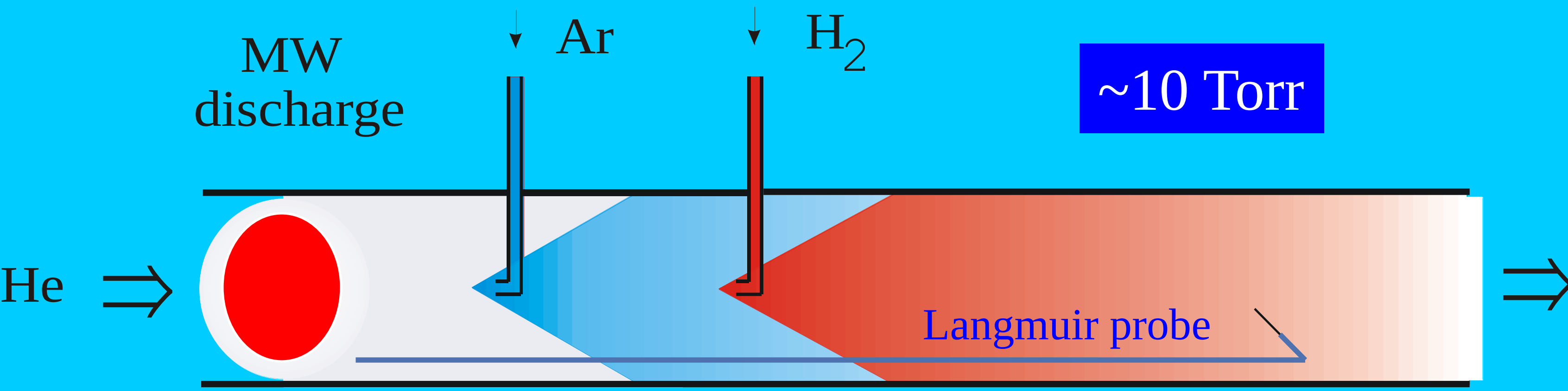

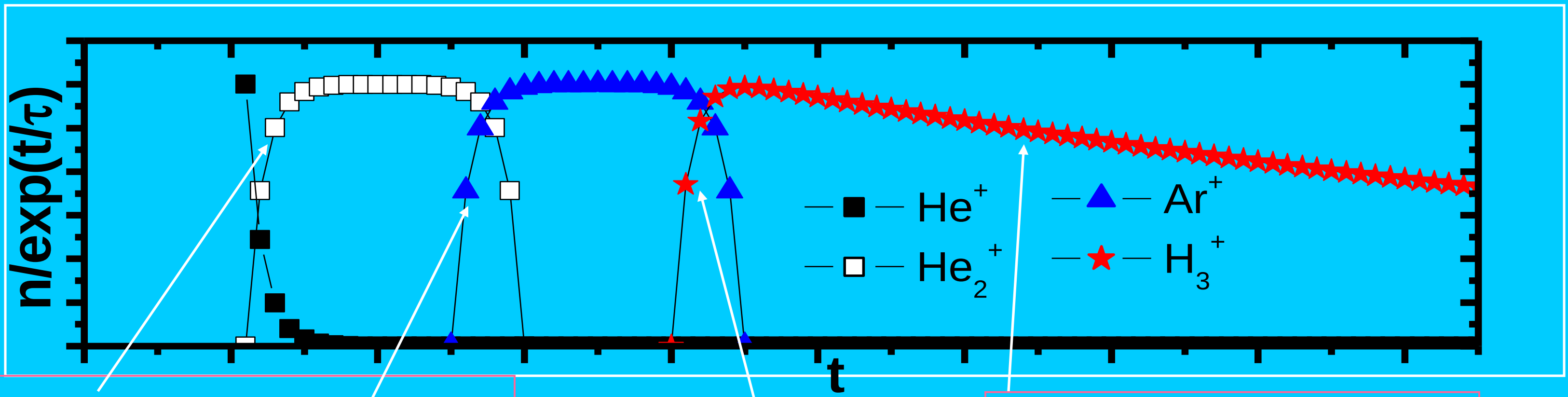

$He^+ + 2He \rightarrow He_2^+ + He$

$He_2^+ + Ar \rightarrow Ar^+ + 2He$

$He^m + Ar \rightarrow Ar^+ + He$

$Ar^+ + H_2 \rightarrow ArH^+ \ldots$

$ArH^+ + H_2 \rightarrow H_3^+ \ldots$

$H_3^+ + H_2 + He \rightarrow H_5^+ \ldots$

$H_3^+ + e^- \rightarrow \ldots$

$H_5^+ + e^- \rightarrow \ldots$

Diffusion in FA

Diffusion losses
Ambipolar diffusion

$$[A^+] = [A^+]_0 \exp(-Dt/\Lambda^2) = [A^+]_0 \exp(-Dpt/p\Lambda^2) = [A^+]_0 \exp(-D_0 p_0 L/vp\Lambda^2)$$
$$\sim [A^+]_0 \exp(-D_0 p_0 L/vp\Lambda^2) \sim [A^+]_0 \exp(-const.L/Q)$$

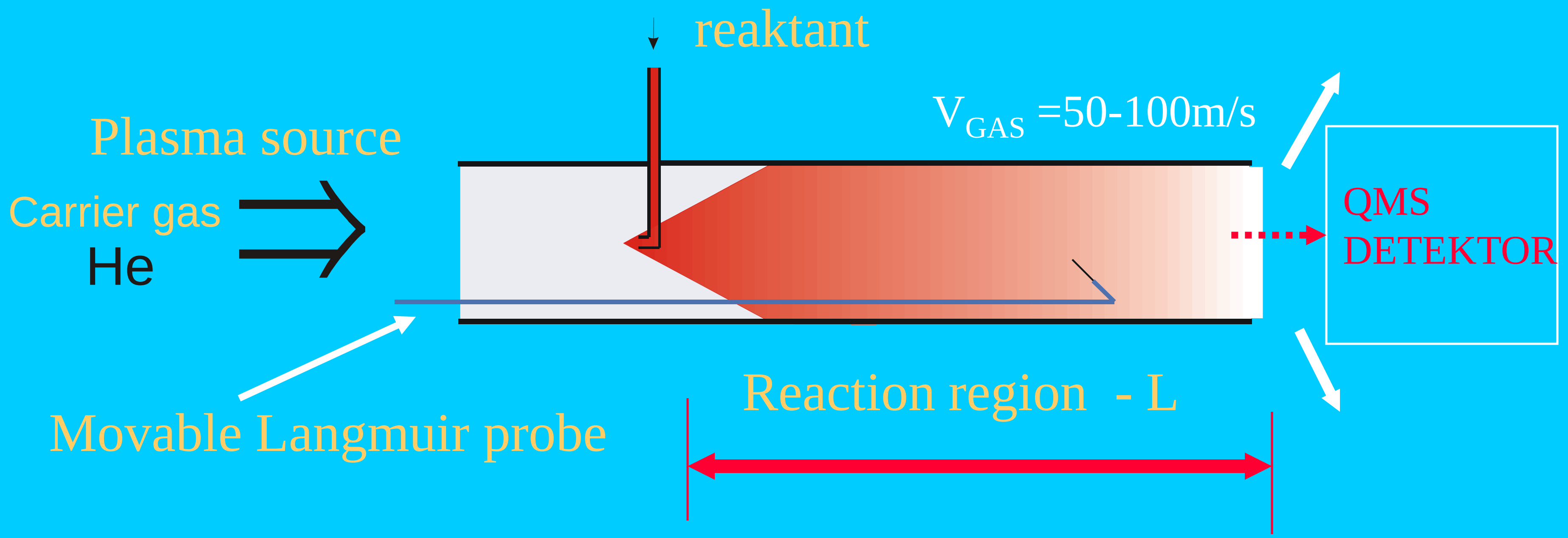

$$[A^+] \sim [A^+]_0 \exp(-const.L/Q)$$

Flowing afterglow/Langmuir probe (FALP)
D. Smith, N. G. Adams and P. Spanel

- A schematic diagram of the **FALP apparatus** showing the relative positions of the microwave discharge that generates the afterglow plasma and the three reactant gas entry ports **P1**, **P2** and **P3**. The distance (*z*) scale is referenced to the downstream mass spectrometer sampling orifice. The complete flow tube is surrounded by a **vacuum jacket** to facilitate high and low temperature operation (ranging from 80 to 600K).

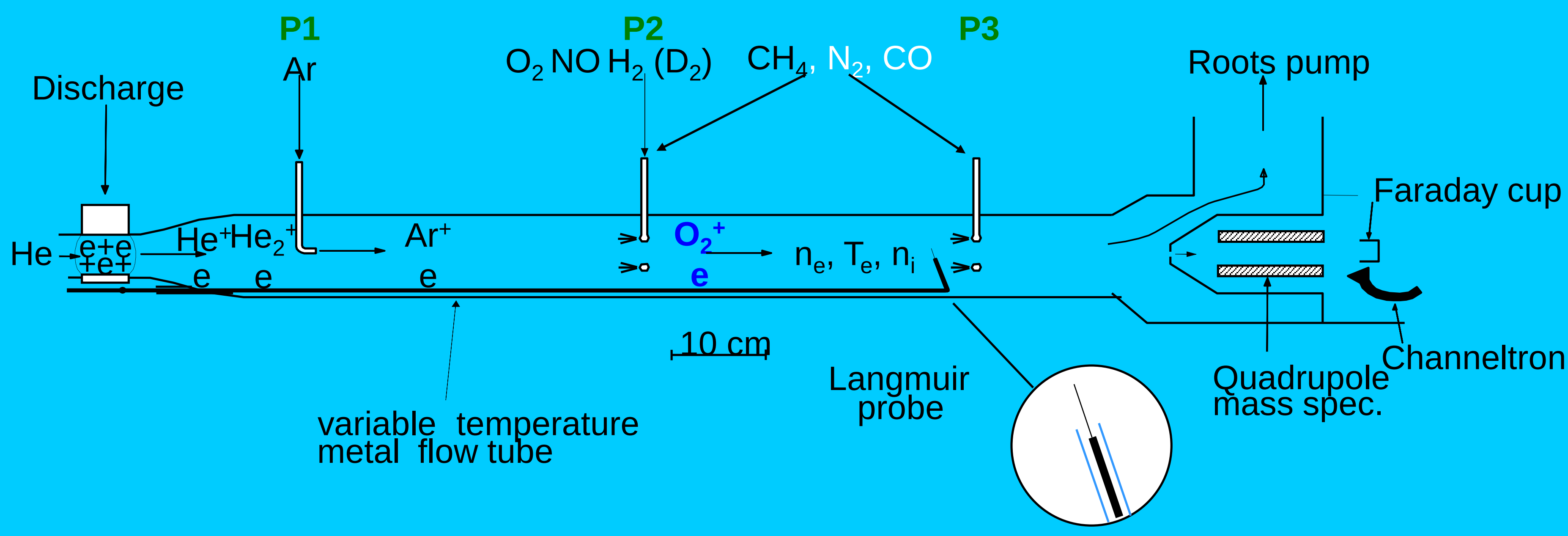

Positive ion/electron dissociative recombination

- e.g. $NO^+ + e \rightarrow N + O$

$$\frac{dn_e}{dt} = -\alpha\, n_e^2 + D_a \nabla^2 n_e \quad \text{diffusion}$$

$$\frac{dn_e}{dt} = -\alpha\, n_e^2 - \frac{D_a}{\Lambda^2} n_e$$

$$\frac{1}{n_e} - \frac{1}{n_0} = \alpha (t_e - t_0)$$

$$\frac{1}{n_e} = \alpha \;\frac{\exp(\nu t) - 1}{\nu} + \frac{1}{n_0} \exp(\nu t) \;\; ; \nu = D_a / \Lambda^2$$

International Journal of Mass Spectrometry and Ion Processes 129 (1993) 183–191
0168-1176/93/$06.00

FALP studies of the dissociative recombination coefficients for O_2^+ and NO^+ within the electron temperature range 300–2000 K[1]

Patrik Španěl, Libuše Dittrichová[†], David Smith*

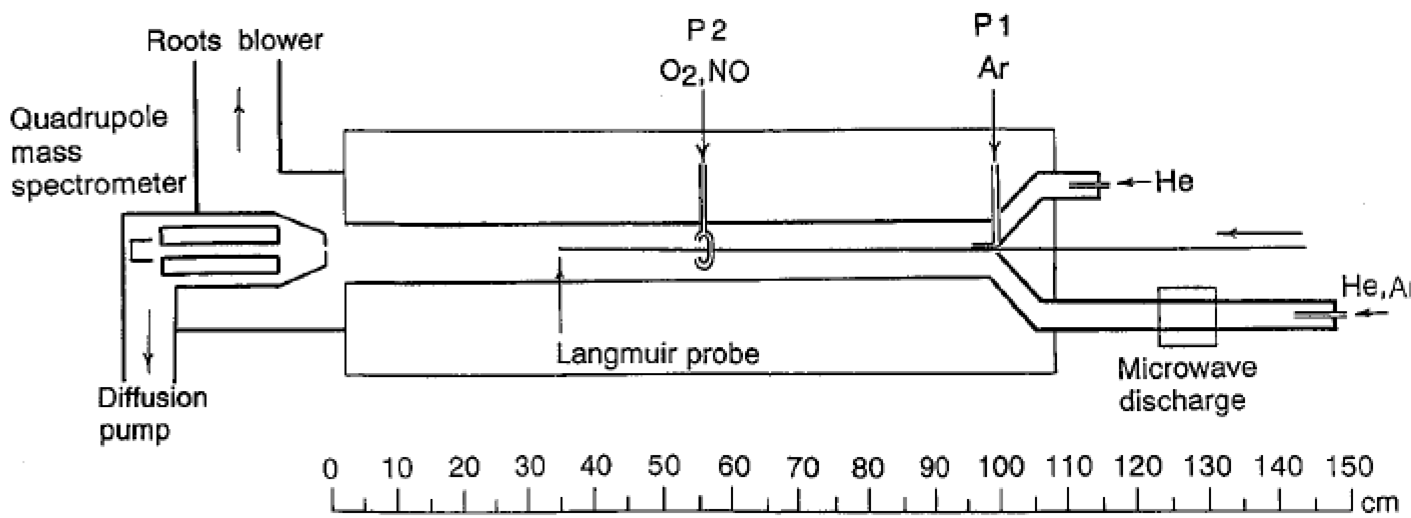

Fig. 1. A line diagram (approximately to scale) of the FALP apparatus, indicating the positions of the microwave discharge, the entry port of helium coolant gas (for the argon afterglow plasmas), the entry ports P1 for argon (for the helium afterglow plasmas) and P2 for O_2 and NO, and the mass spectrometer. The Langmuir probe can be positioned at any point on the axis of the flow tube. Also indicated is the outline of the vacuum jacket which facilitates the heating and cooling of the complete flow tube.

e

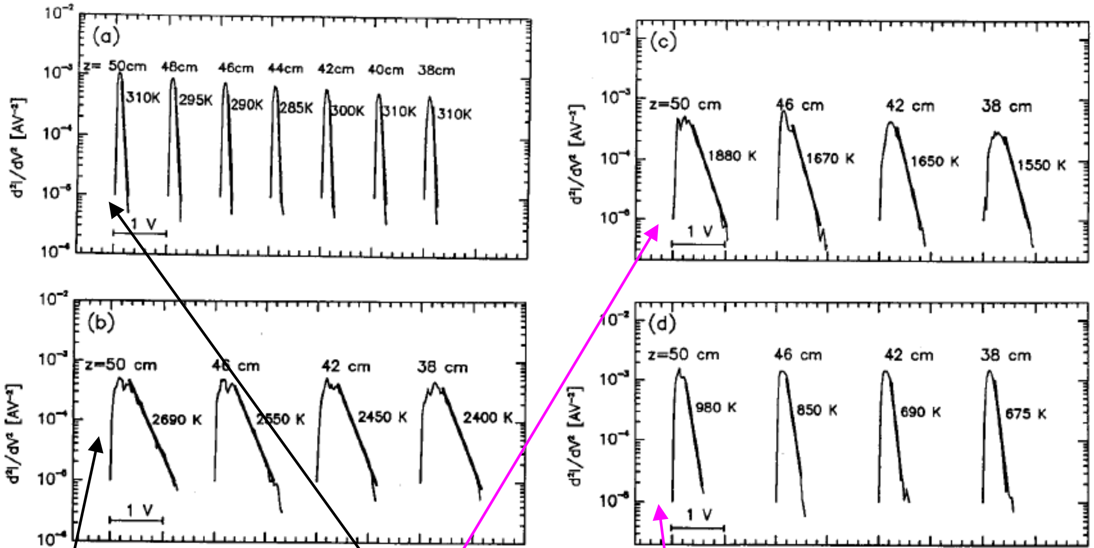

Fig. 2. Representative plots of d^2i/dV^2 against V obtained from the Langmuir probe current (i)–voltage (V) characteristics from which electron temperatures T_e are obtained. In every case the carrier gas temperature is 300 K. The good linearity of a plot is indicative of a Maxwellian electron energy distribution function (EEDF). The z values are the positions of the probe along the axis of the flow tube (referenced to the mass spectrometer sampling orifice; see Fig. 1). The entry port P2 via which the O_2 and NO ion source gases were introduced into the afterglows is located at $z = 56$ cm. (a) Obtained in helium afterglows (at a pressure of 1 Torr) with a small admixture of argon to destroy helium metastable atoms. Note the excellent linearity of the plots and the small scatter of T_e about T_g (= 300 K) along z. (b) Obtained in pure argon afterglows (at a pressure of 0.7 Torr). Note the much higher T_e values (compared with those in (a)) and the small (but obvious) T_e gradient along z. (c) Obtained in argon afterglows into which O_2 (partial pressure of ≈ 5 mTorr) has been added to generate an O_2^+/electron plasma. Note the somewhat greater fractional decrease in T_e compared with that in the pure argon afterglow in (b), this being due to the additional cooling of the electron gas on the O_2 molecules. (d) Obtained in argon afterglows into which first helium (partial pressure 50 mTorr) has been added to cool the electron gas (see Fig. 1), and then into which O_2 (partial pressure 5 mTorr) has been added to produce the O_2^+/electron plasma at a lower T_e than that in (c). Note that the fractional decrease in T_e is greater than in (c) because of the combined cooling effects of the helium and the O_2. It is this T_e gradient along the reaction zone which limits the T_e resolution in these experiments.

$$v_p \frac{dn_e}{dz} = -\alpha n_e^2 + D_a \nabla^2 n_e \quad (4)$$

As a reasonable approximation, we assume that diffusive loss is via the fundamental mode only and then

$$v_p \frac{dn_e}{dz} = -\alpha n_e^2 - \frac{D_a}{\Lambda^2} n_e \quad (5)$$

where D_a is the ambipolar diffusion coefficient and Λ is the characteristic diffusion length (for the flow tube used here, $\Lambda^2 = 2.76\,cm^2$), and v_p is the plasma flow velocity ($1.1 \times 10^4\,cm\,s^{-1}$). When recombination is the dominant loss process, such as is the case in these studies of both $\alpha(O_2^+)$ and $\alpha(NO^+)$ at the lower T_e, (and certainly at 300 K in the helium carrier gas), then the diffusion term in Eq. (5) can be neglected, and the solution to Eq. (5) is then

$$\frac{1}{n_t} - \frac{1}{n_0} = \frac{\alpha(z_t - z_0)}{v_p} \quad (6)$$

Electron temperature measurement

D.Smith and P.Spanel

(a) Obtained in **helium** afterglow (at a pressure of 1 Torr) with a small admixture of argon to destroy helium metastable atoms.

(b) Obtained in pure **argon** afterglow (at a pressure of 0.7 Torr).

(c) Obtained in **argon** afterglow into which $\mathbf{O_2}$ (partial pressure of ~5mTorr) has been added to generate an O_2^+/electron plasma.

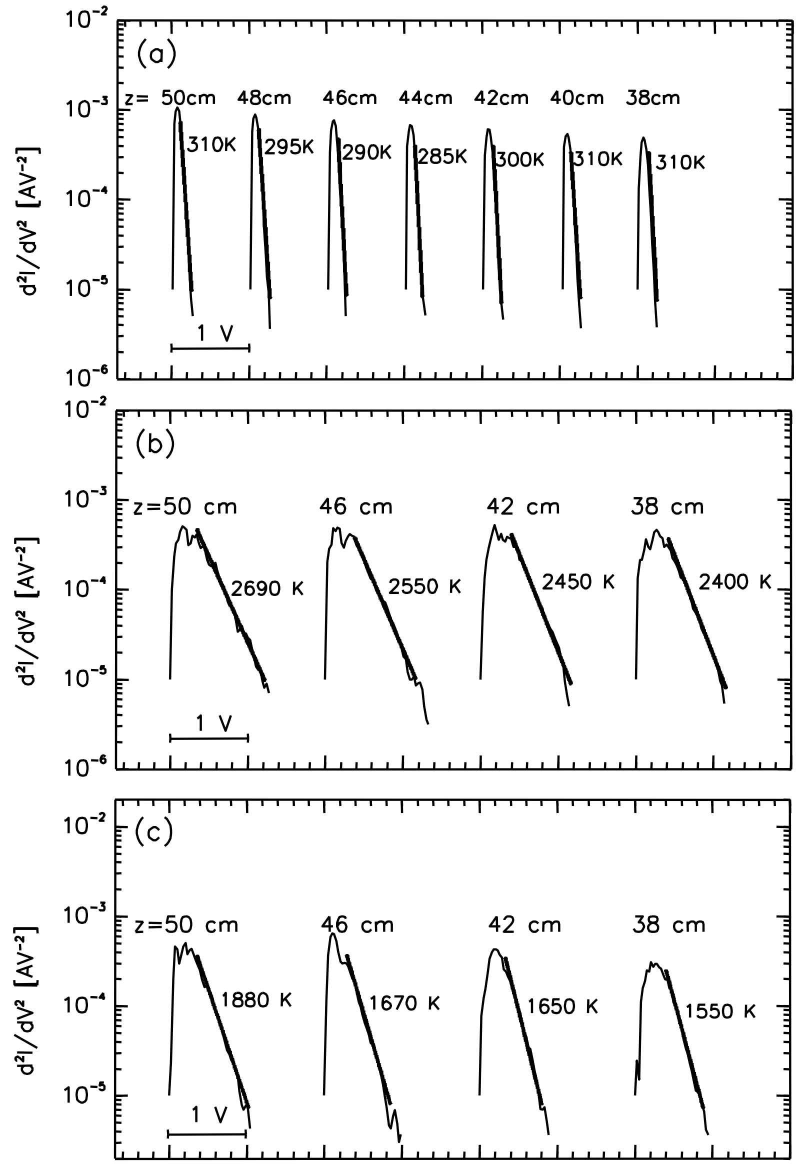

Electron temperature dependence

Plots of $1/n_e$ against the distance z along the flow tube obtained in O_2^+/electron afterglow plasmas from which values for $\alpha(O_2^+)$ are obtained.

The data indicated by filled circles were obtained in helium carrier gas when $T_e = T_i = T_g$ = 300 K; the linearity of the plot over a factor of about ten indicates that dissociative recombination is the dominant loss process for electrons and ions.

The data represented by open circles (T_e=650 K) were obtained in argon carrier gas at T_g = 300 K, and at elevated T_e.

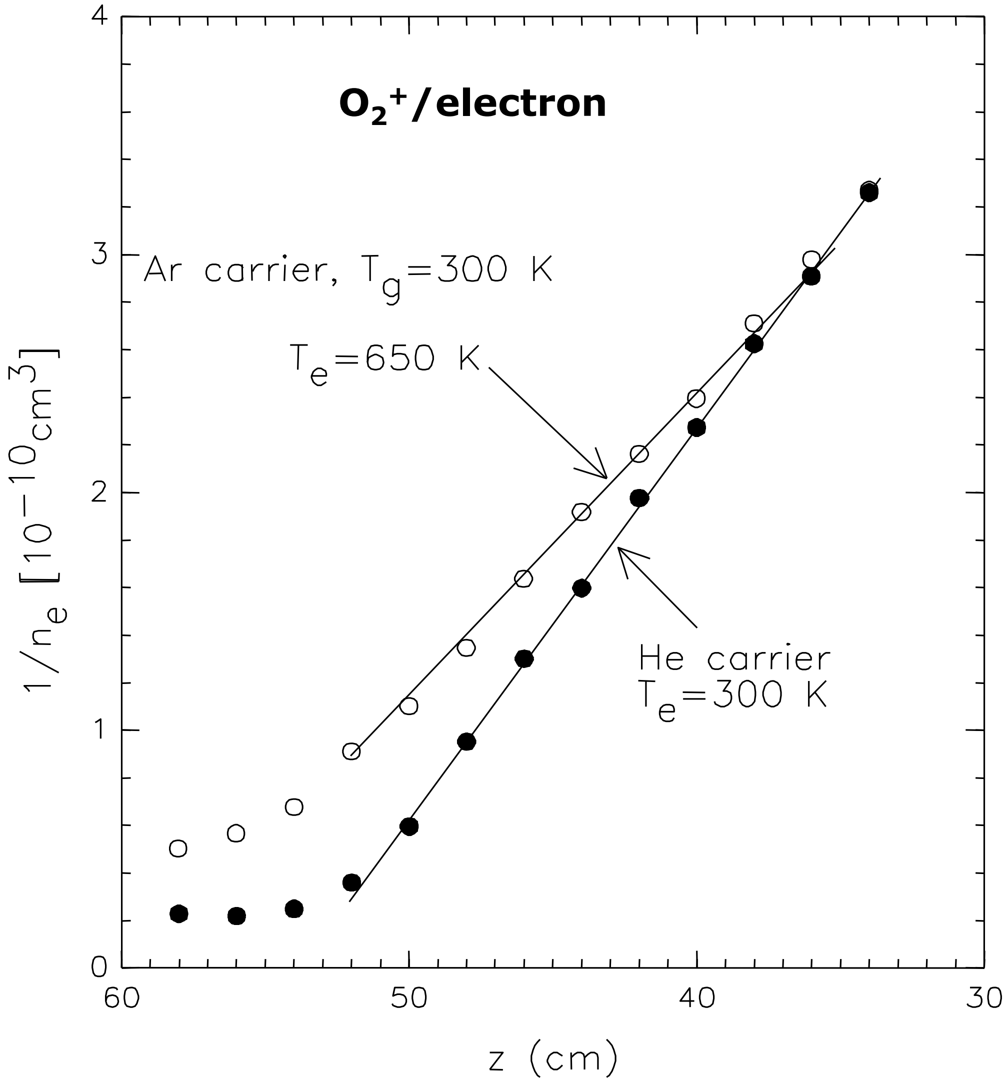

FALP and in-situ data

The points indicated by blue triangles are the $\alpha(NO^+)$ deduced from in-situ satellite data by

M. R. Torr, J. P. St-Maurice and D. G. Torr, J. Geophys. Res., **82** (1977) 3287.

The agreement between these data and the laboratory data is remarkable.

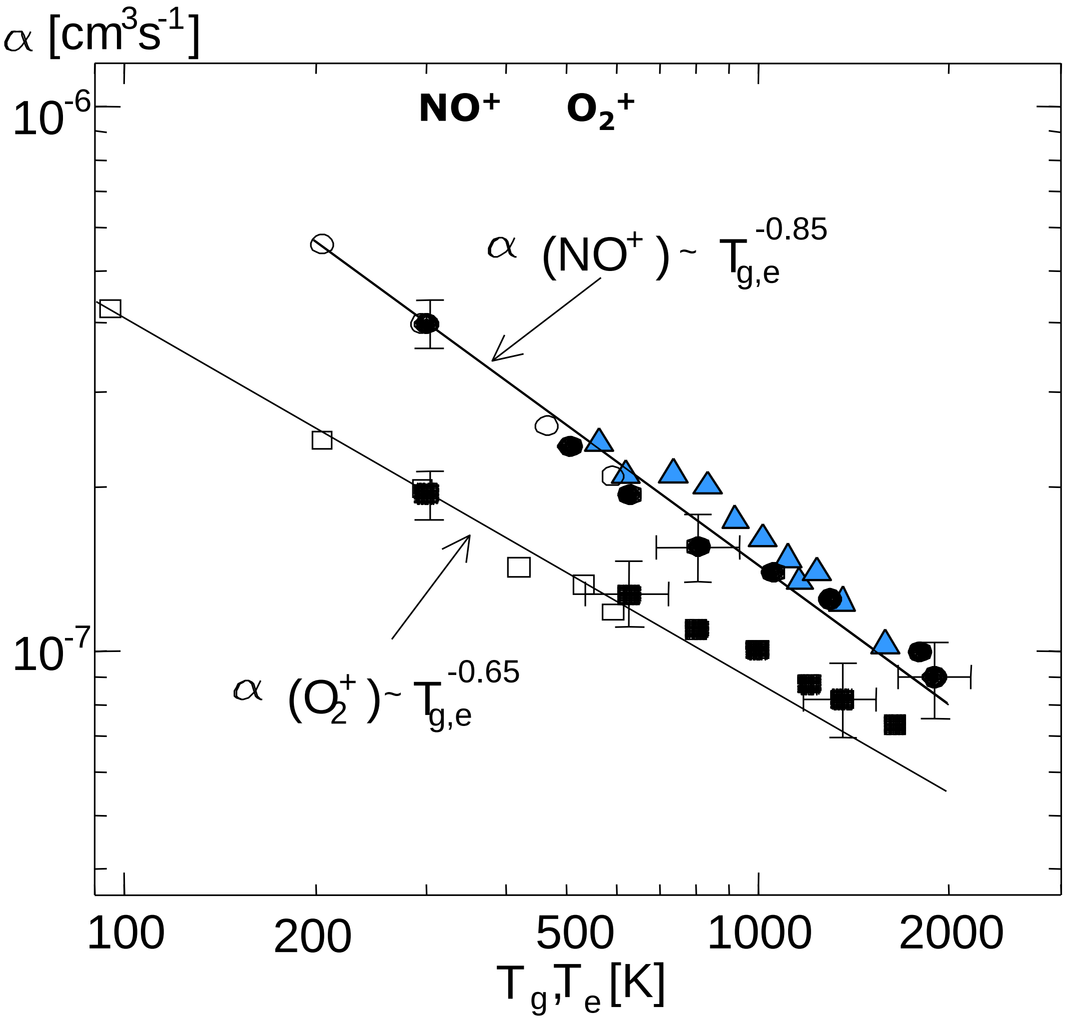

Dissociative recombination of different ions

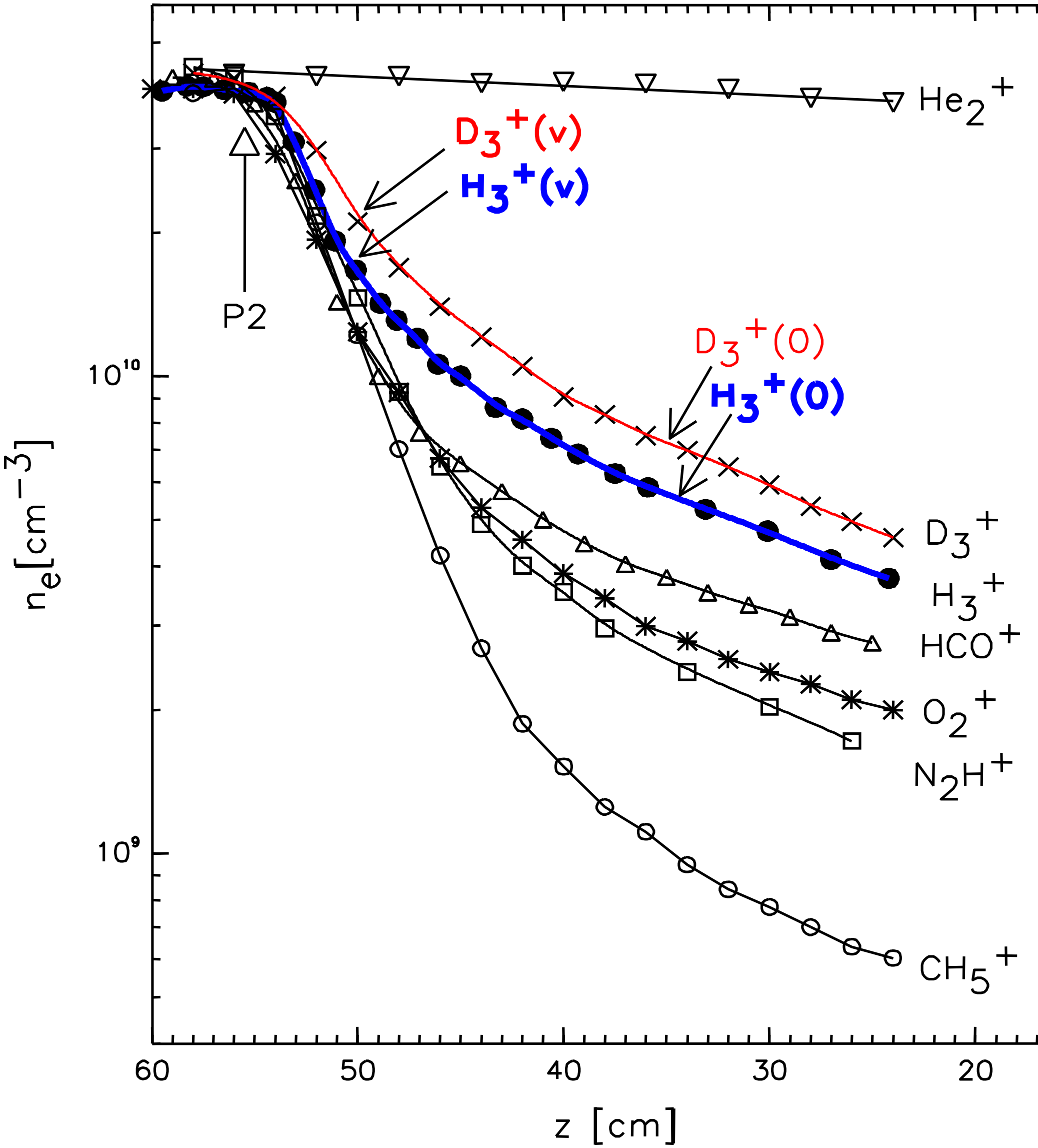

RENNES MS - FALP

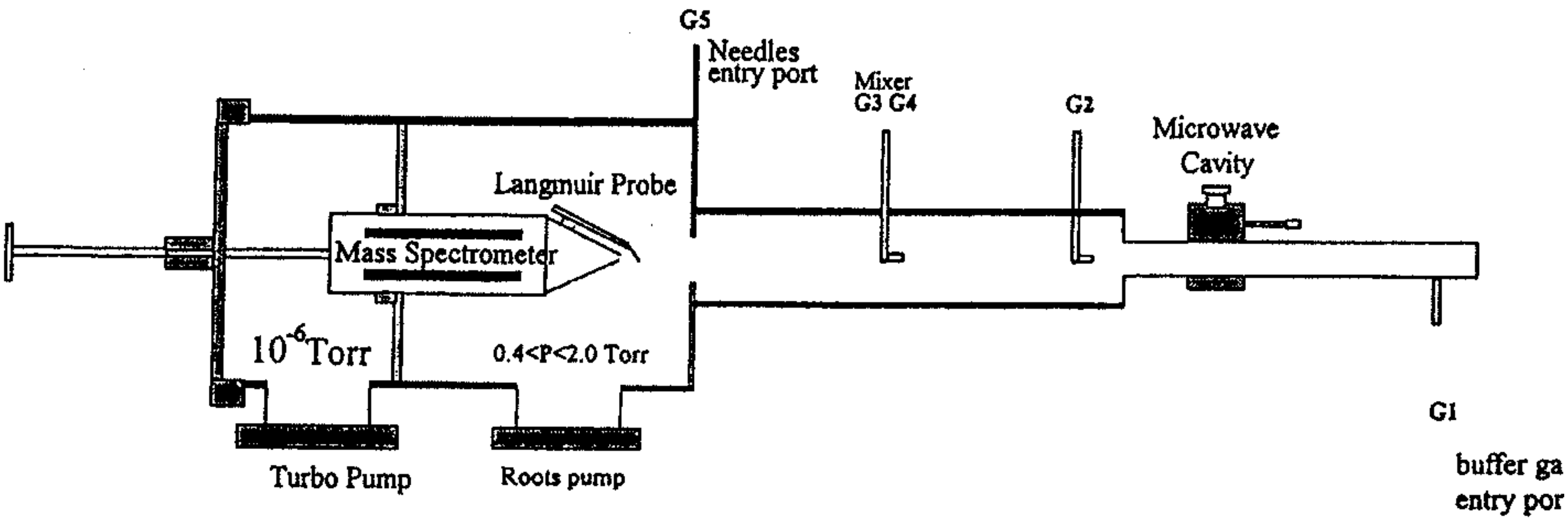

Figure 1. Sketch of the FALP apparatus.

RENNES absorption studies

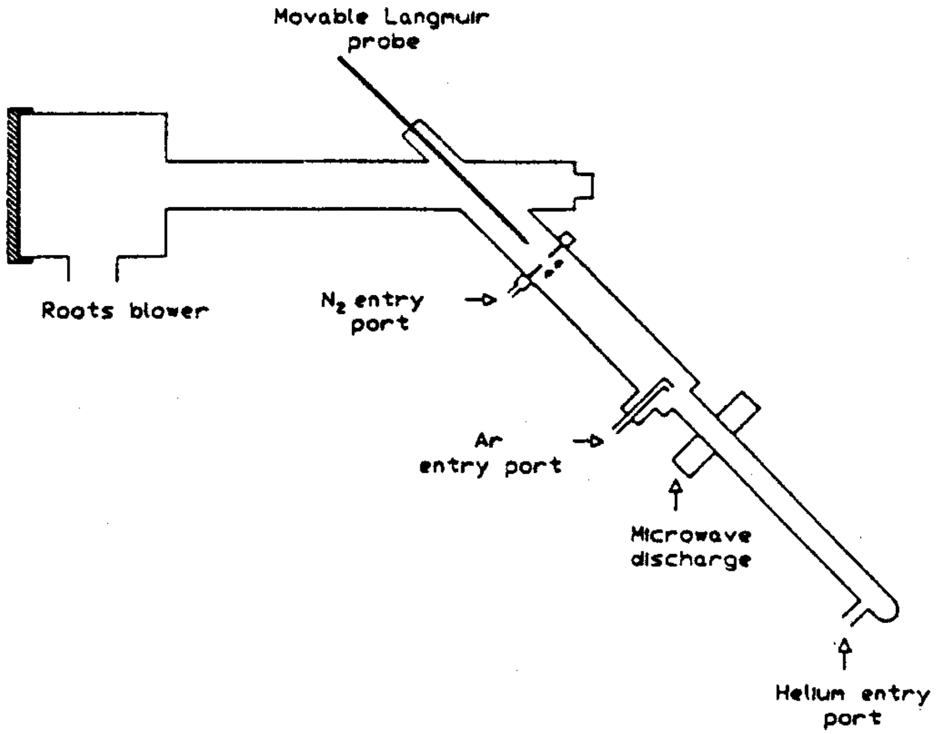

FIG. 1. Sketch of the apparatus.

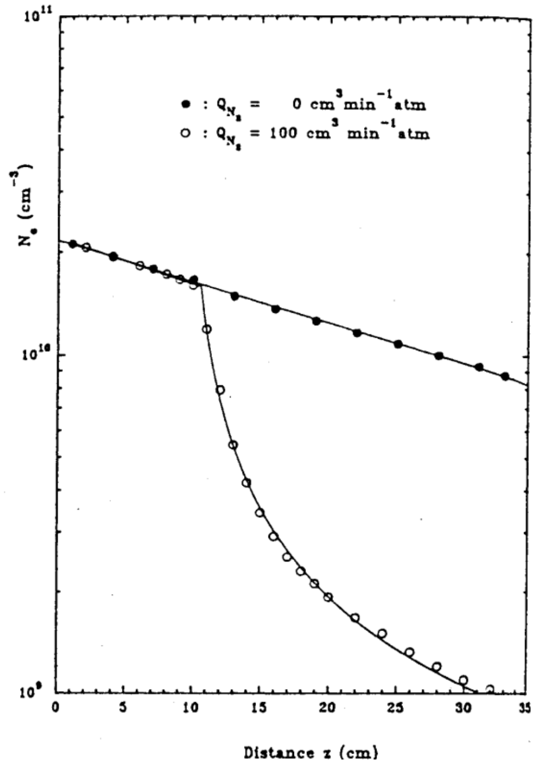

Pittsburg Rainer Johnsen FALP

Emission spectroscopy for identification products of recombination collisional radiative recombination of argon ions

$$Ar^{+} + e^{-} + e^{-} \rightarrow Ar + e^{-}$$

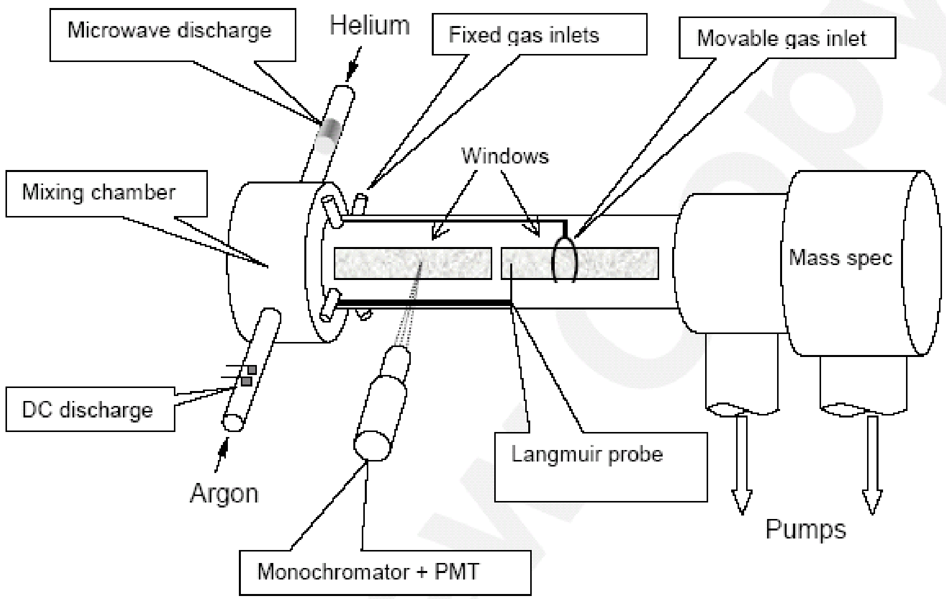

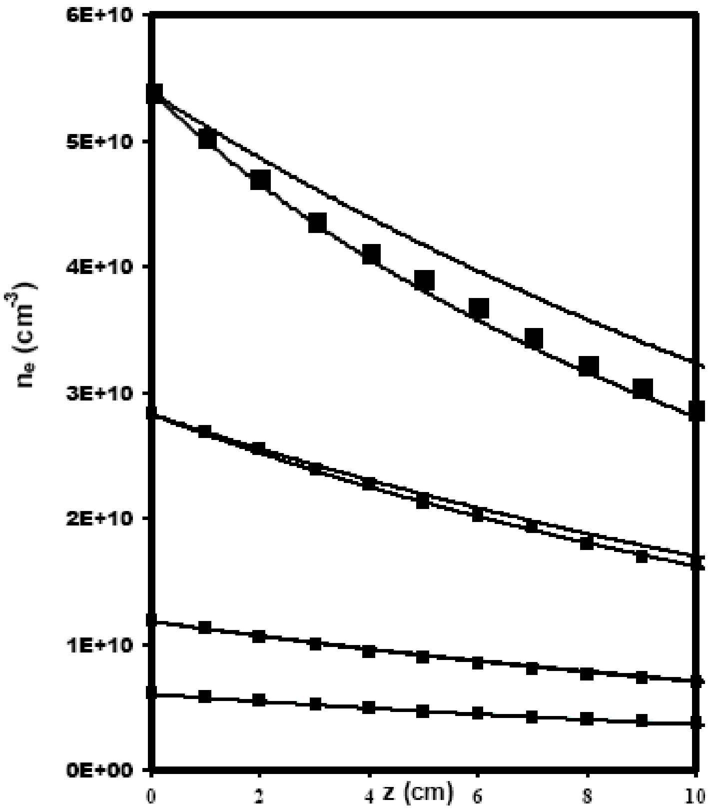

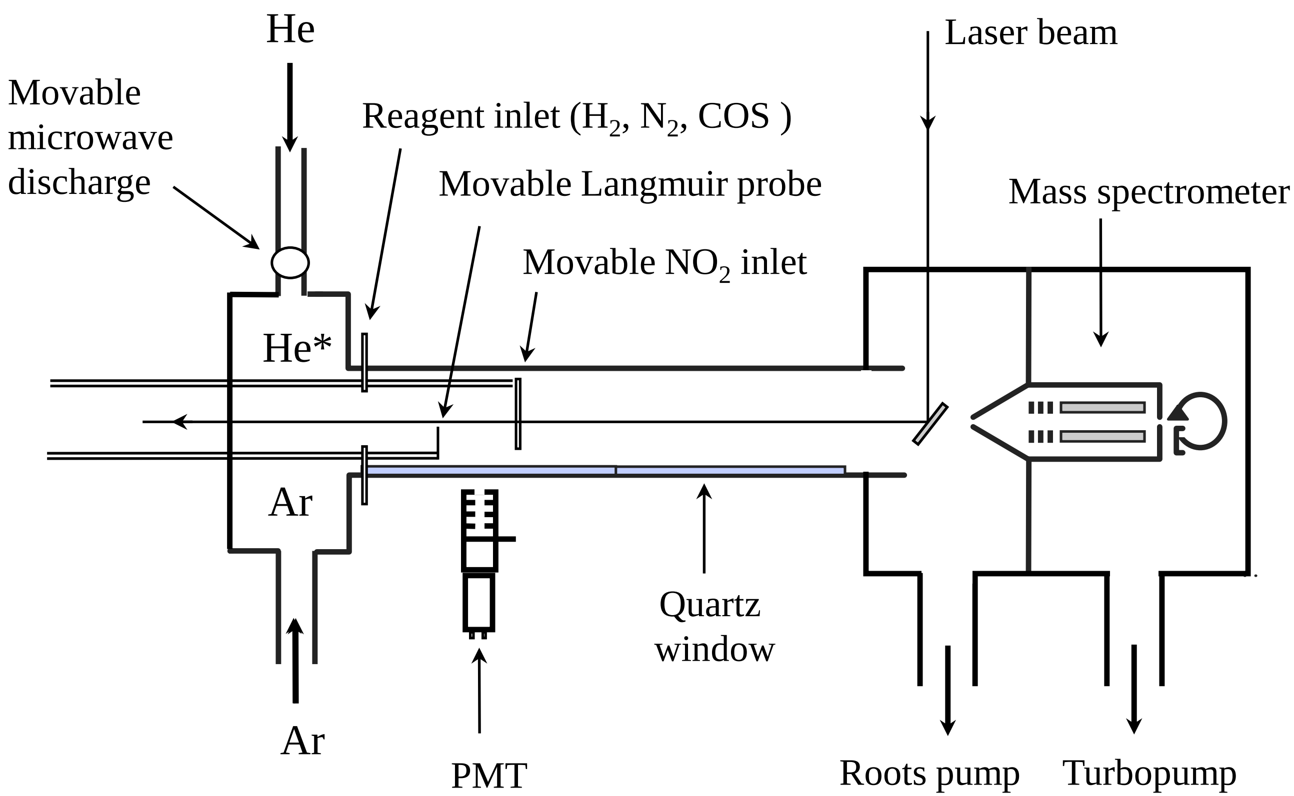
He
Movable
microwave
discharge
Reagent inlet (H2, N2, COS)
Movable Langmuir probe
Movable NO2 inlet
Laser beam
Mass spectrometer
He*
Ar
Quartz
window
Ar
PMT
Roots pump
Turbopump

The Pittsburgh flow tube

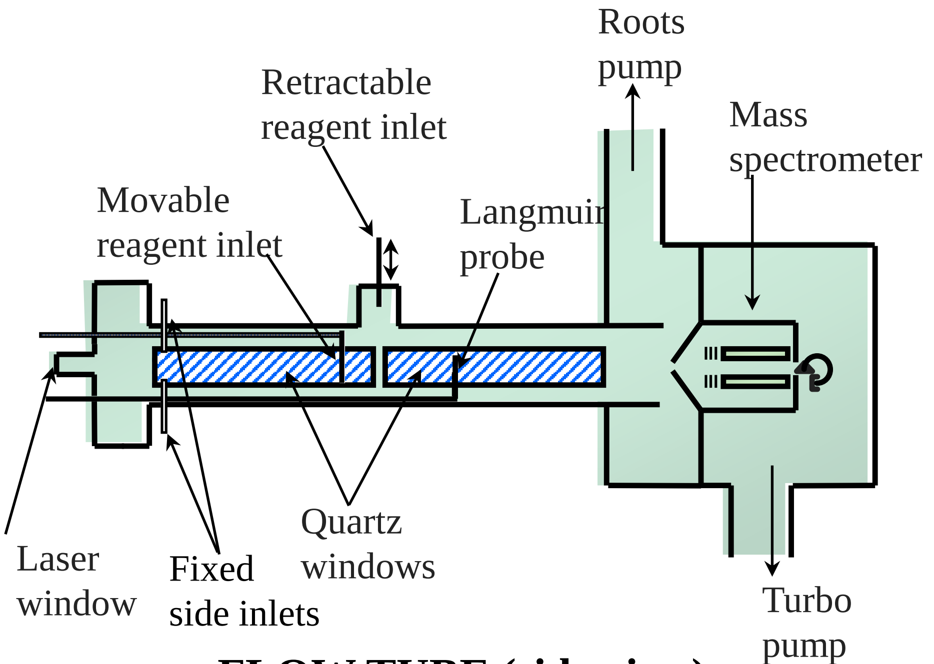

FLOW TUBE (side view)

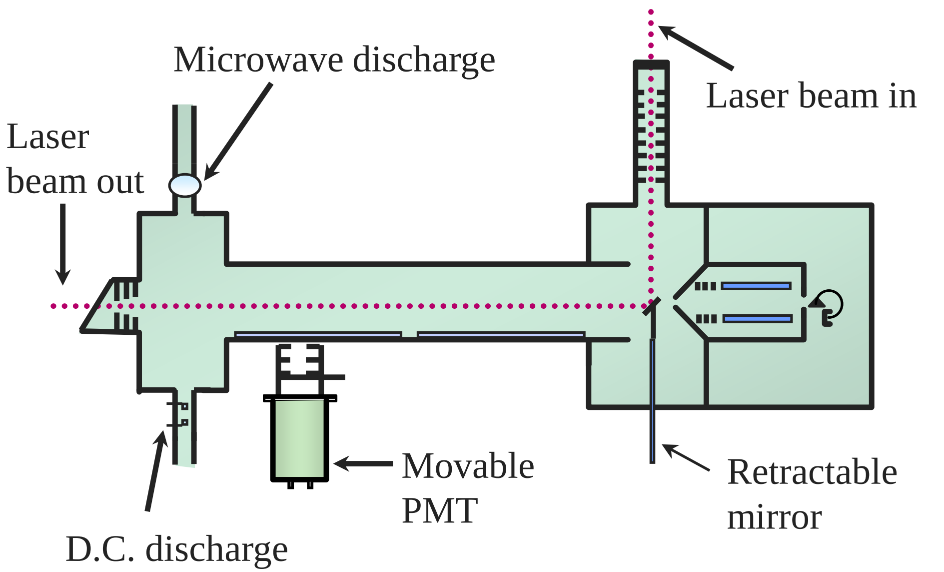

FLOW TUBE (top view)

$$Ar^+ + H_2 \rightarrow ArH^+ + H \quad (+\ 1.53 eV)$$

$$ArH^+ + H_2 \rightarrow Ar + H_3^+ \quad (+\ 0.57\ eV)$$

N.G.ADAMS University of Georgia, Viktoria Poterya

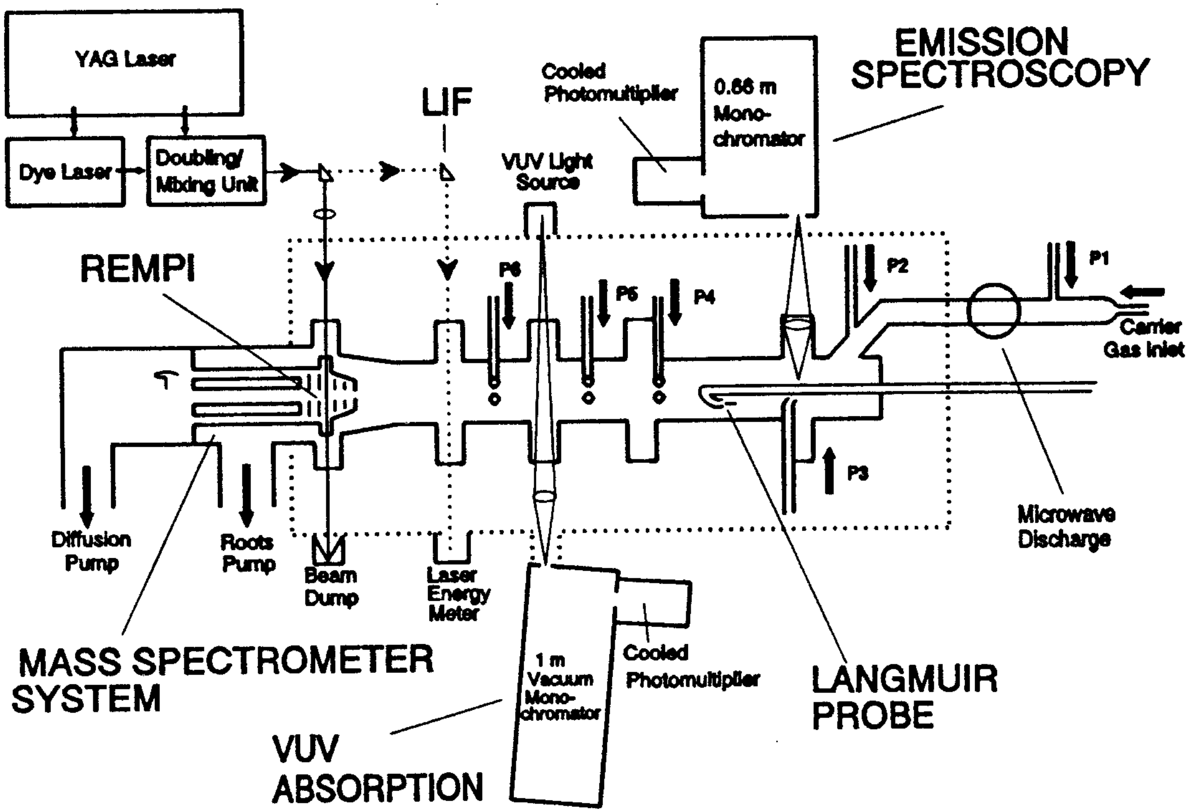

Figure 1. A schematic of the University of Georgia flowing afterglow. Illustrated are the axially movable Langmuir probe, the downstream mass spectrometer, a 0.66 m monochromator with red sensitive photomultiplier for emission studies, a vuv light source and 1 m vacuum monochromator with uv enhanced photomultiplier for detection of atoms and a YAG pumped dye laser with doubling and mixing capabilities for detection of radical species by LIF and REMPI. All photomultipliers are cooled to reduce the background noise and photon counting is used throughout. Further details of this apparatus are described in a separate review.[27]

FALP High pressure UHV version - PRAGUE

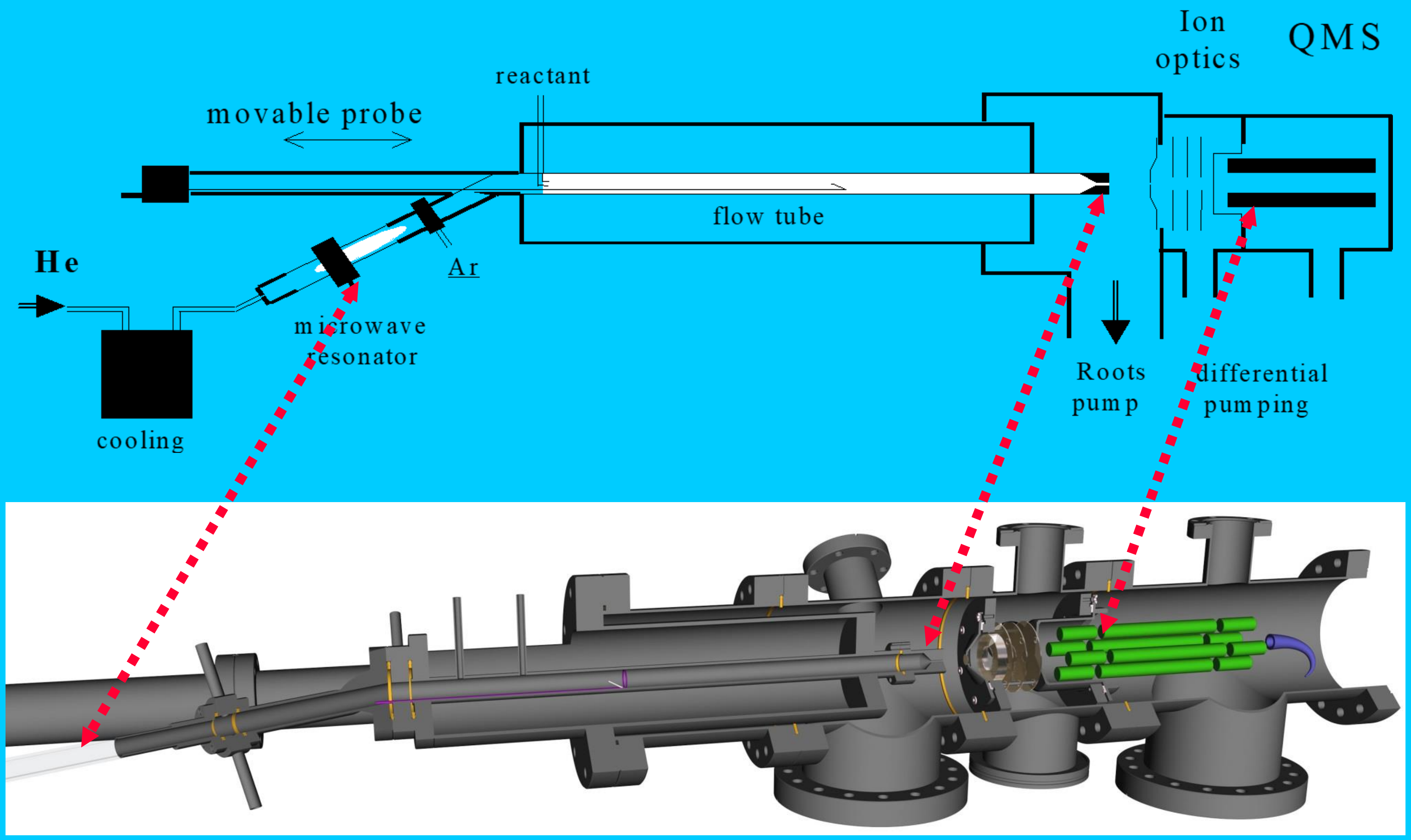

FALP – Ion detection system

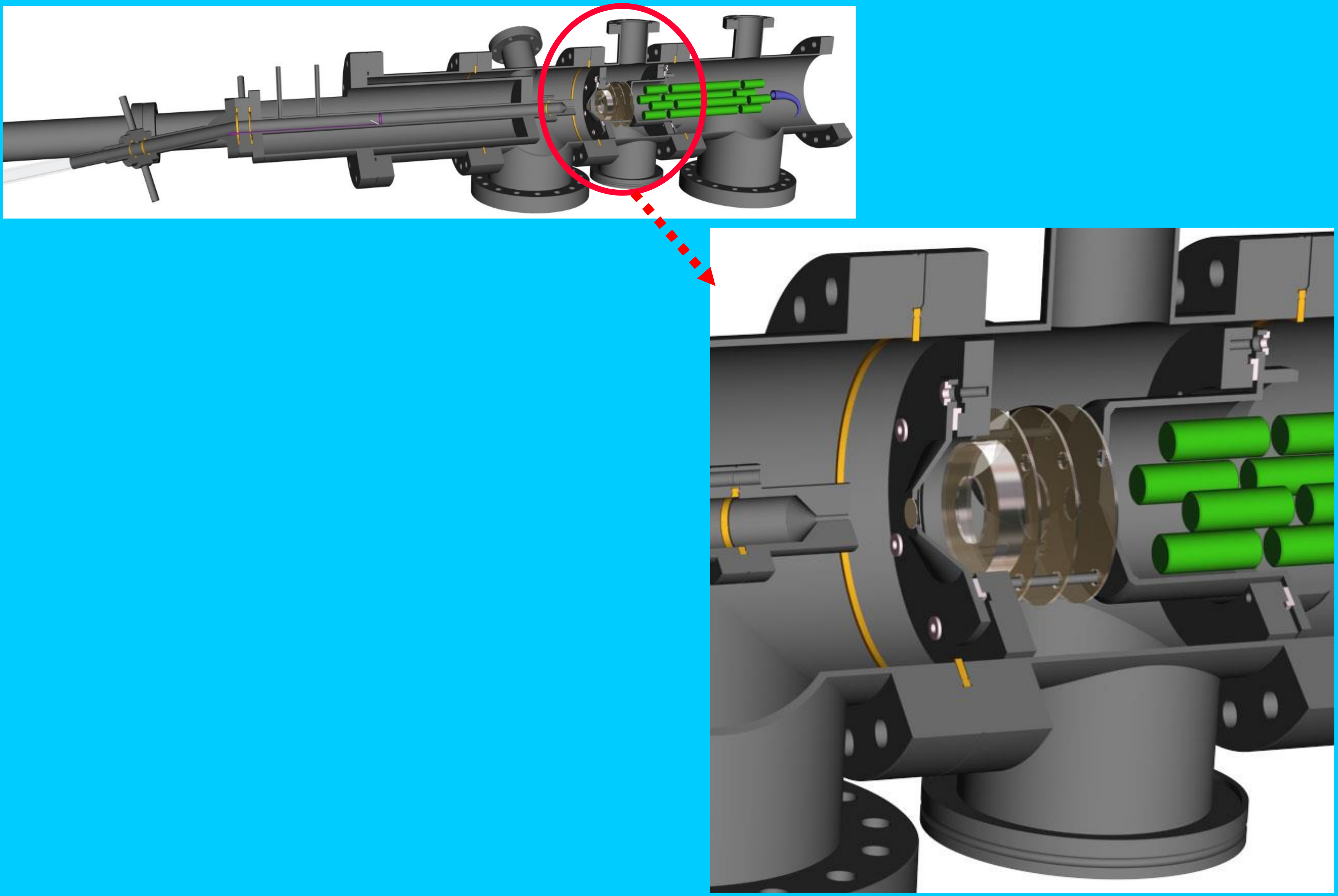

FALP - Pumping units and gas handling system

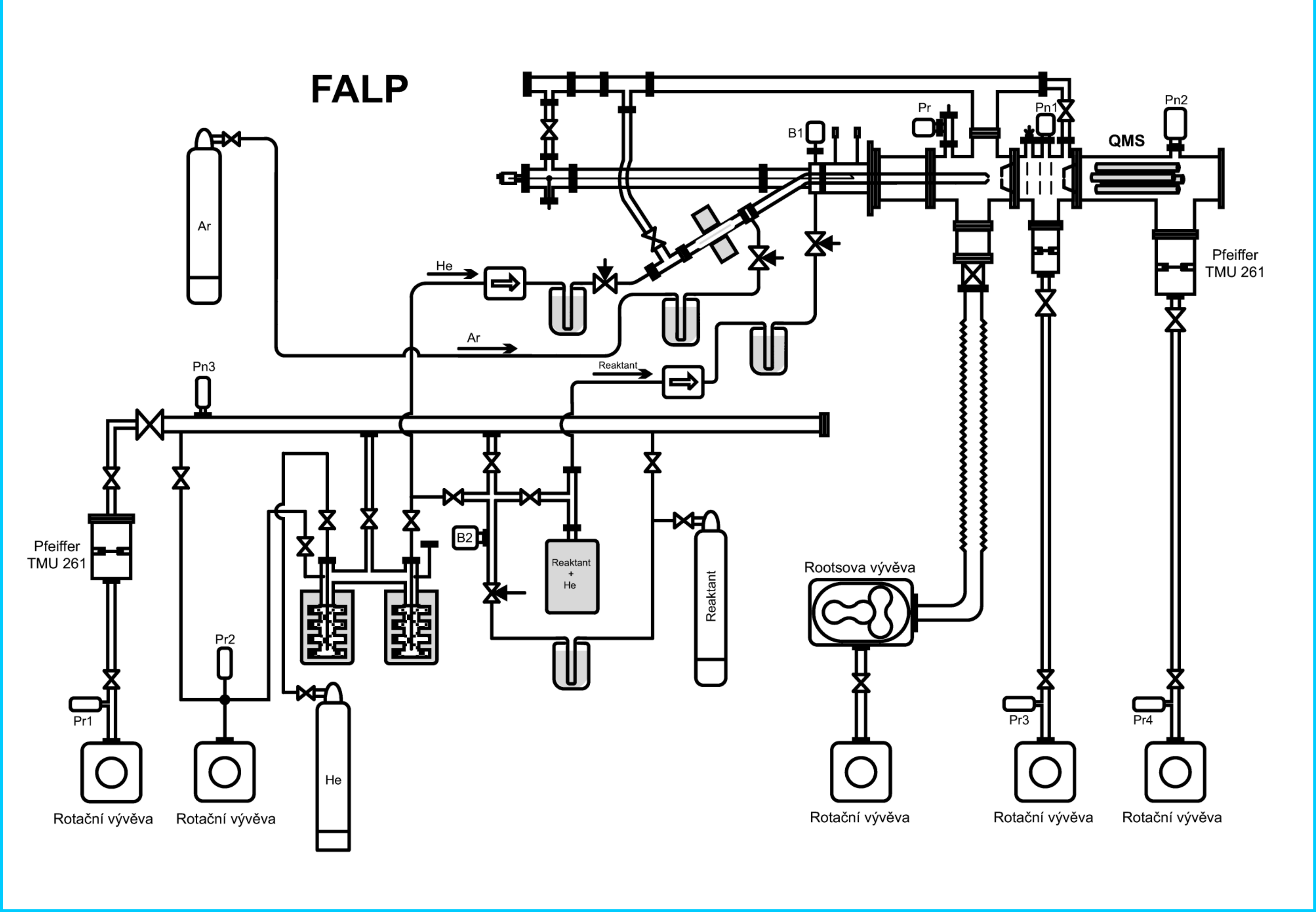

FALP high pressure version

To demonstrante how simple it is in reality

2 men experiment

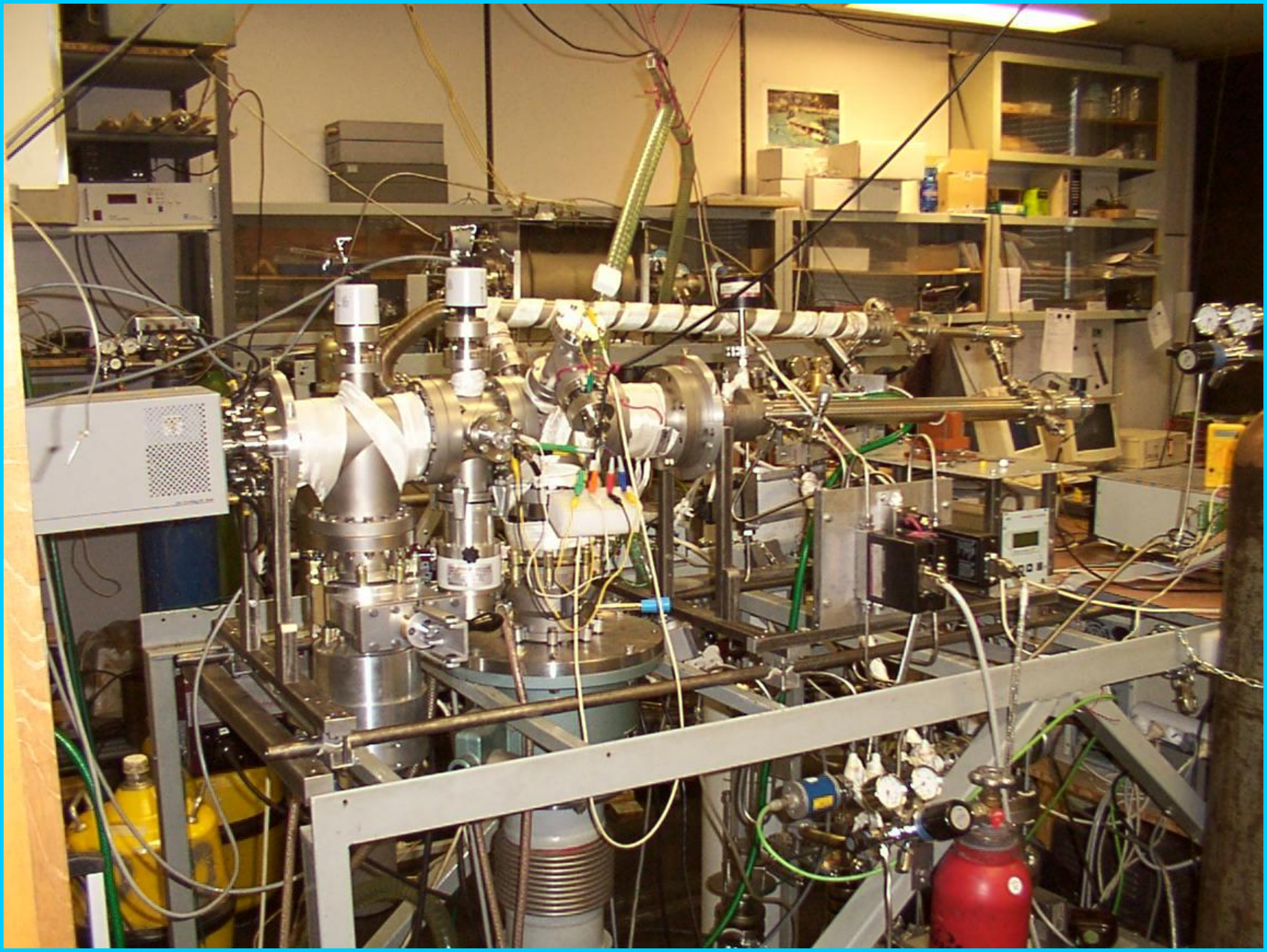

Variation of the probe characteristics along the flow tube

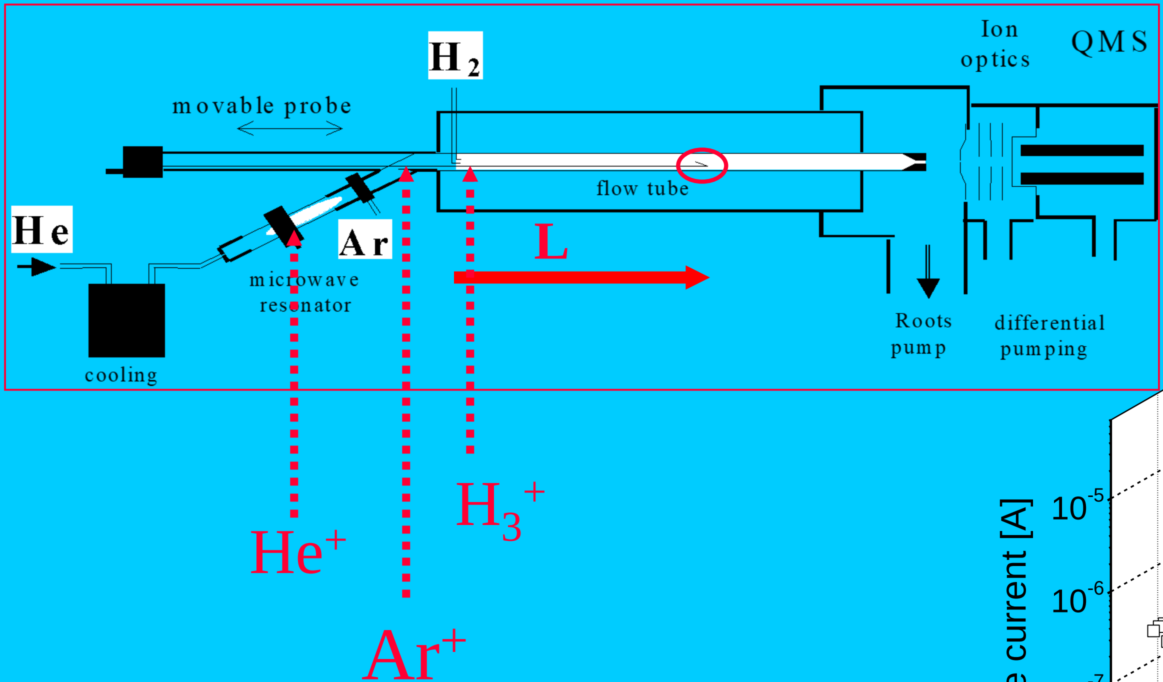

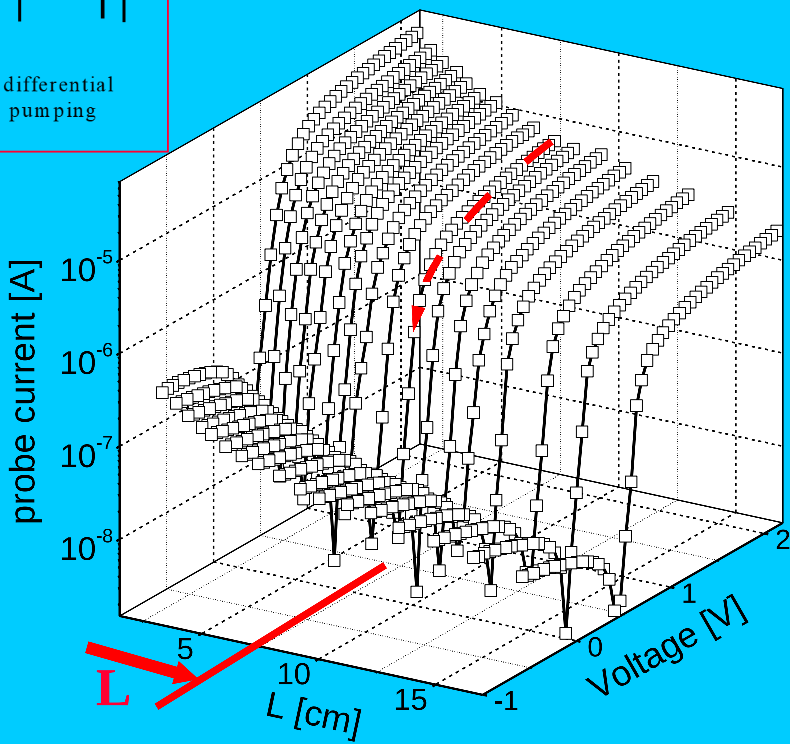

The decay time is correlated with the position in the flow tube.

He pressure 8.8 Torr, temperature 190 K, [Ar] 1.4 mTorr), [H_2] = 9.6×10^{14} cm^{-3}.

Evolution of the probe characteristics along the flow tube

Study of H_3^+ and H_5^+ recombination

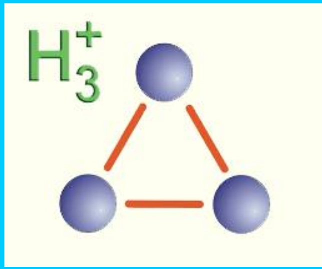

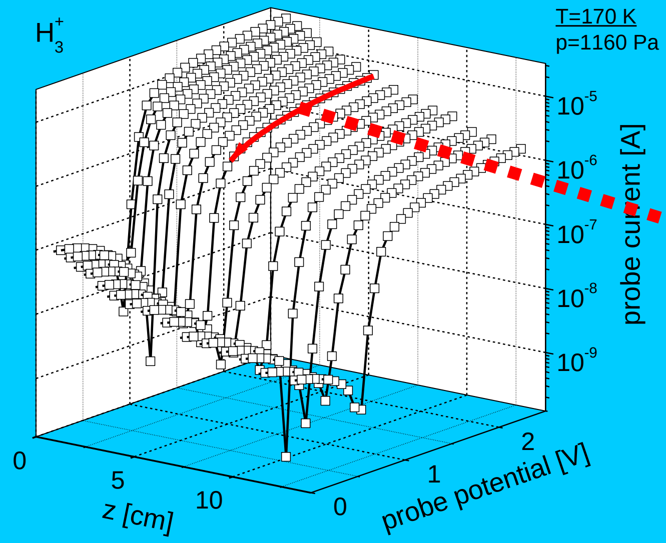

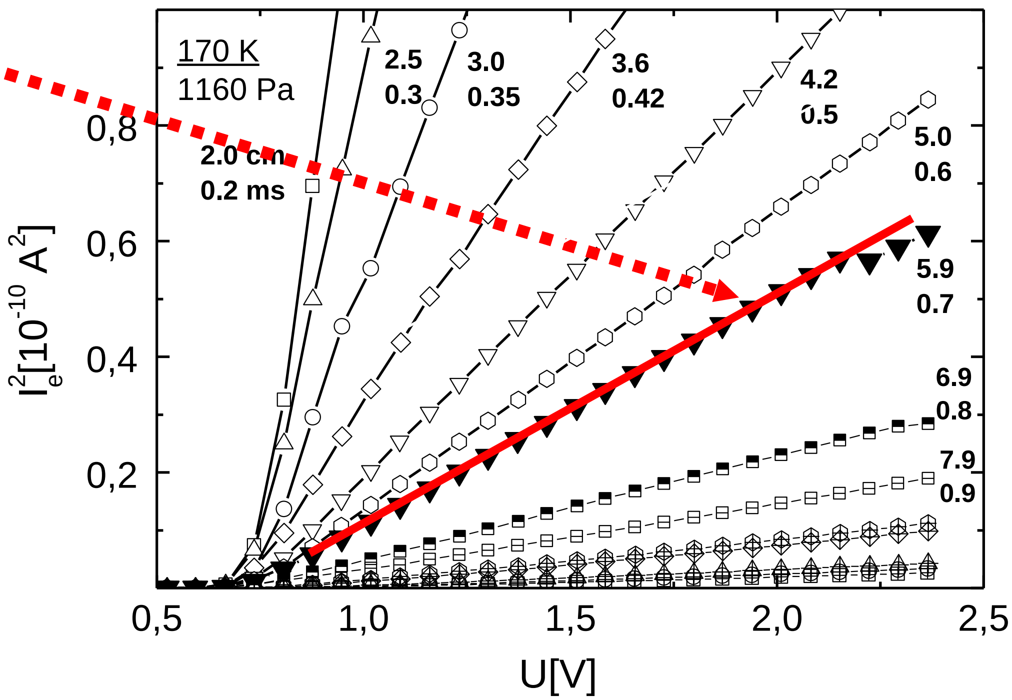

$$I_e^2 \sim n_e A_{Pr}(V_{probe} - V_{plasma})$$

PLASMA DECAY
H_3^+ and H_5^+ in thermodynamic equilibrium

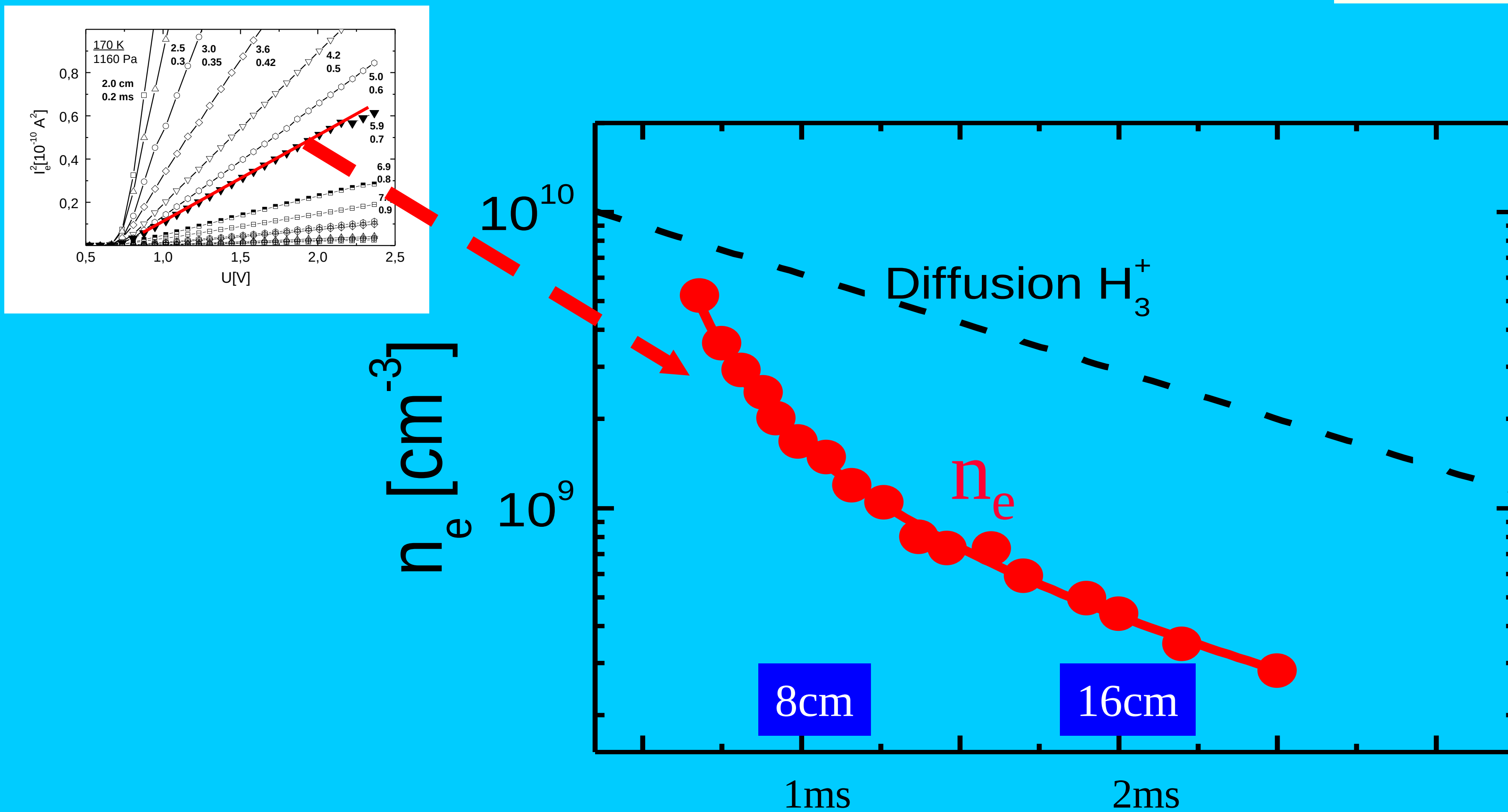

190 K, 9 Torr

Note very different time scale!!!

Plasma parameters along the flow tube

$NH_4^+(NH_3)_2 + e^-$

$\vec{E}_L$

V_P

T_e

n_e

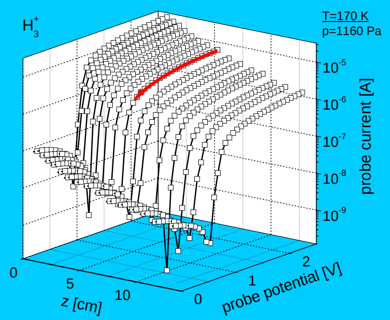

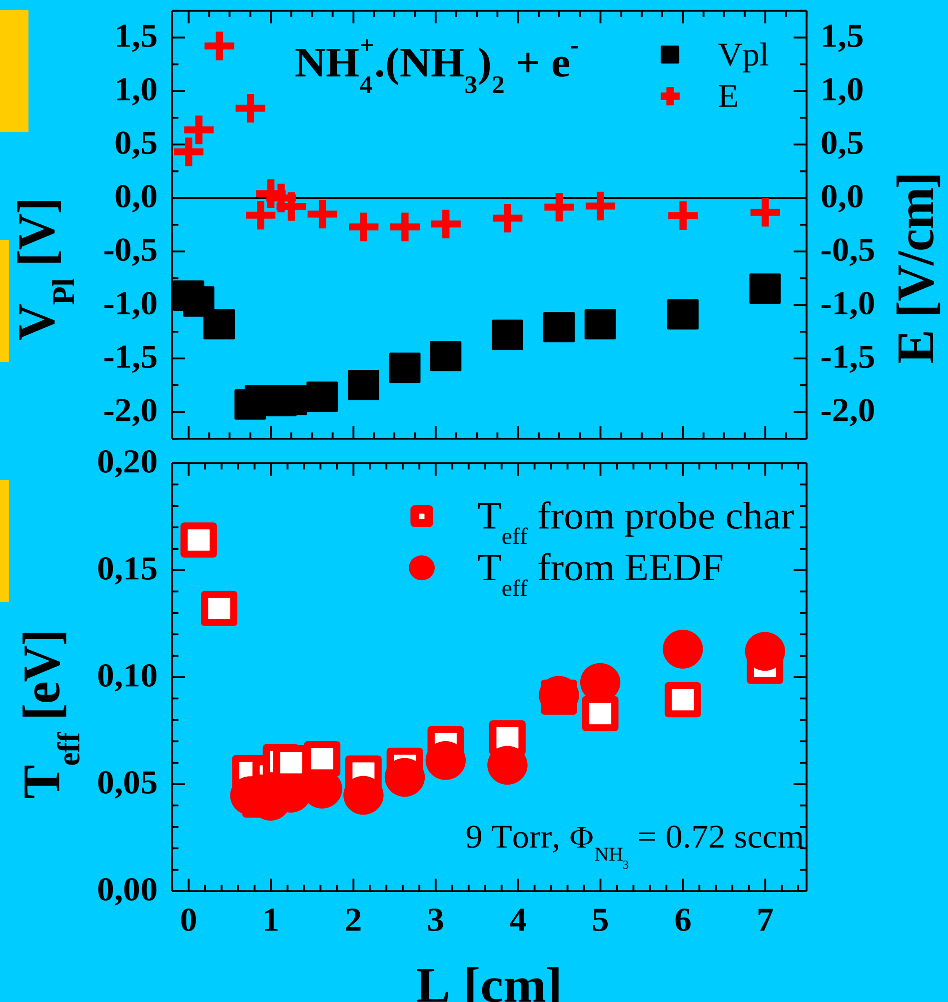

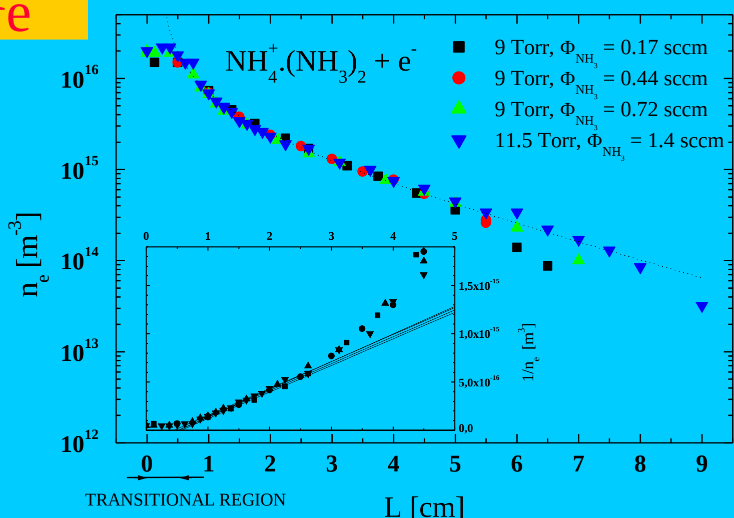

He buffer

EEDF measurements

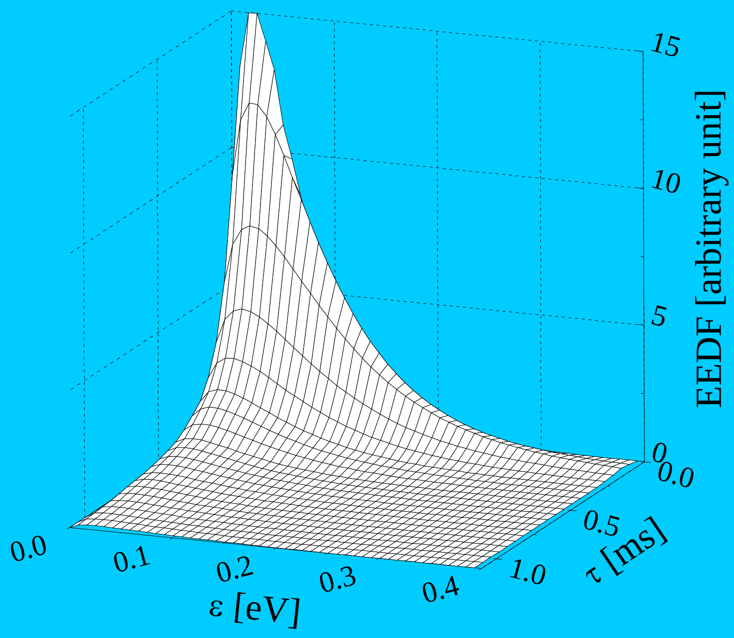

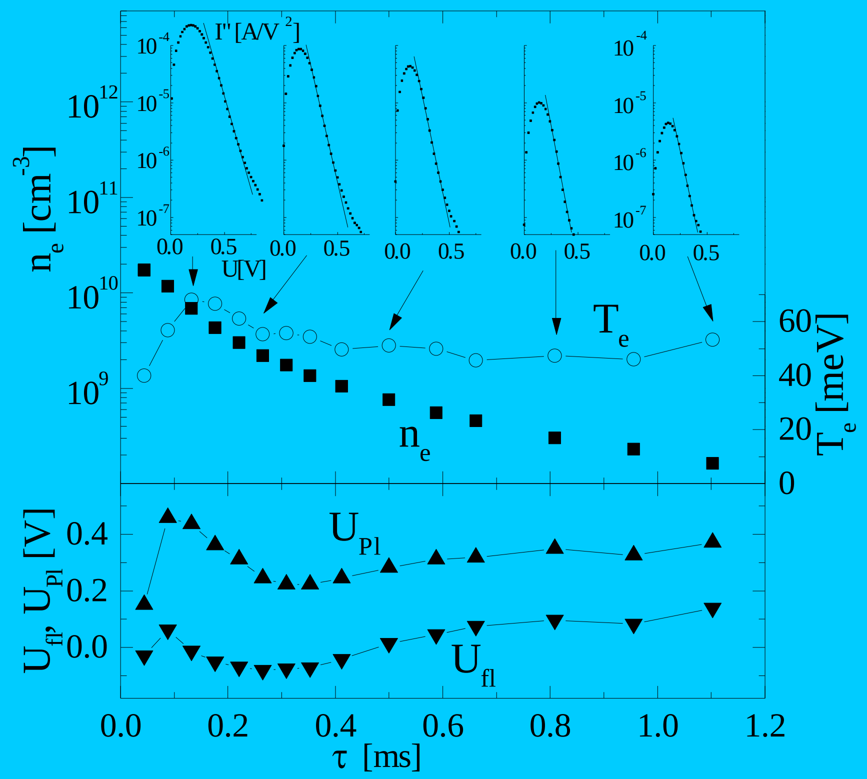

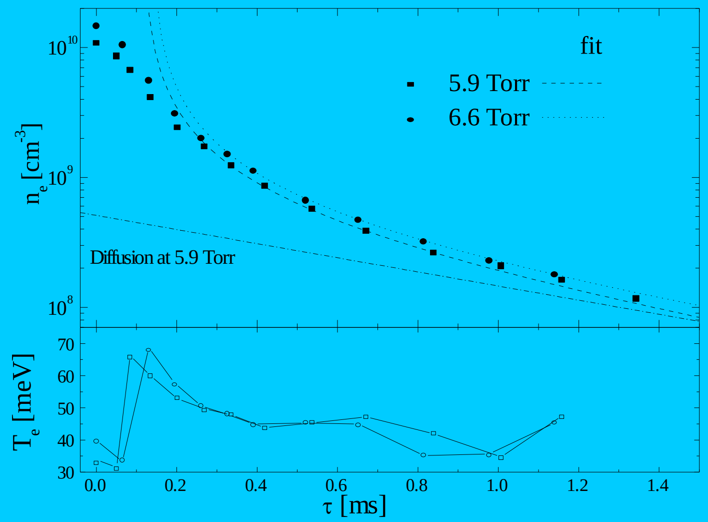

The time evolution of the EEDF in the recombination dominated FA plasma In He (p= 9 Torr) with small admixture of HCOH (0.05 %).
EEDF is normalized to the electron number density.

The CRESU technique at Rennes

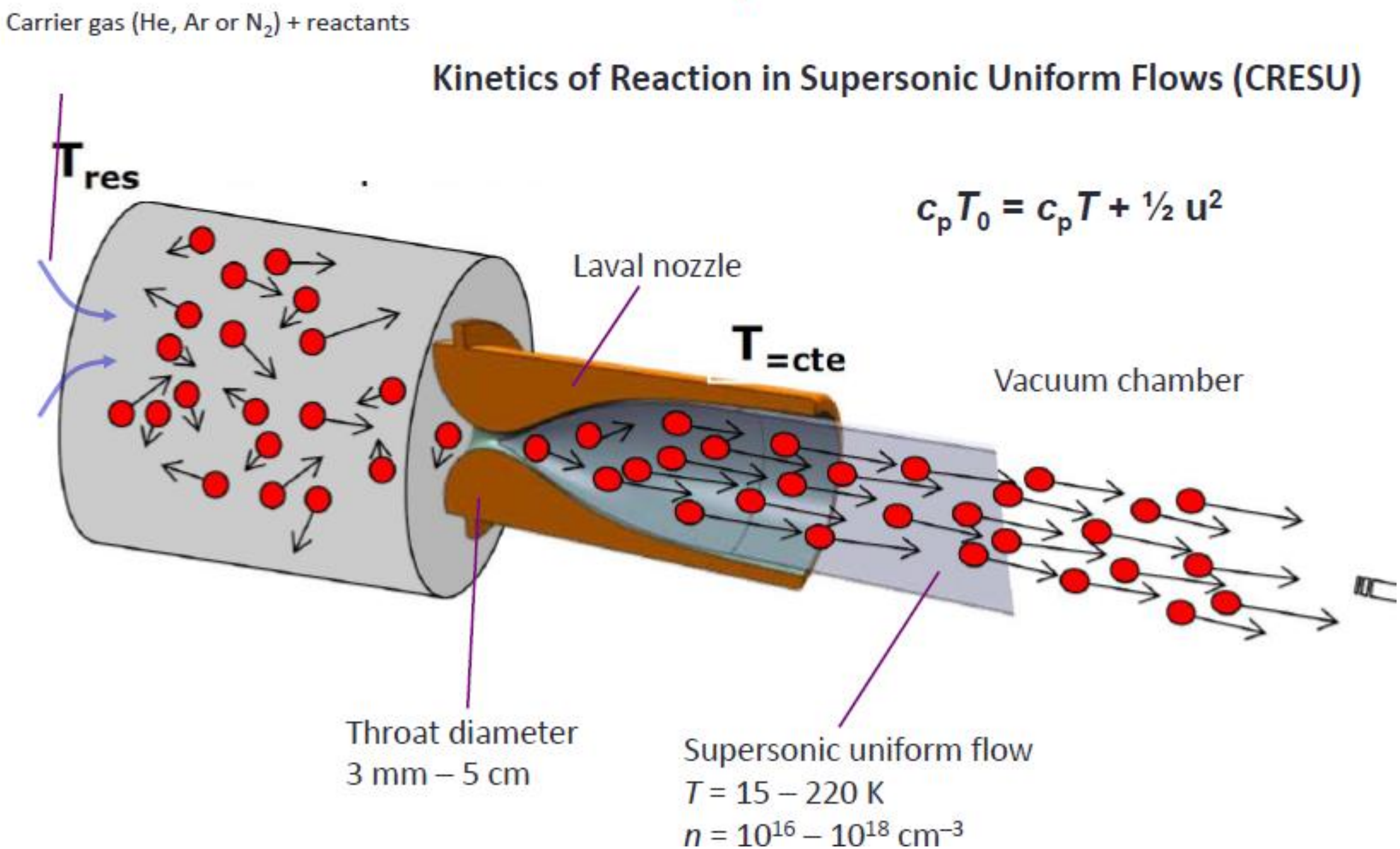

Kinetics of anion-molecule reactions at low temperature

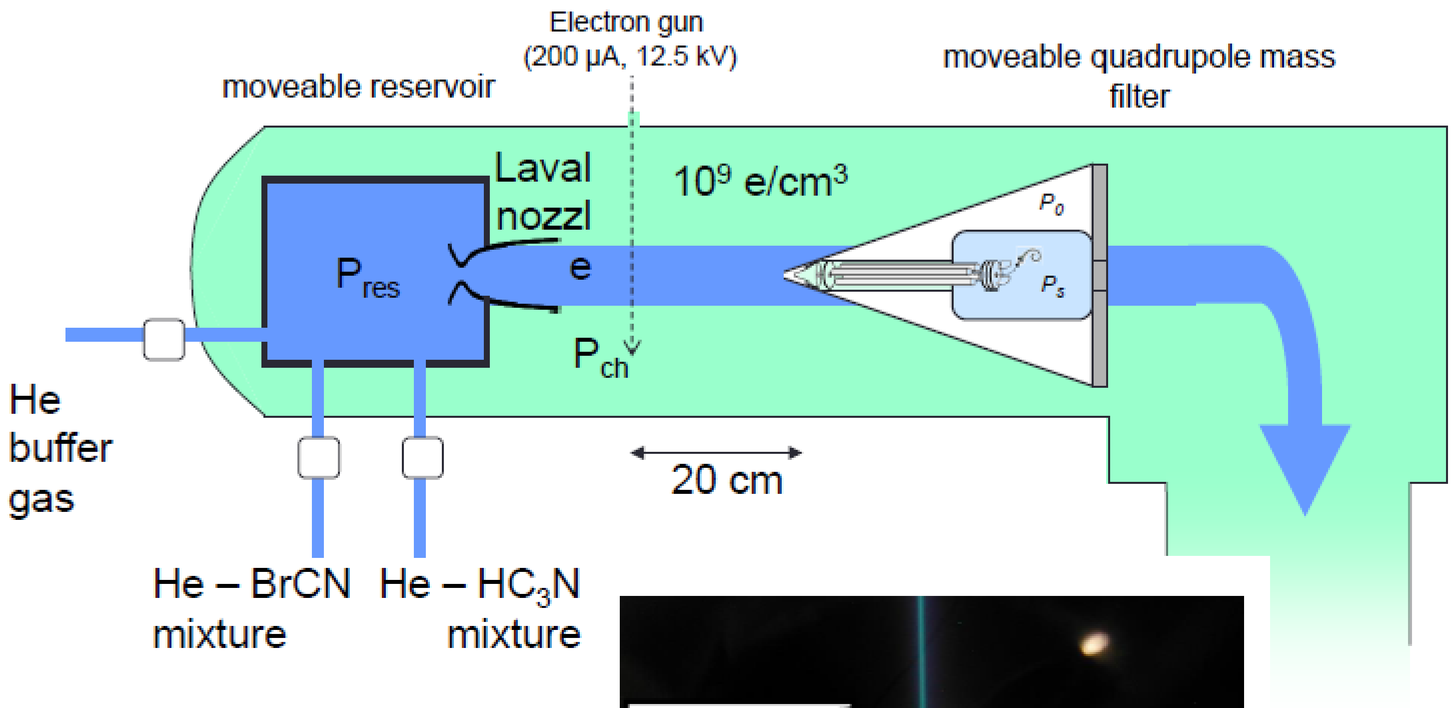

- CN^- + HC_3N (L. Biennier, S. Carles, J-C Guillemin et al. Icarus, 227, 123, 2014)
- C_3N^- + HC_3N (in progress)
- Collaboration with C. Alcaraz and co-workers (Orsay and Prague)

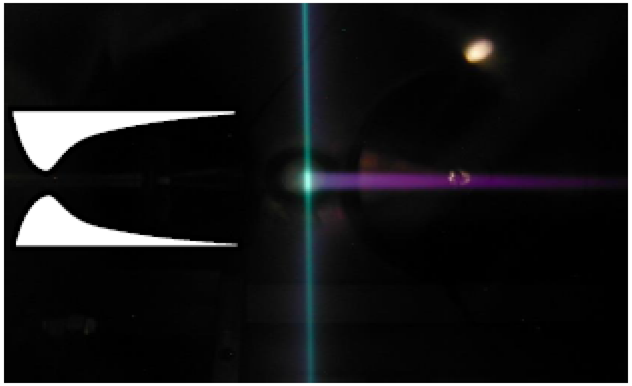

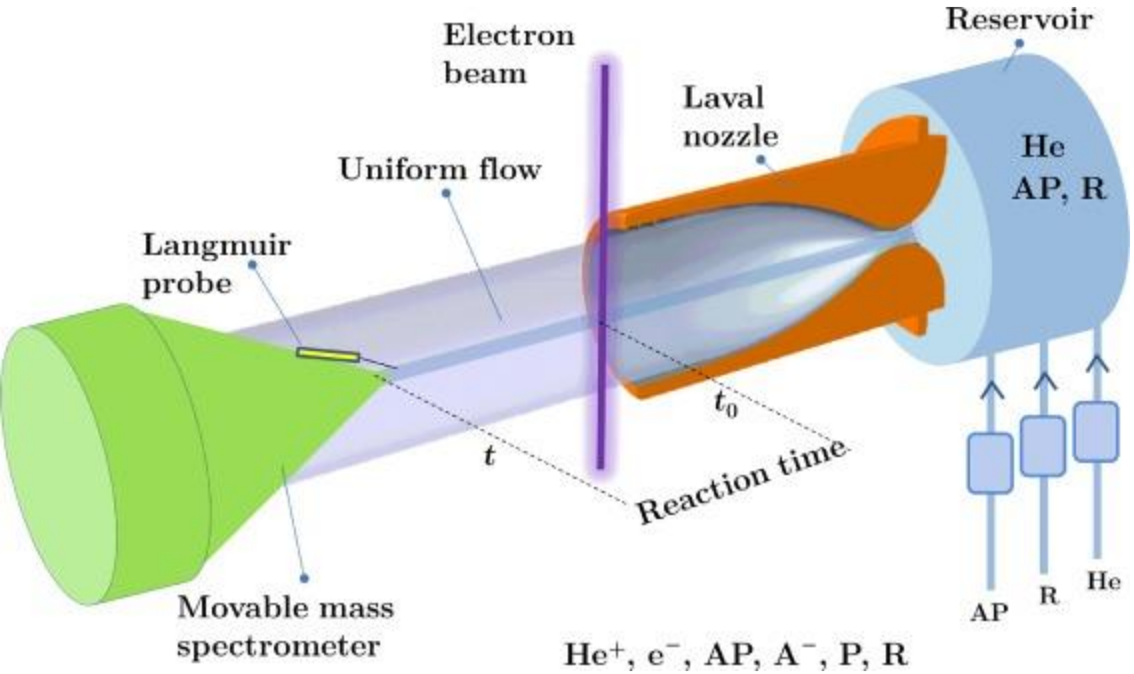
Electron beam
Reservoir
Laval nozzle
Uniform flow
He
AP, R
Langmuir probe
t_0
t
Reaction time
Movable mass spectrometer
AP
R
He
He$^+$, e$^-$, AP, A$^-$, P, R

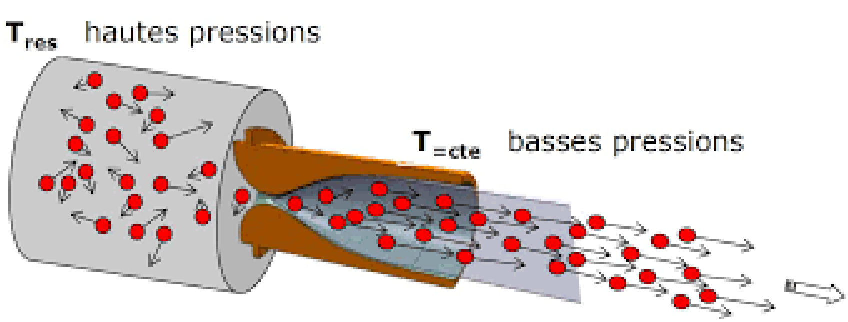
T_{res} hautes pressions
$T_{=cte}$ basses pressions

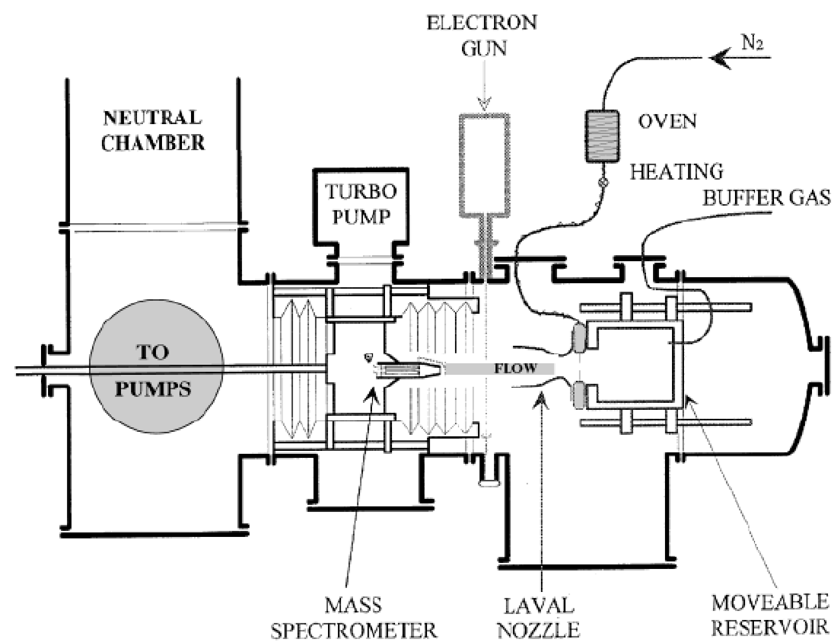
ELECTRON GUN
N_2
NEUTRAL CHAMBER
OVEN
HEATING BUFFER GAS
TURBO PUMP
TO PUMPS
FLOW
MASS SPECTROMETER
LAVAL NOZZLE
MOVEABLE RESERVOIR

Outlook: Electron-beam collision studies

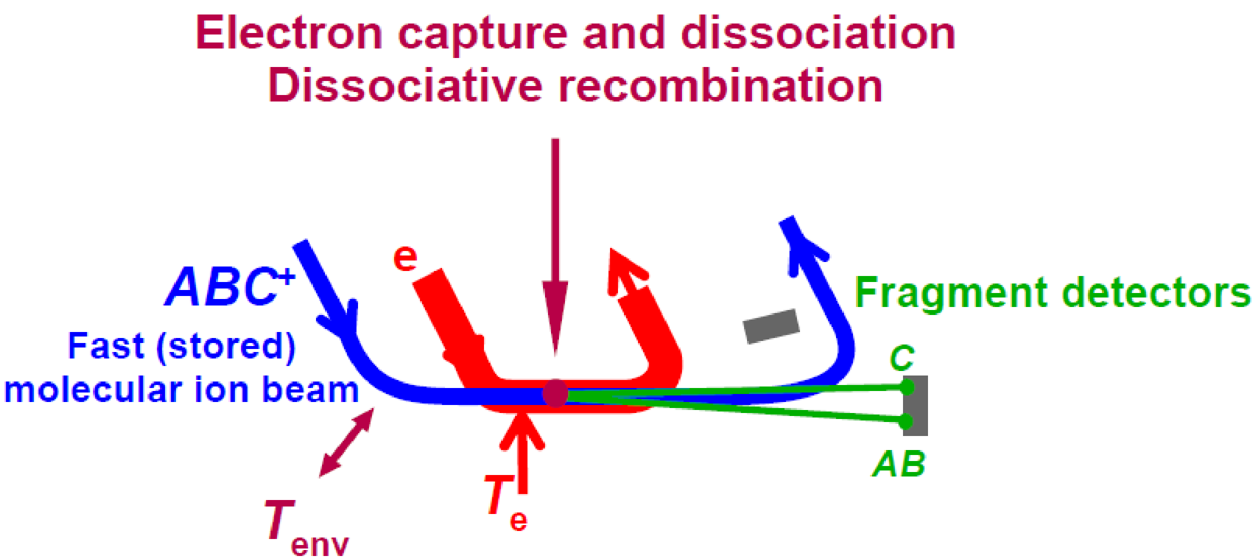

$$E_{coll} = \frac{1}{2} m_e (v_e - v_i)^2$$

can be scanned from ~ 1 meV ... 50 eV

Electron-cold molecular ion reaction: Dissociative Recombination → Merged Beam Kinematics

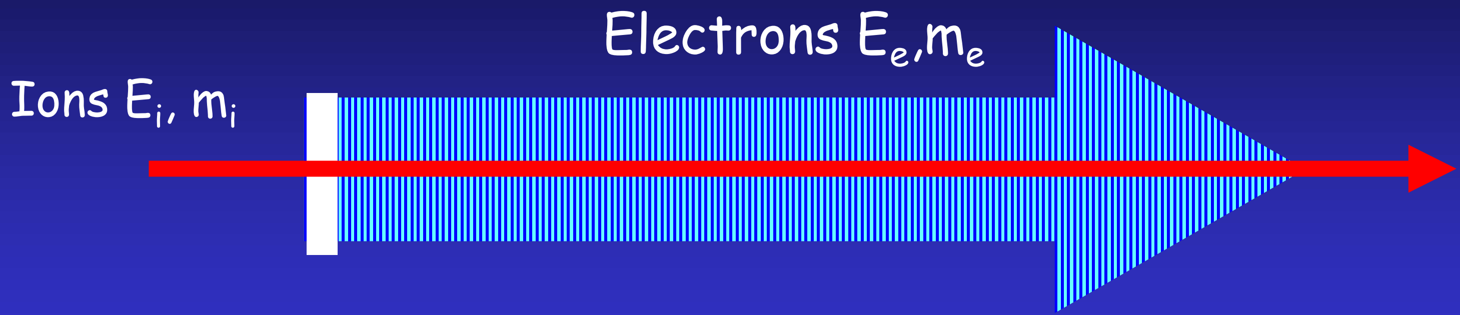

$$E_{cm} = \frac{1}{2} m_e v_{cm}^2 \approx \left[\sqrt{\frac{m_e}{m_i} E_i} - \sqrt{E_e} \right]^2$$

Center of mass resolution:

$$\Delta E_{cm} = \left\{ \left[\left(1 - \frac{v_e}{v_i} \right) \frac{m_e}{m_i} \Delta E_i \right]^2 + \left[\left(1 - \frac{v_i}{v_e} \right) \Delta E_e \right]^2 \right\}^{1/2}$$

~ meV resolution for zero relative kinetic energy!

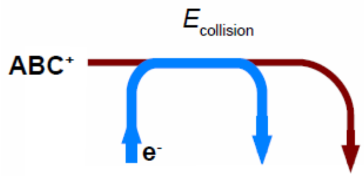

Merged ion and electron beams

- Tunable collision energy

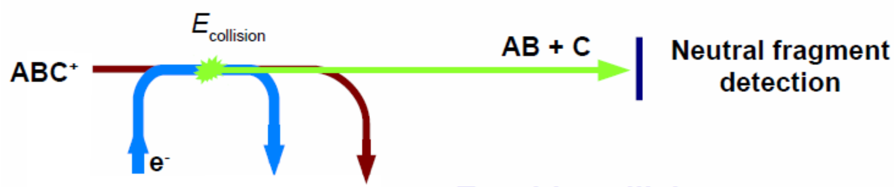

Merged ion and electron beams

- Tunable collision energy

- Forward dissociation cone
→ full detection possible

- Velocity conservation
→ calorimetry mass detection

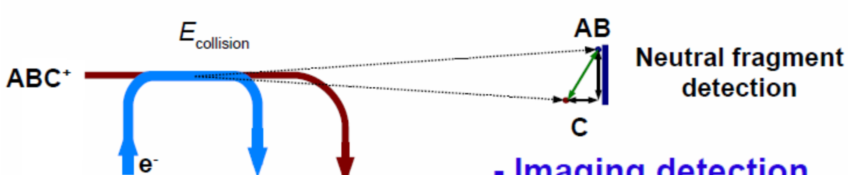

- Imaging detection
→ kinetic energy released
→ product excitation

Experiments

PLASMA experiments SA and FA - multi collisions $\{\alpha(T)\}$
Crossed beam experiments - single collisions $\{\sigma(v_r)\}$
Marched beam, Storage rings - TSR, Cryring, Astrid - single collisions $\{\sigma(v_r)\}$

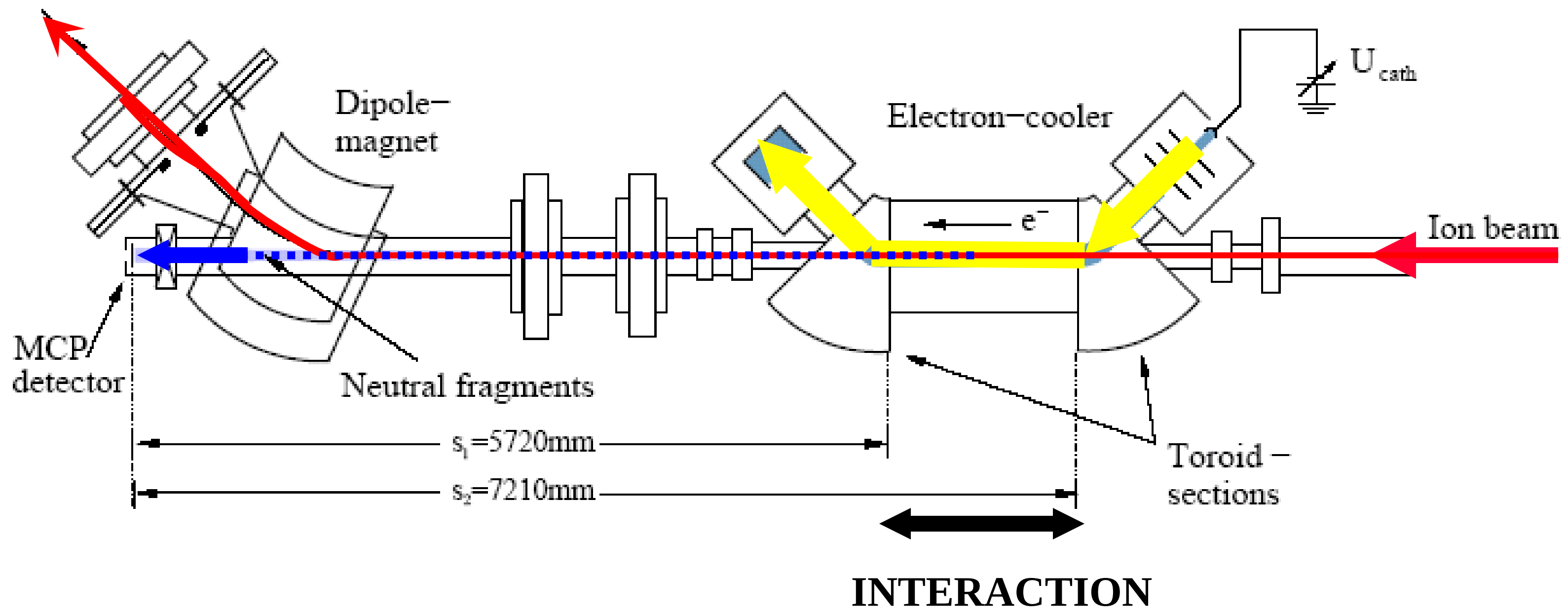

$$H_3^+ + e^- \rightarrow H, H_2$$

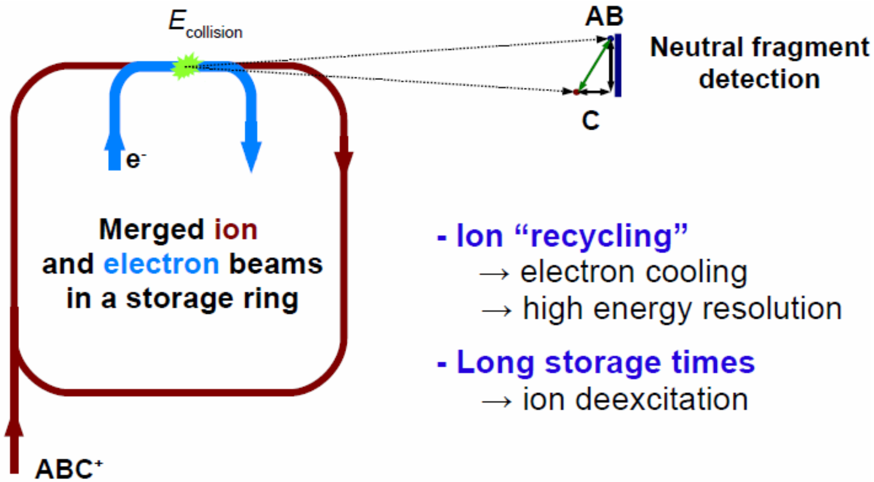

- **Ion "recycling"**
  - → electron cooling
  - → high energy resolution
- **Long storage times**
  - → ion deexcitation

TSR heavy ion storage ring

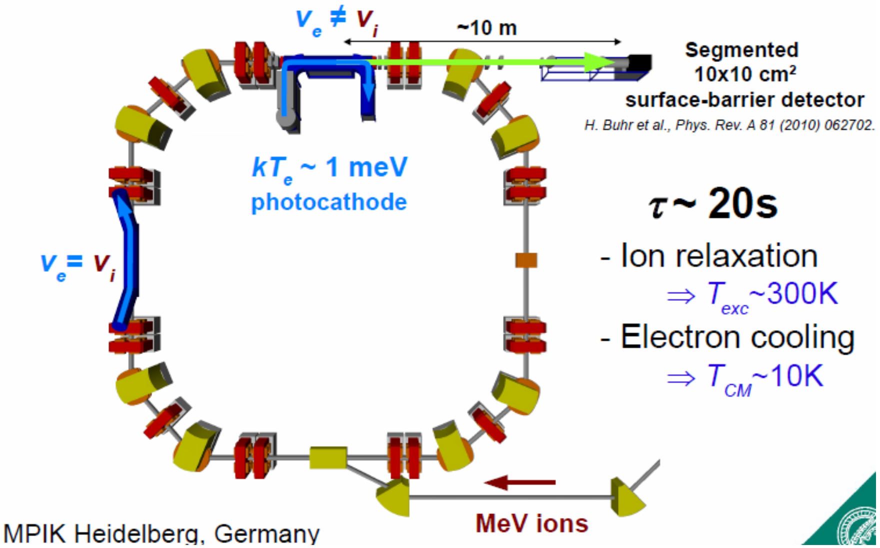

τ ~ 20s

- Ion relaxation
  - ⇒ T_{exc}~300K
- Electron cooling
  - ⇒ T_{CM}~10K

MPIK Heidelberg, Germany

TSR electron target

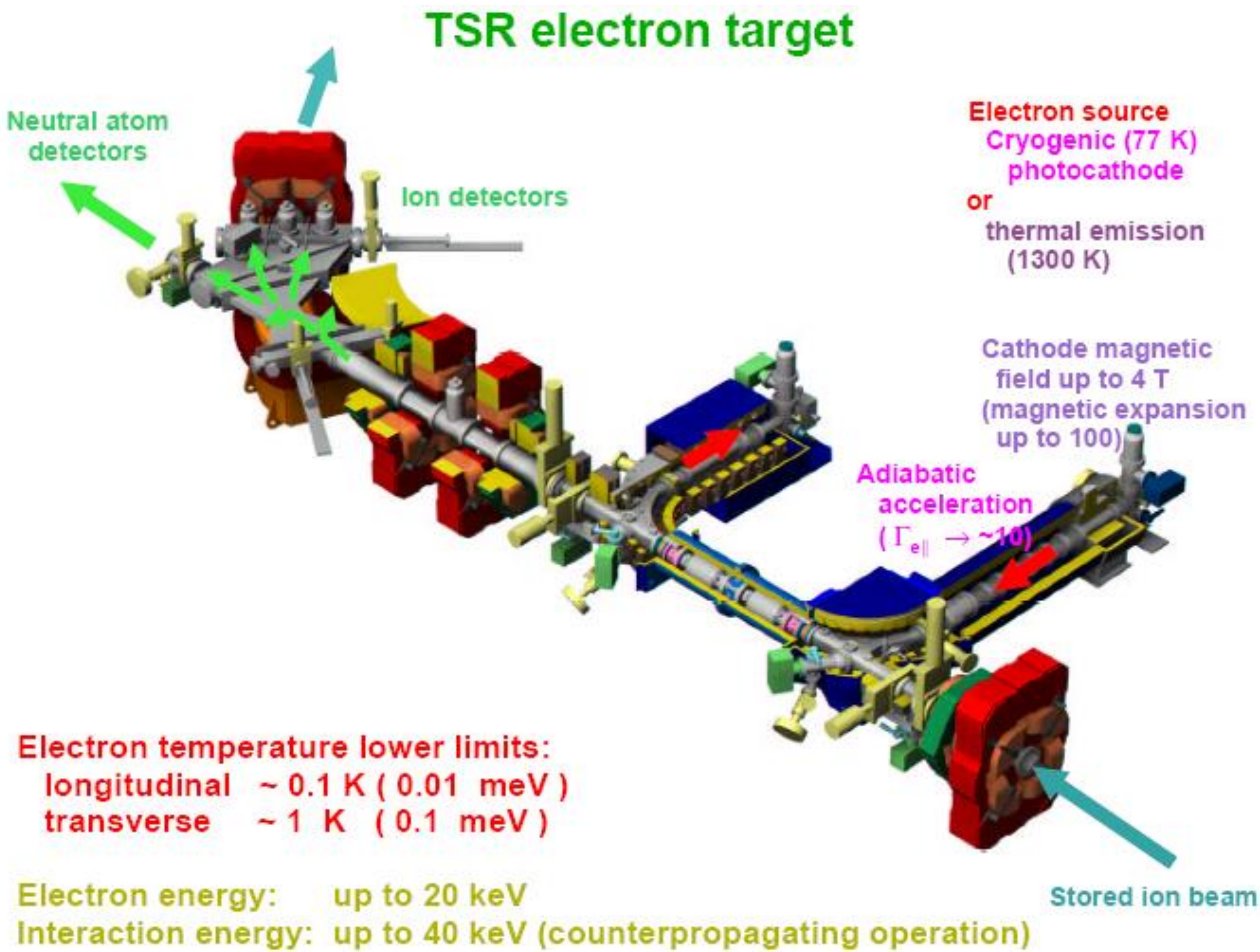

Electron cooling

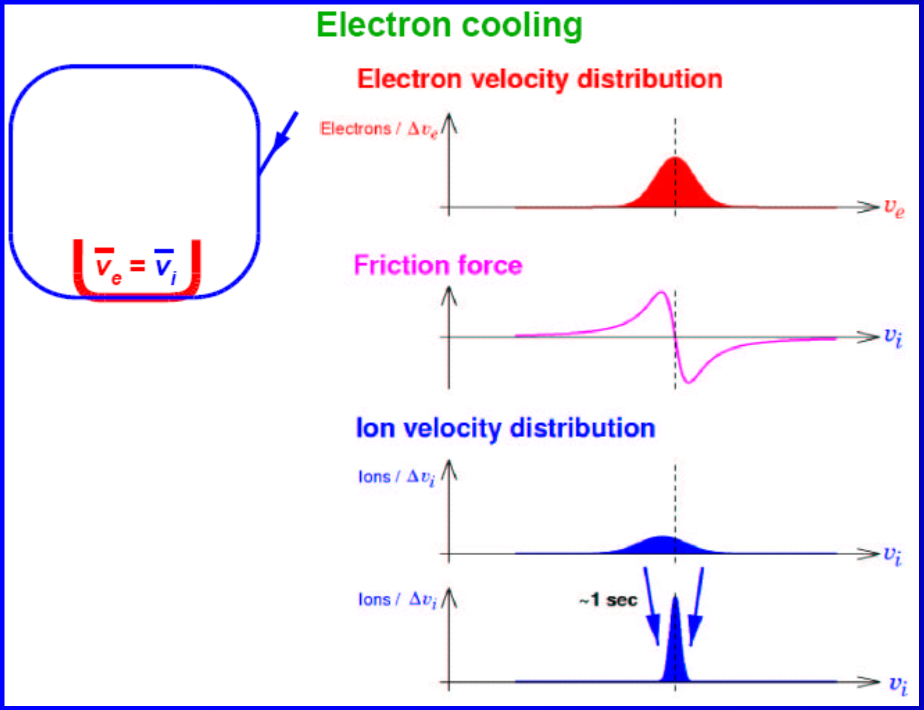

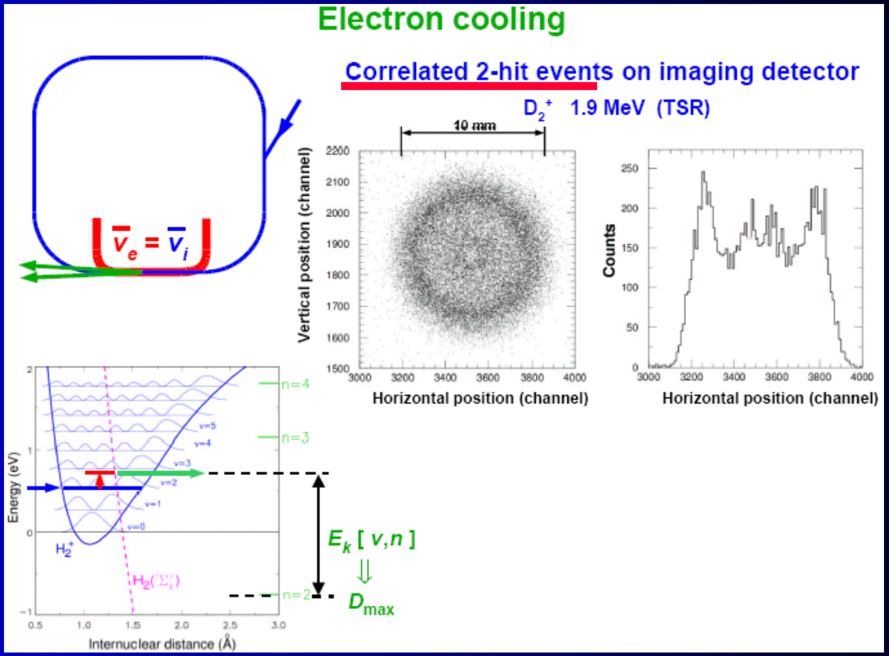

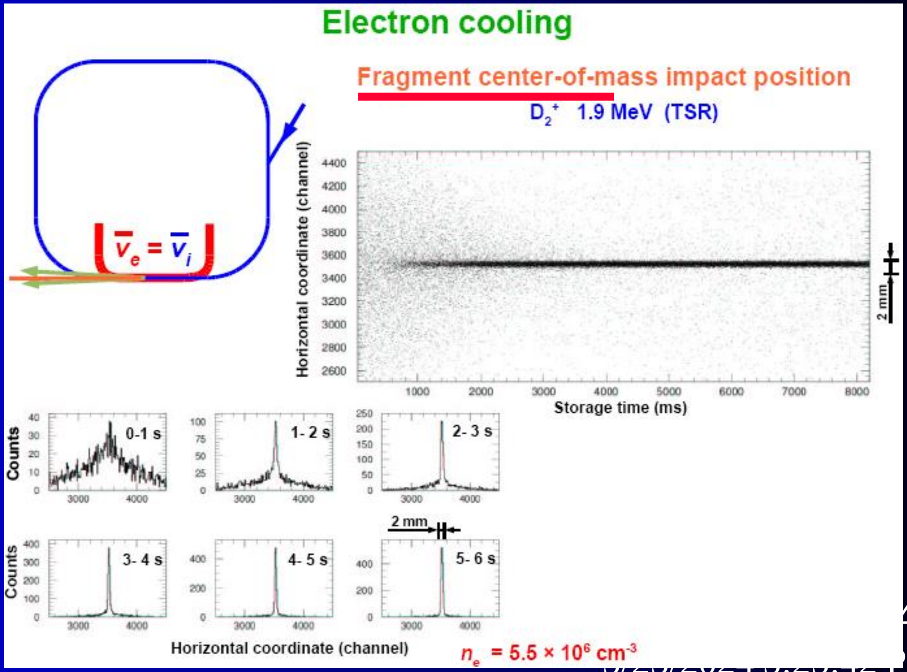

Reality - TSR (MPIK Heidelberg)

Injection of INTERNALY COLD H_3^+ IONS(12-50K) with kinetic energy 1-2 MeV

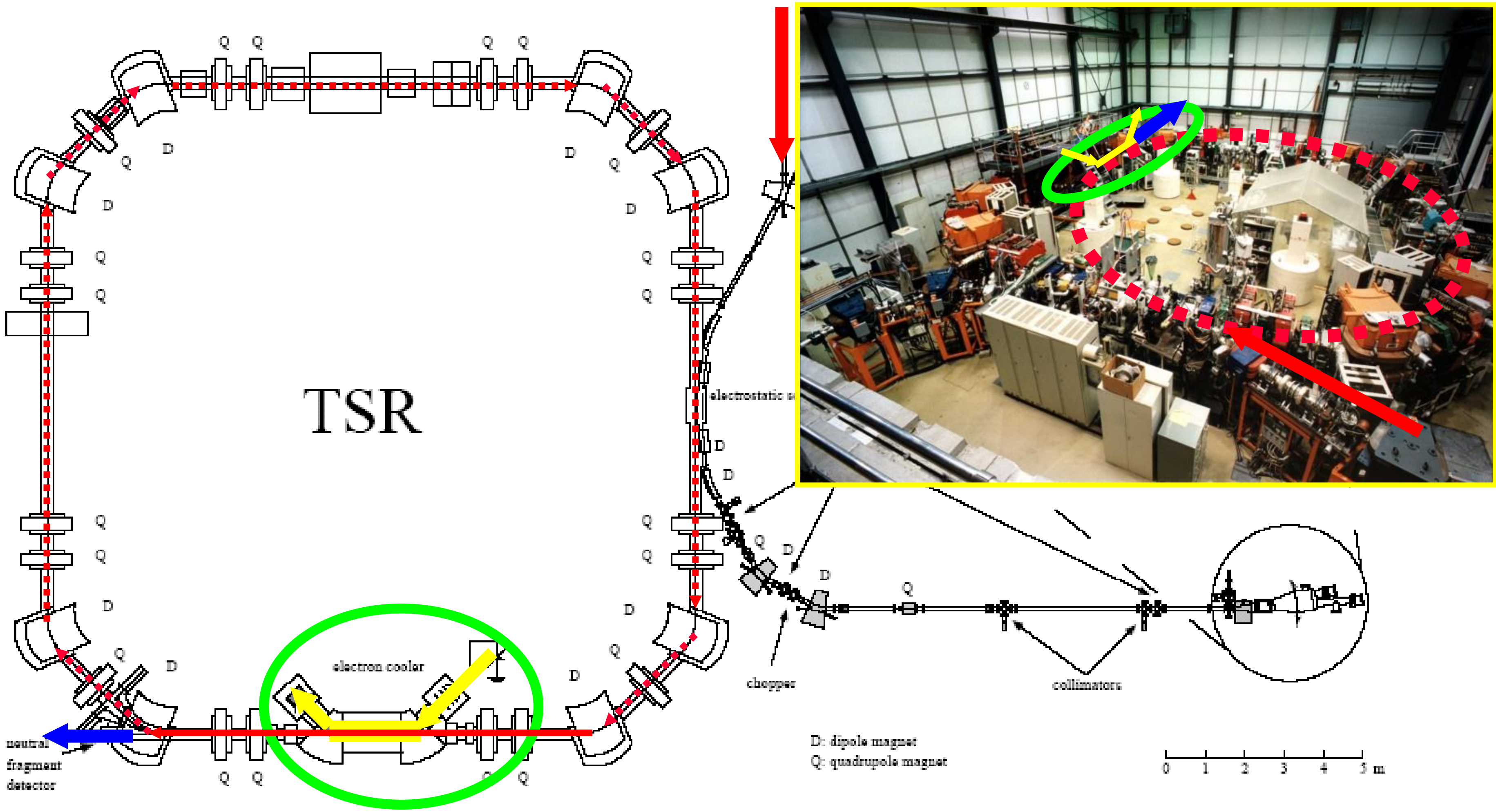

Detection of neutrals

INTERACTION at meV collision energies

Detection of $H_3^+(v,j)$

TSR Heidelberg, ion injection and ion source

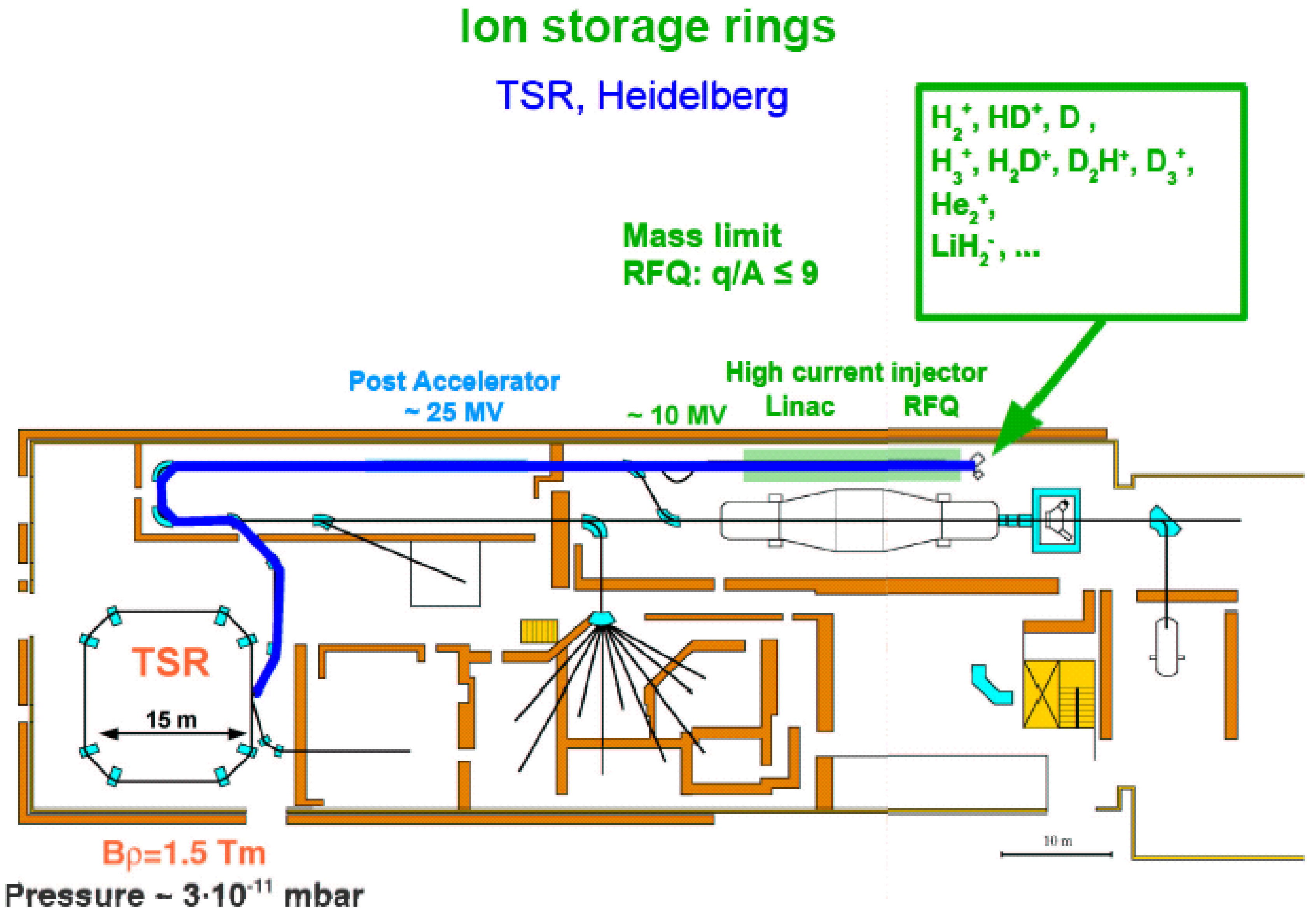

Ion storage rings

Ion storage rings

Mean storage lifetimes of molecular ions in the TSR

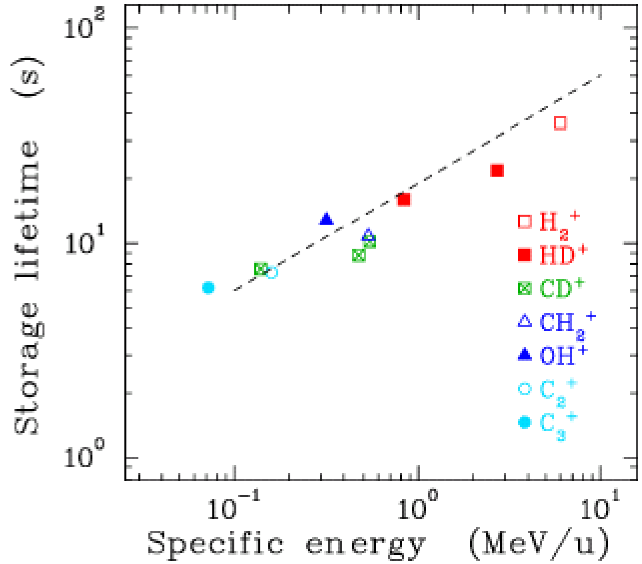

DR with electrons can reduce the beam lifetime !

Internal cooling

Asymmetrical molecules: **Cooling by spontaneous electric dipole radiation (typ. ~0.1 sec for vibration, ~1-10 sec for rotation) Thermal equilibrium with blackbody radiation (300 K)**

Symmetrical molecules: No significant cooling by radiation

Internal cooling by electrons (present electron temperature ~ 20 ... 200 K)

TSR instrumentation

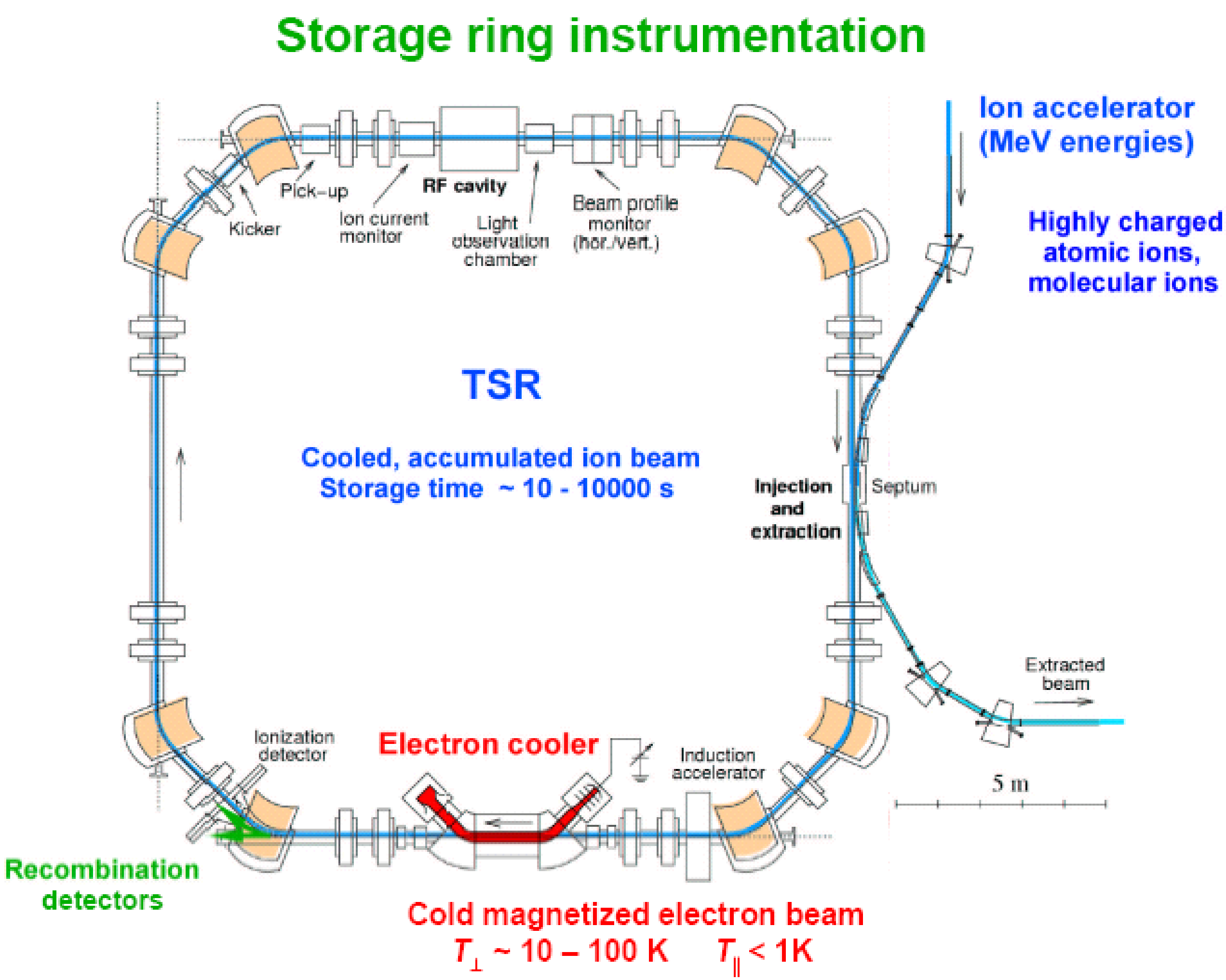

Electron cooling

Electron cooling

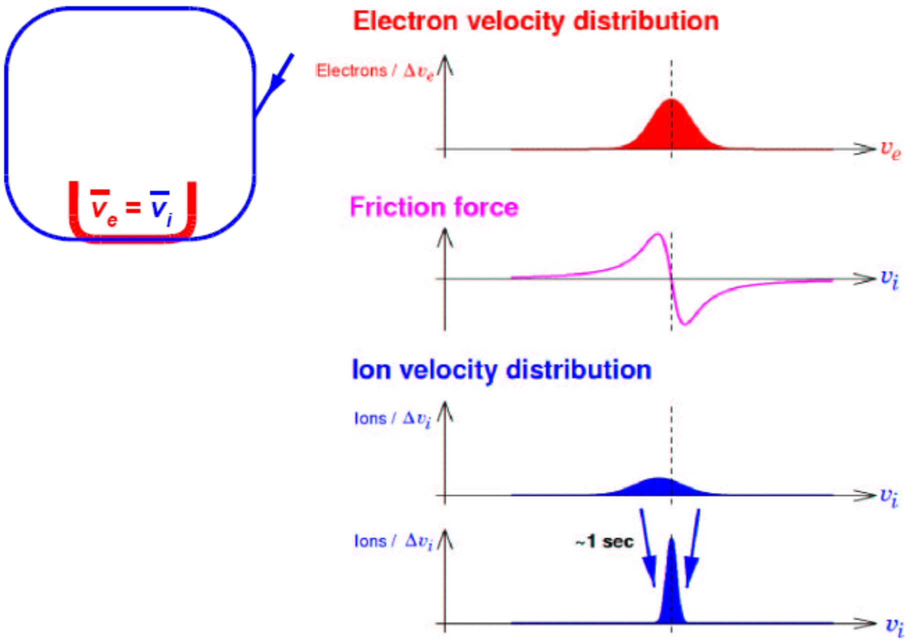

Electron cooling

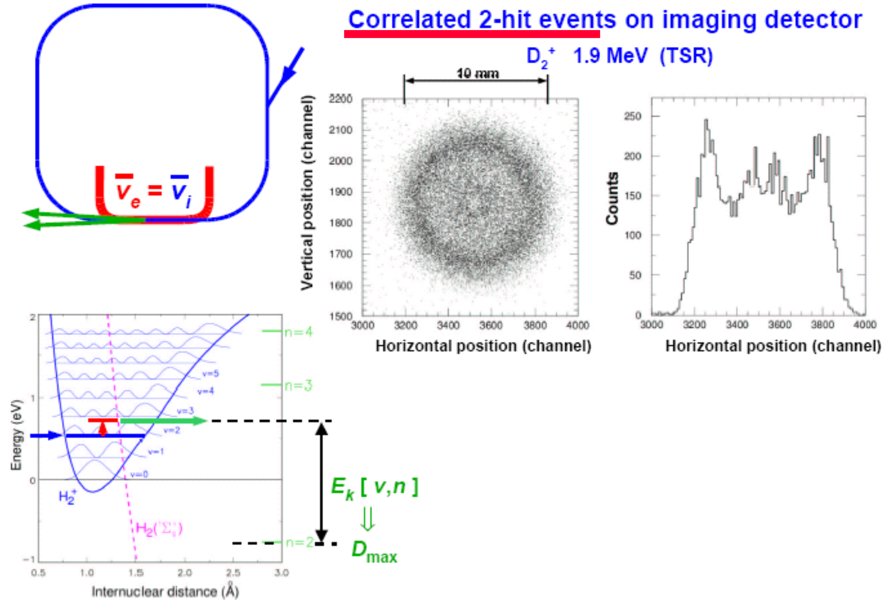

Electron cooling

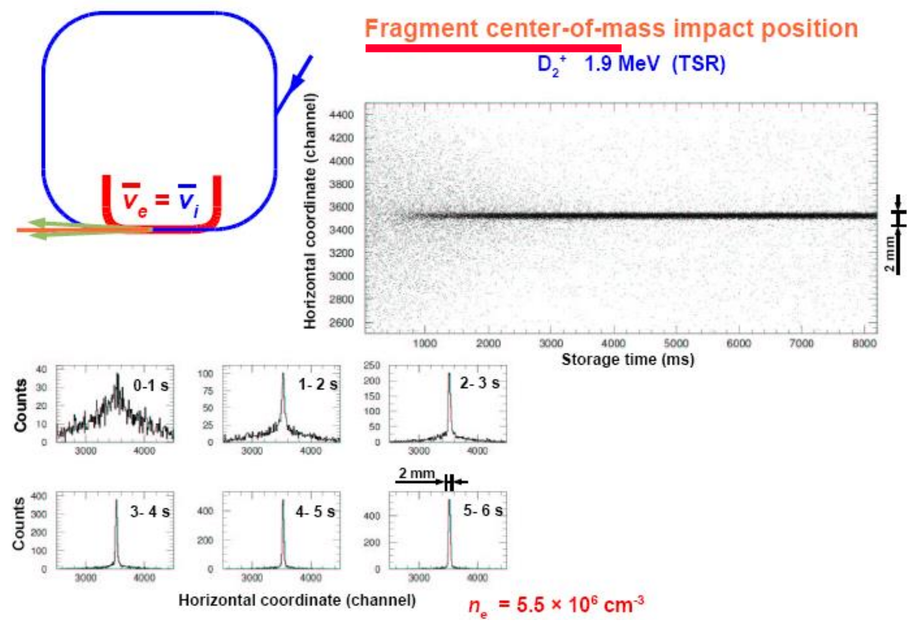

State diagnostics

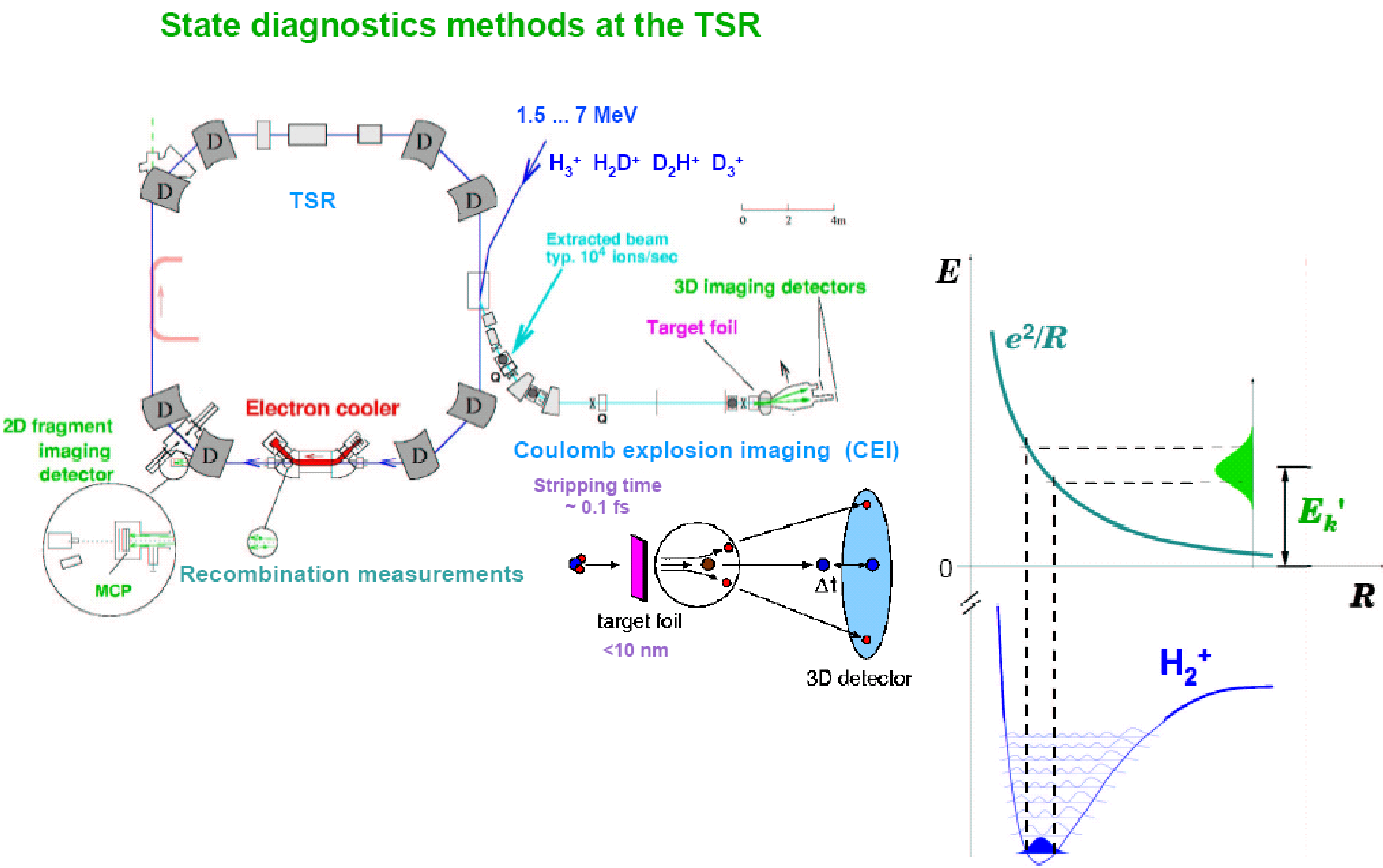

Recombination H_2^+

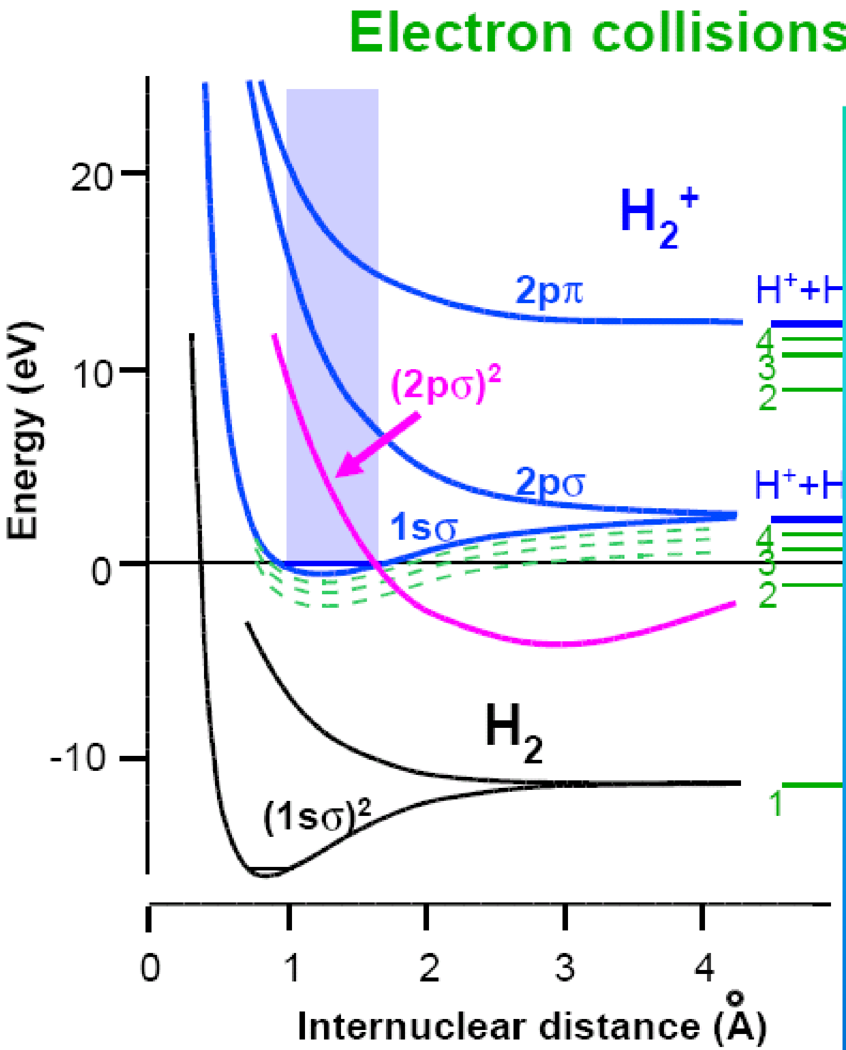

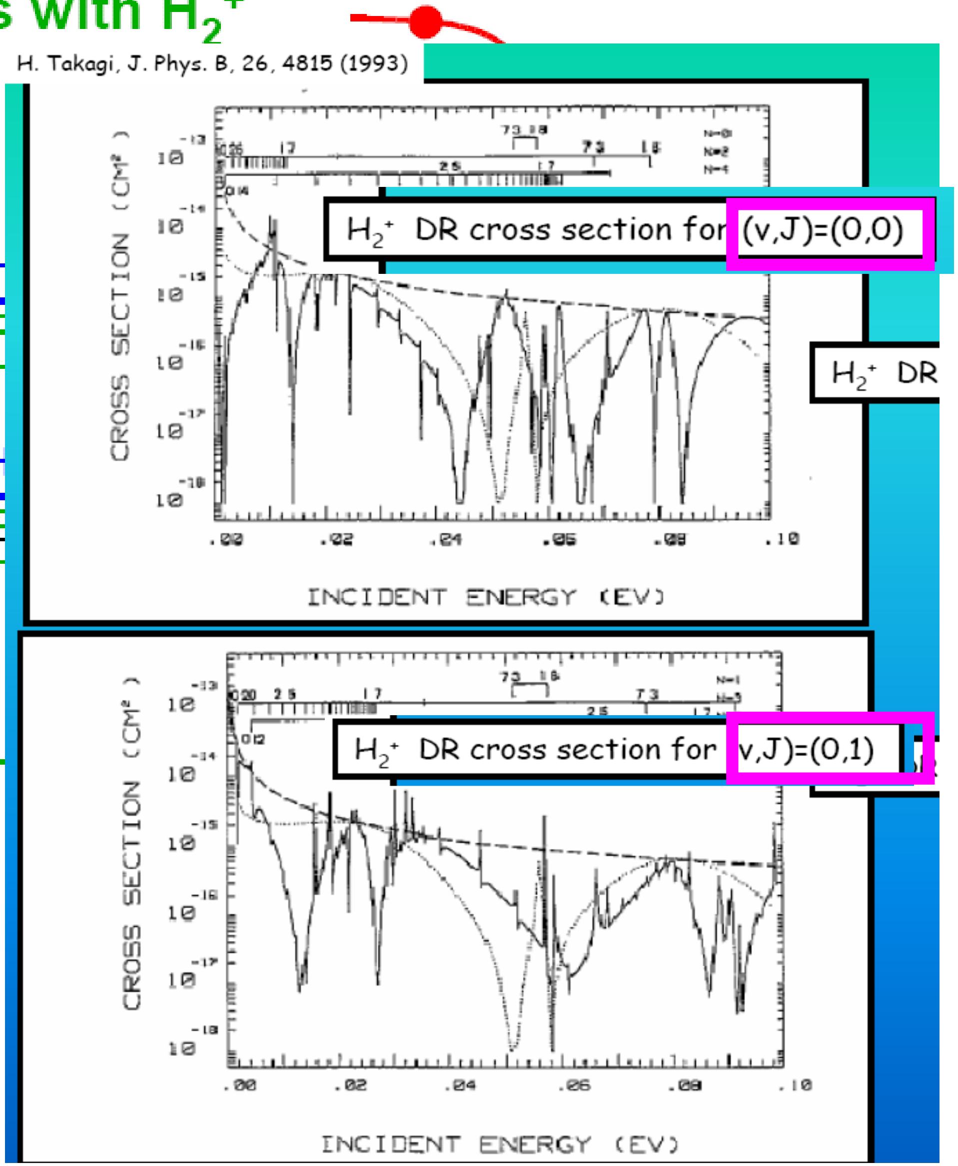

E.M. Staicu-Casagrande, N. de Ruette, A. Le Padellec*, E.A. Naji, T. Nzeyimana, X. Urbain $H_2^+ + O^- \rightarrow H_2O^+ + e / OH^+ + H + e$

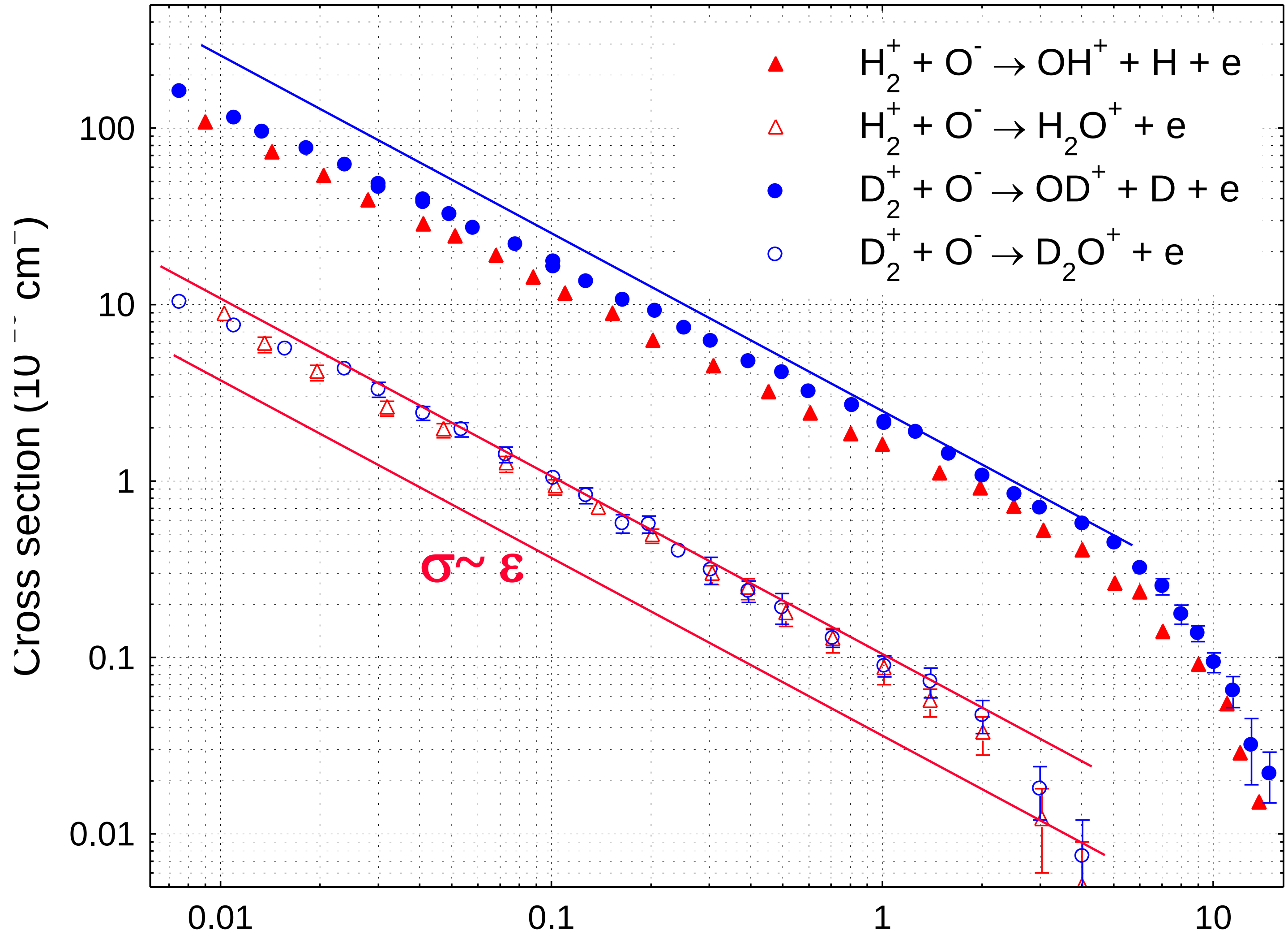

TSR (MPIK Heidelberg

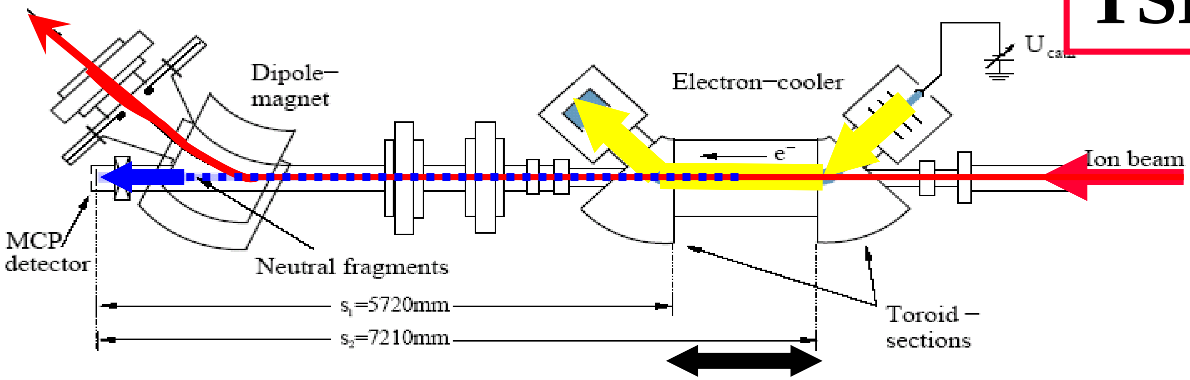

INTERACTION

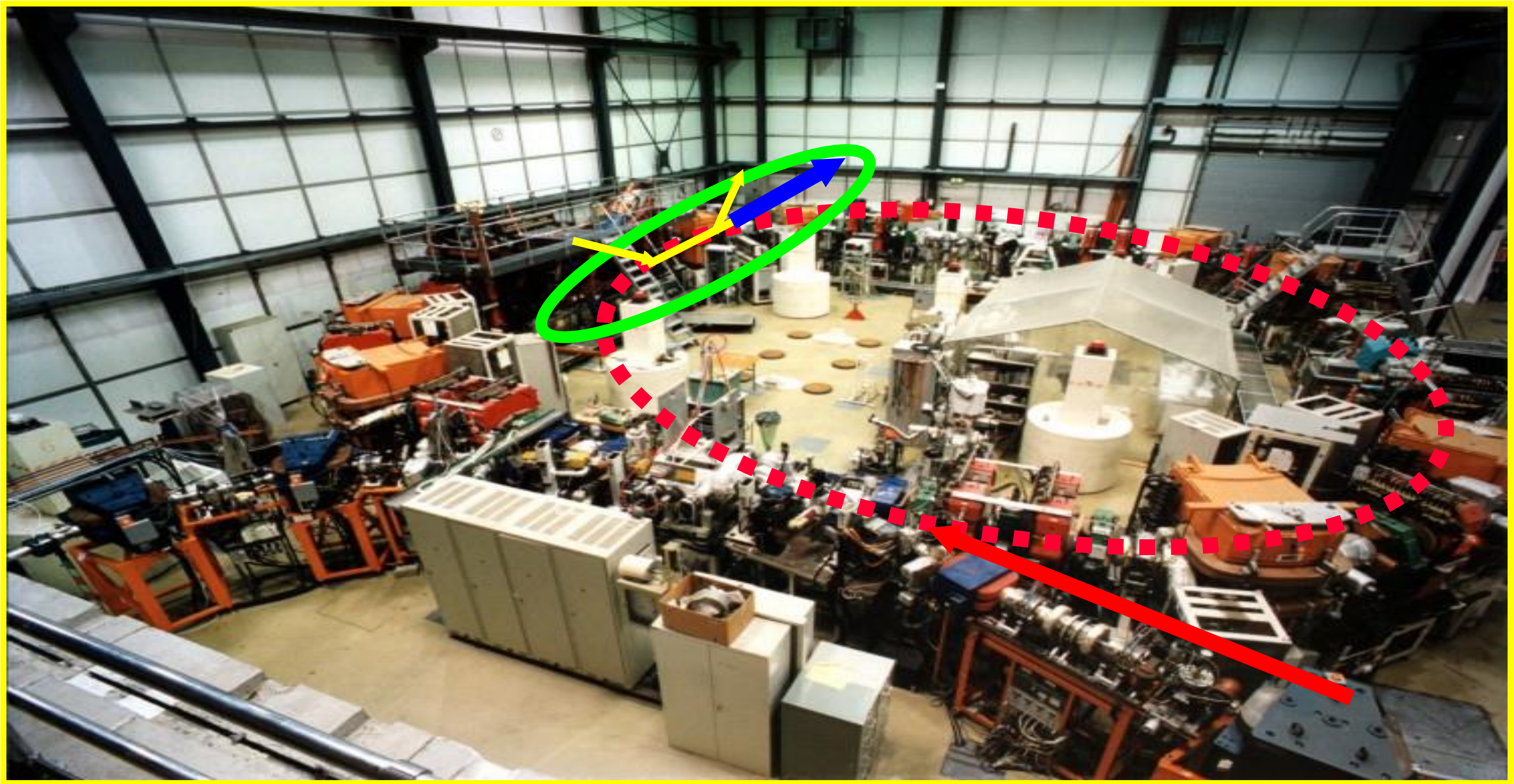

Thanks for your attention!

A. Becker
K. Blaum
C. Breitenfeldt
F. Fellenberger
S. George
J. Göck
M. Grieser
F. Grussie
R. von Hahn
P. Herwig
J. Karthein
C. Krantz
H. Kreckel
S. Kumar S.
M. Lange
J. Lion
S. Lohmann
C. Meyer
P. M. Mishra
O. Novotný
P. O'Connor
R. Repnow
S. Saurabh
S. Schippers
C. D. Schröter
D. Schwalm
L. Schweikhard
K. Spruck
X. Urbain
S. Vogel
A. Wolf
D. Zajfman

JUSTUS-LIEBIG-UNIVERSITÄT GIESSEN

CSR – machine view

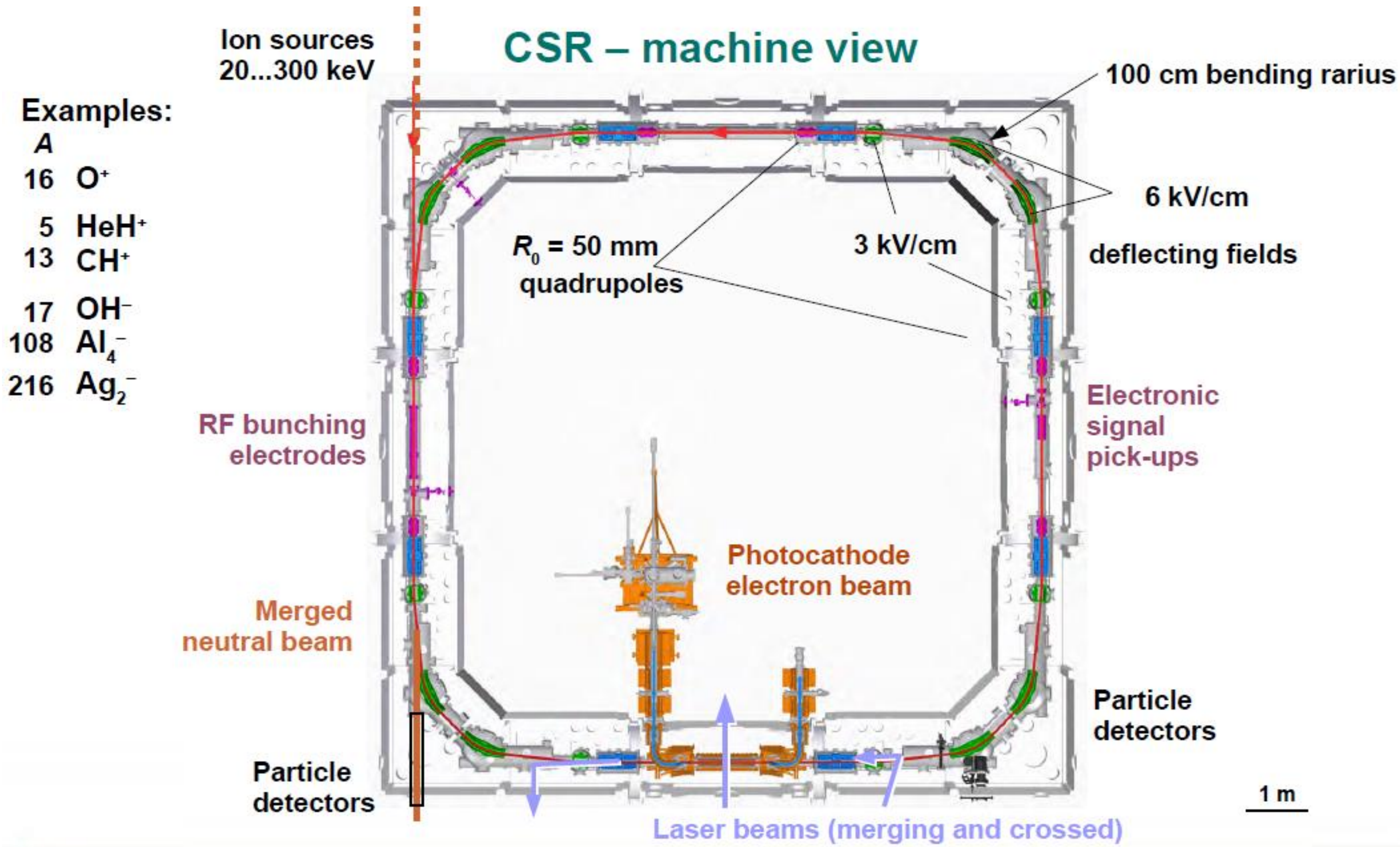

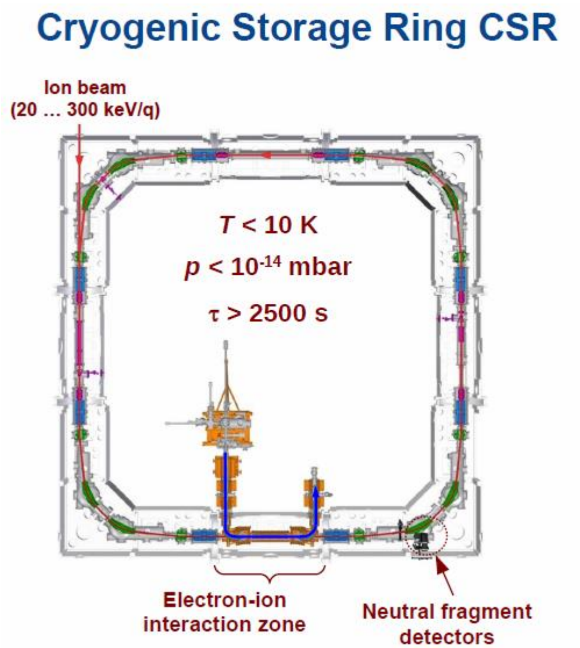
Cryogenic Storage Ring CSR
Ion beam
(20 … 300 keV/q)
T < 10 K
p < 10-14 mbar
τ > 2500 s
Electron-ion
interaction zone
Neutral fragment
detectors

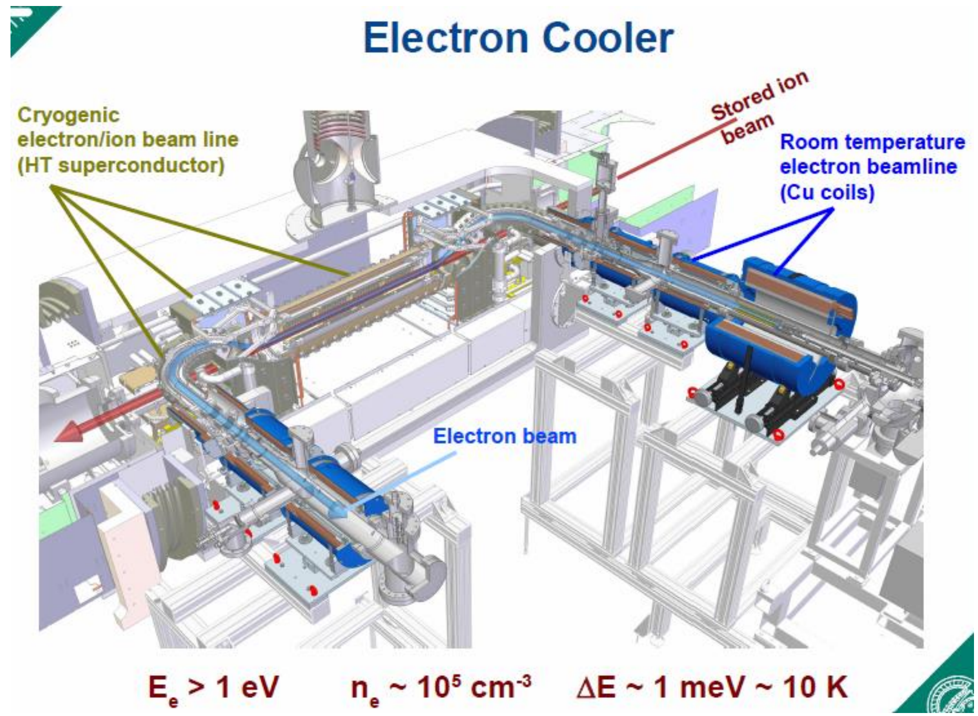
Electron Cooler
Cryogenic
electron/ion beam line
(HT superconductor)
Stored ion
beam
Room temperature
electron beamline
(Cu coils)
Electron beam
Ee > 1 eV
ne ~ 105 cm-3
ΔE ~ 1 meV ~ 10 K

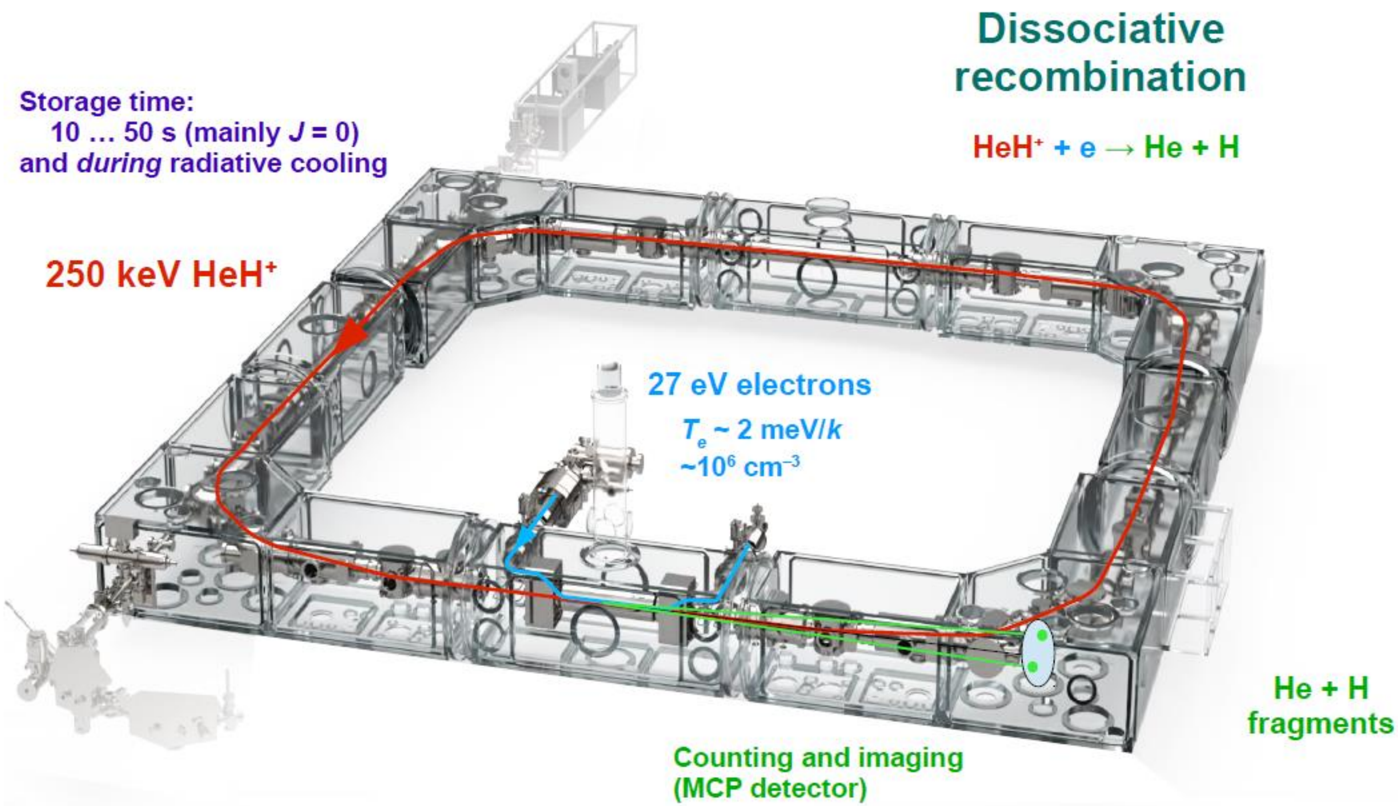

Dissociative recombination
HeH⁺ + e → He + H
Storage time:
10 … 50 s (mainly J = 0)
and during radiative cooling
250 keV HeH⁺
27 eV electrons
Tₑ ~ 2 meV/k
~10⁶ cm⁻³
He + H fragments
Counting and imaging
(MCP detector)

CSR laboratory

Max Planck Institute for Nuclear Physics
Heidelberg, Germany

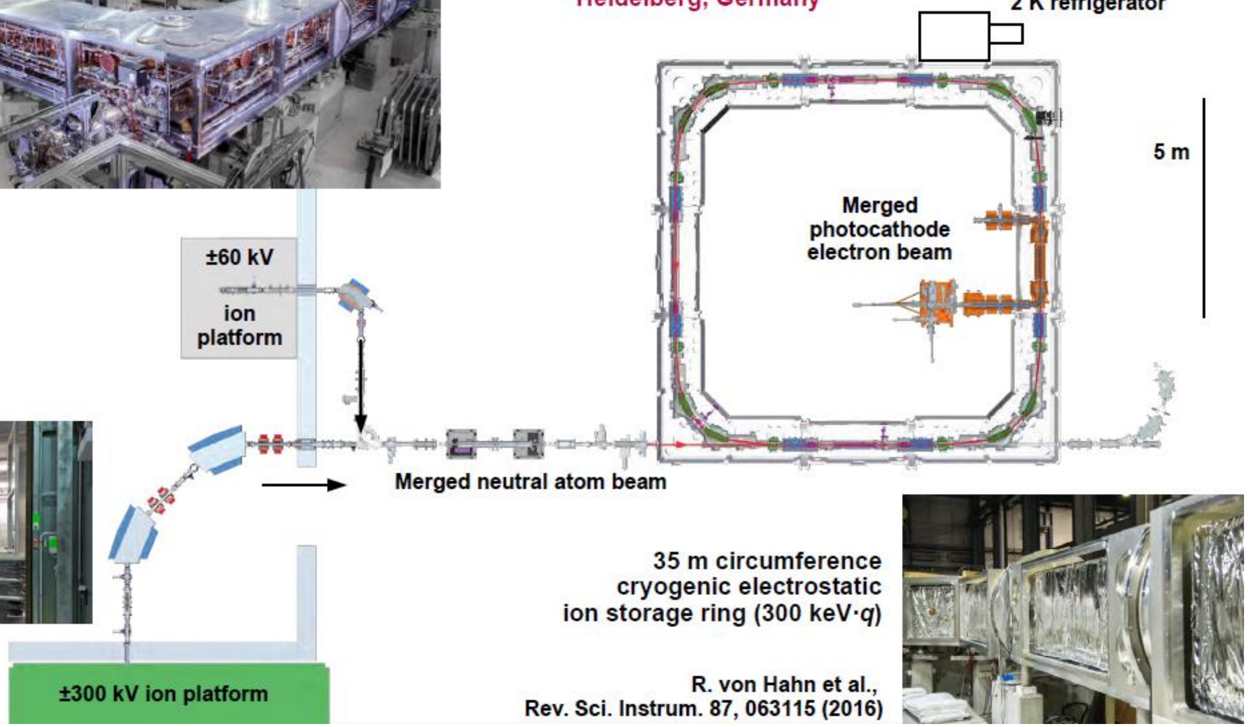

35 m circumference
cryogenic electrostatic
ion storage ring (300 keV·q)

R. von Hahn et al.,
Rev. Sci. Instrum. 87, 063115 (2016)

The CSR – overview

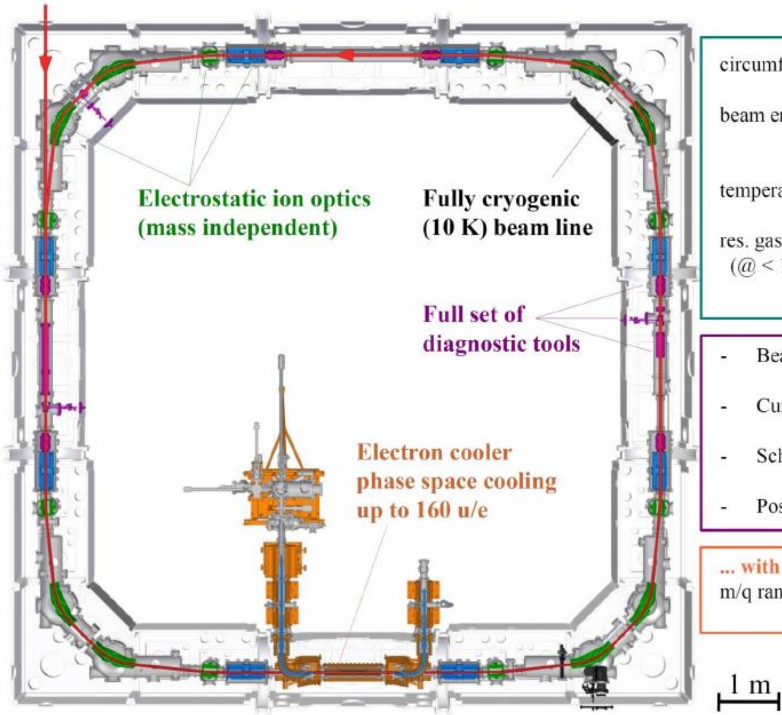

circumference:	35 m
beam energy:	20 keV × q ... 300 keV × q
temperature:	10 ... 300 K
res. gas press. (@ < 10 K):	10^{-14} mbar (~ 100 cm^{-3})

- Beam profile monitors (3x)
- Current pickup
- Schottky pickup
- Position pickups (6x)

... with electron cooling

m/q range:	1 ... 160 u/e (@ 300 kV)

R. v. Hahn
M. Grieser

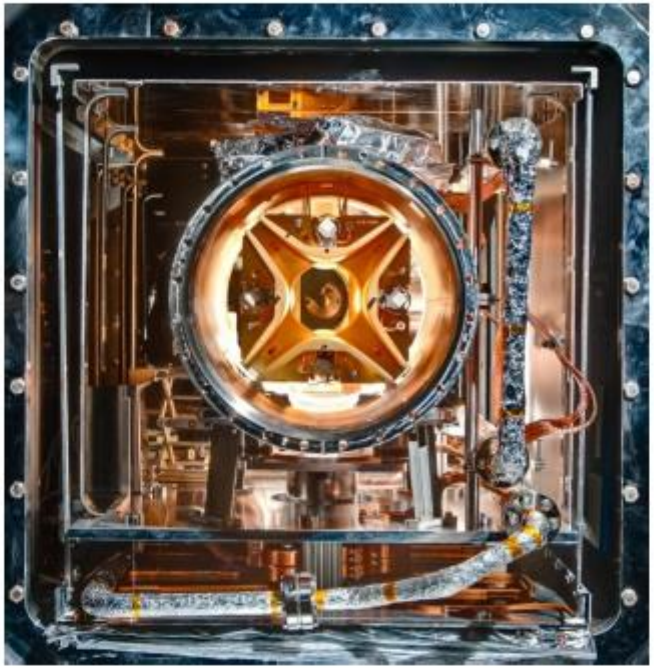

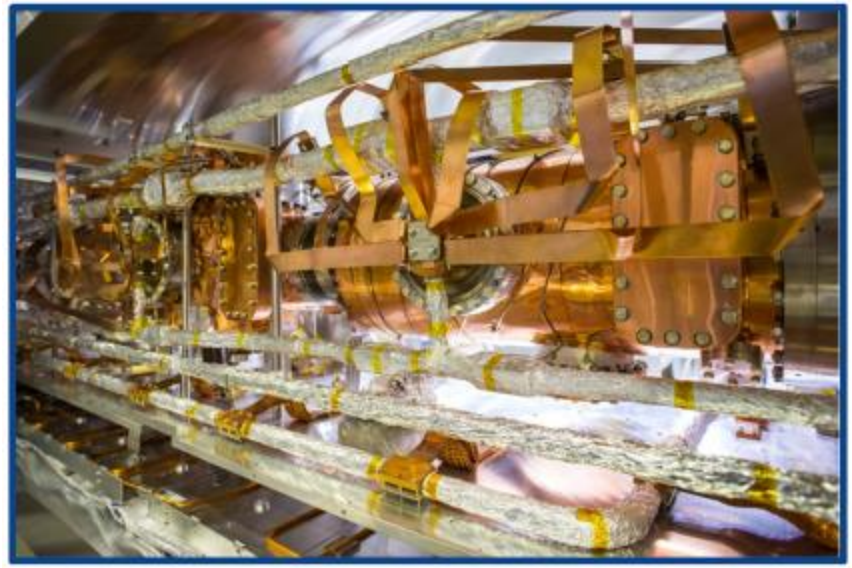

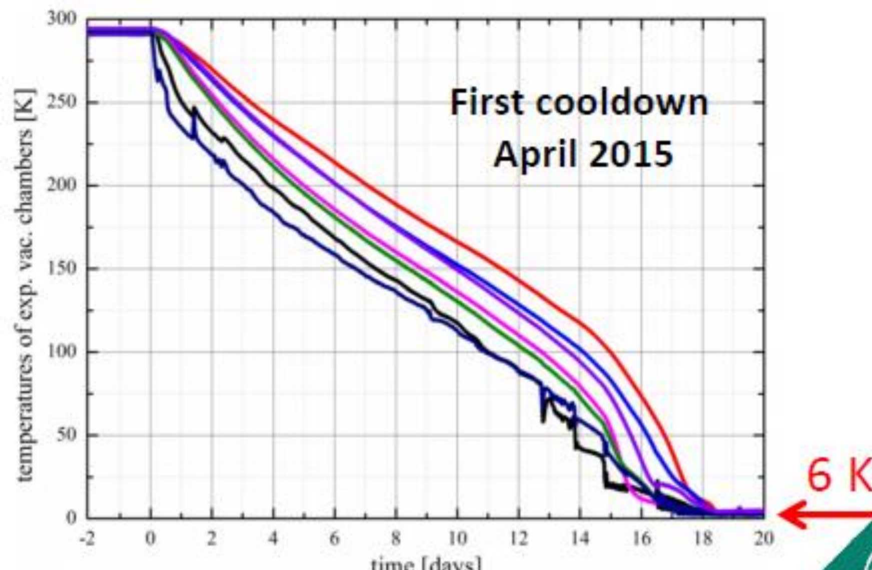
First cooldown
April 2015
6 K
temperatures of exp. vac. chambers [K]
time [days]
0
50
100
150
200
250
300
-2
0
2
4
6
8
10
12
14
16
18
20

The CSR electron cooler

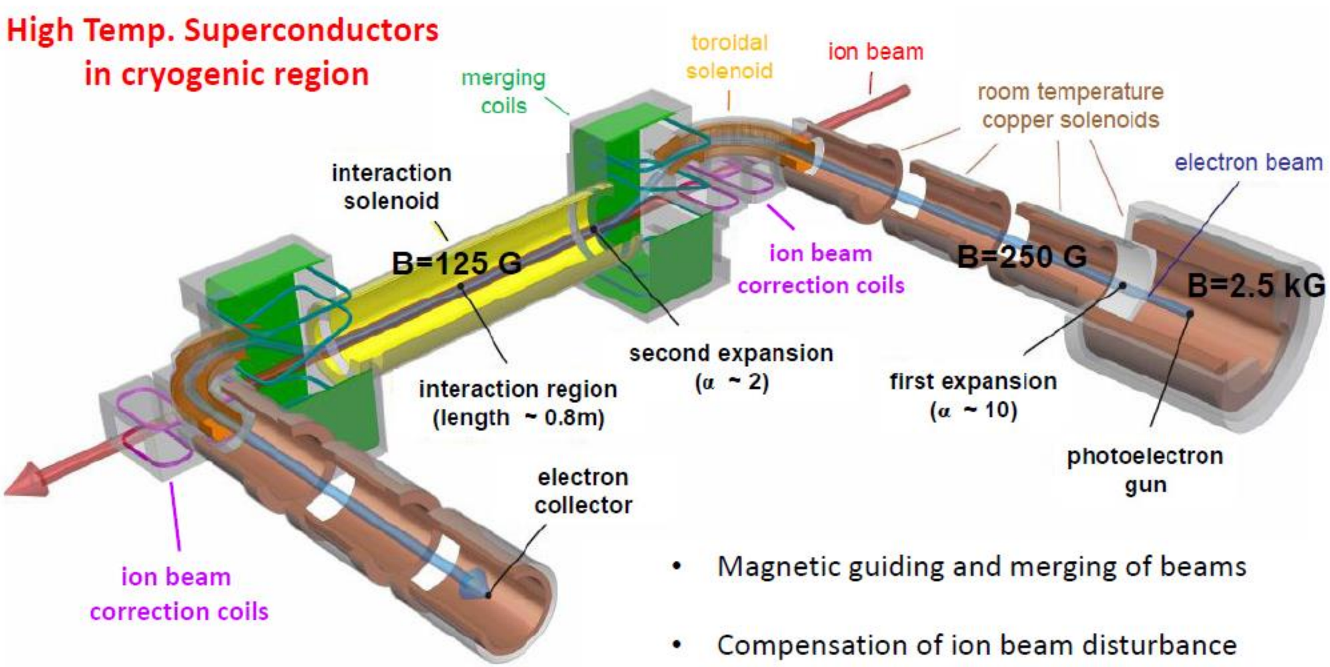

- Magnetic guiding and merging of beams
- Compensation of ion beam disturbance
- Variable electron energy (drift tube)
- Beam diagnostics (two wire scanners)

The CSR electron cooler

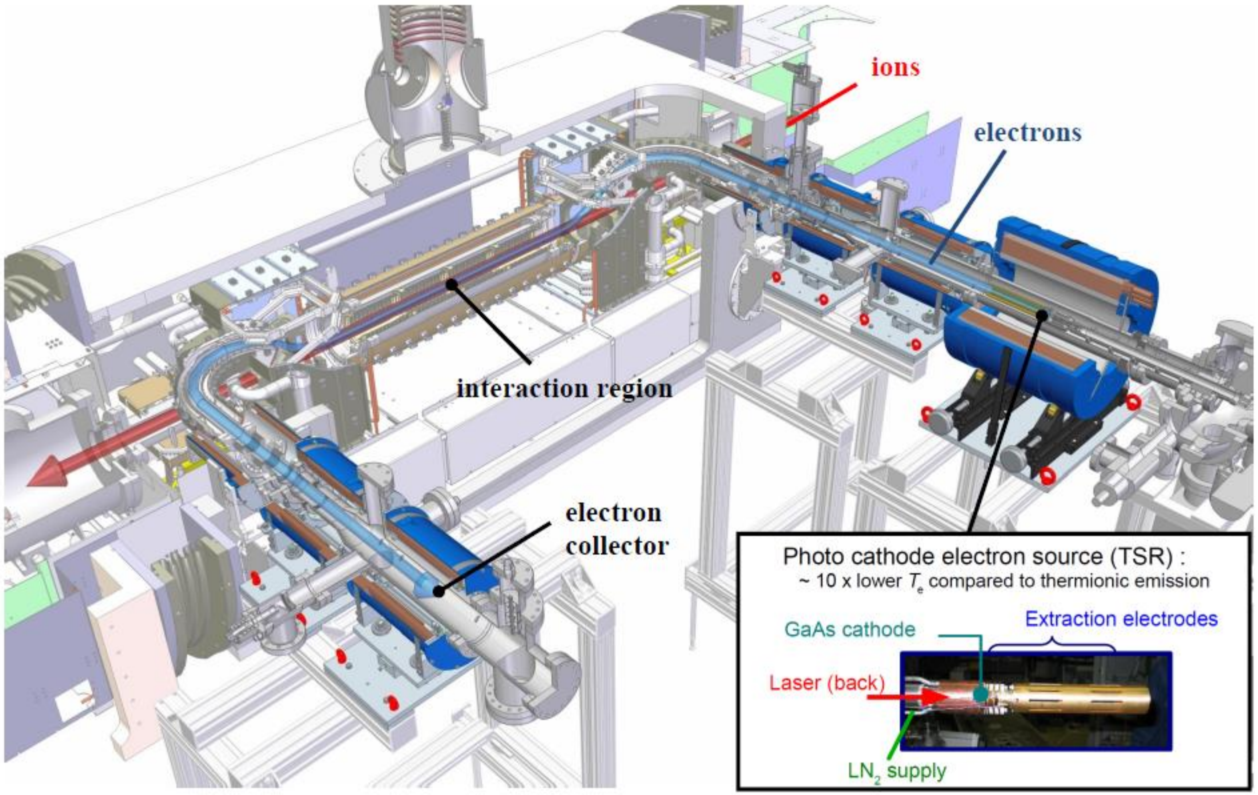

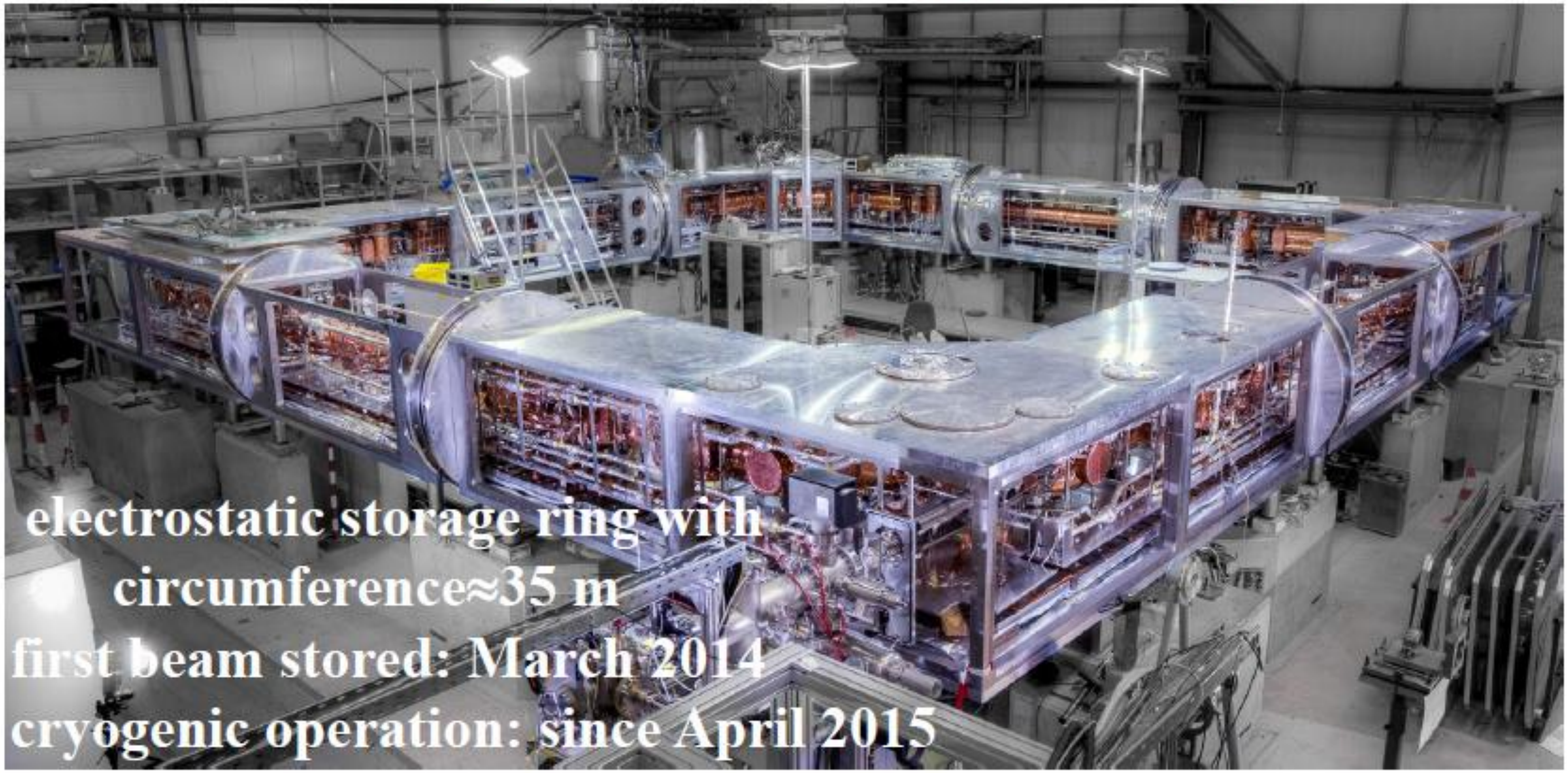
electrostatic storage ring with
circumference≈35 m
first beam stored: March 2014
cryogenic operation: since April 2015

High Voltage platforms

CSR main injector:
ion sources on a high voltage plat form of **±300 kV**

± 40 keV platform with positive and negative ion sources

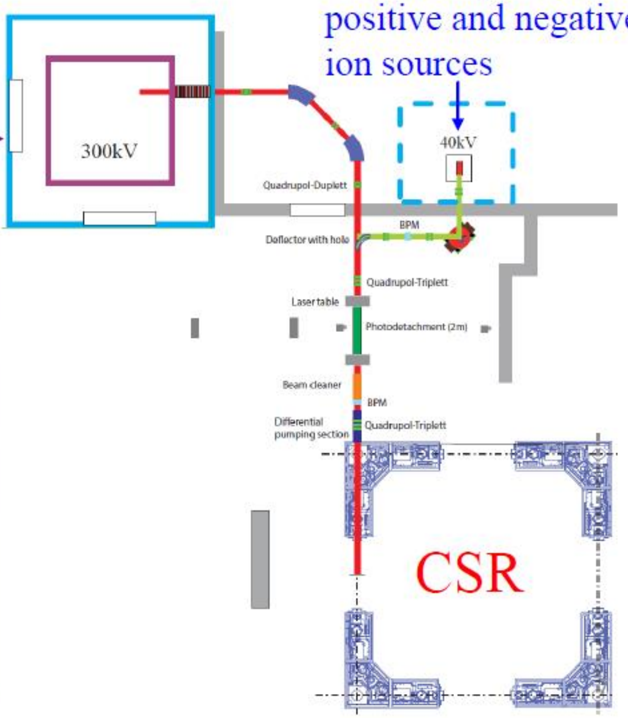

The CSR electron cooler

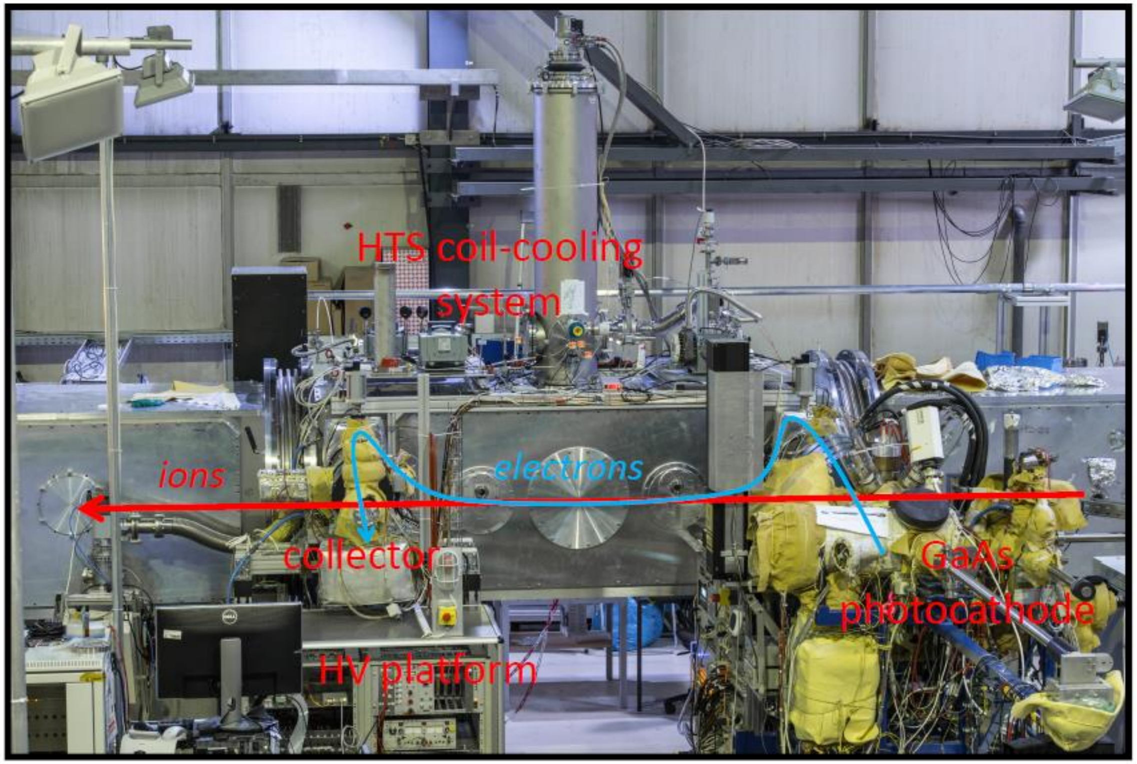

The CSR – storage lifetime

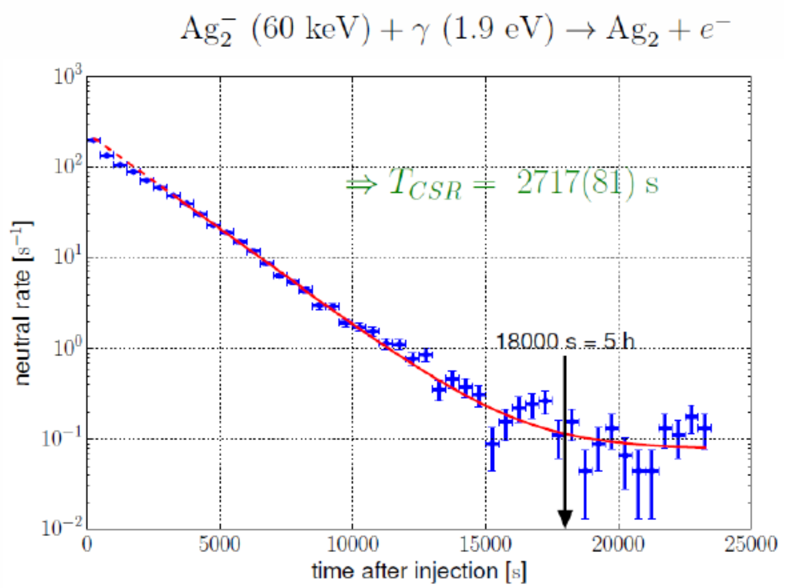

EA (Ag_2^-) = 1.02 eV

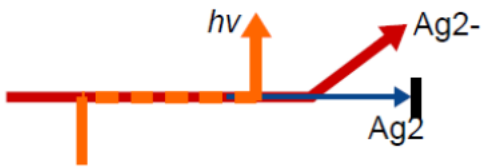

von Hahn et al.,
Rev. Sci. Instr. 87 (2016) 063115

Storage ring (CRYRING)

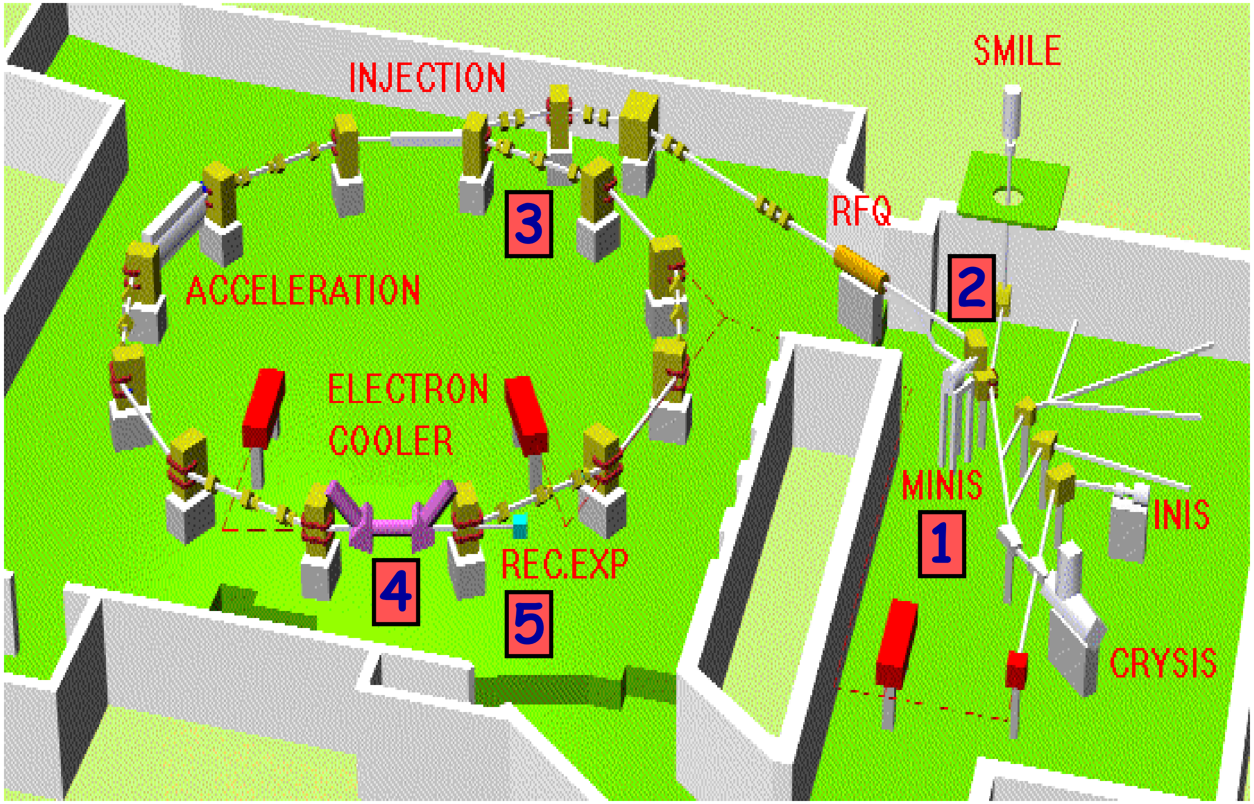

Schematic view of CRYRING

Steps during the experiment

1. Formation of the ions in the source
2. Mass selection by bending magnet
3. Injection via RFQ and acceleration
4. Merging with electron beam
5. Detection of the neutral products

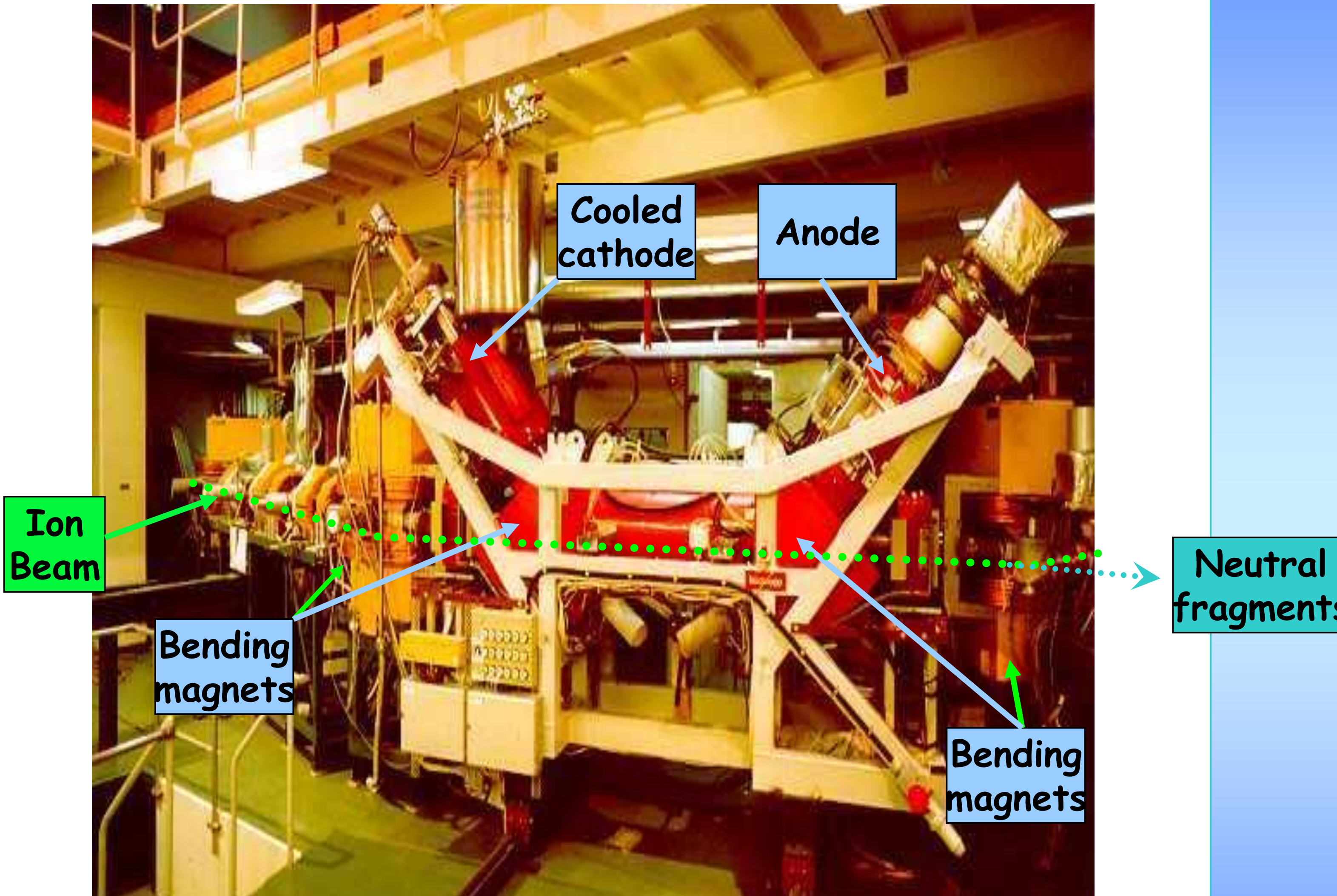

Electron cooler

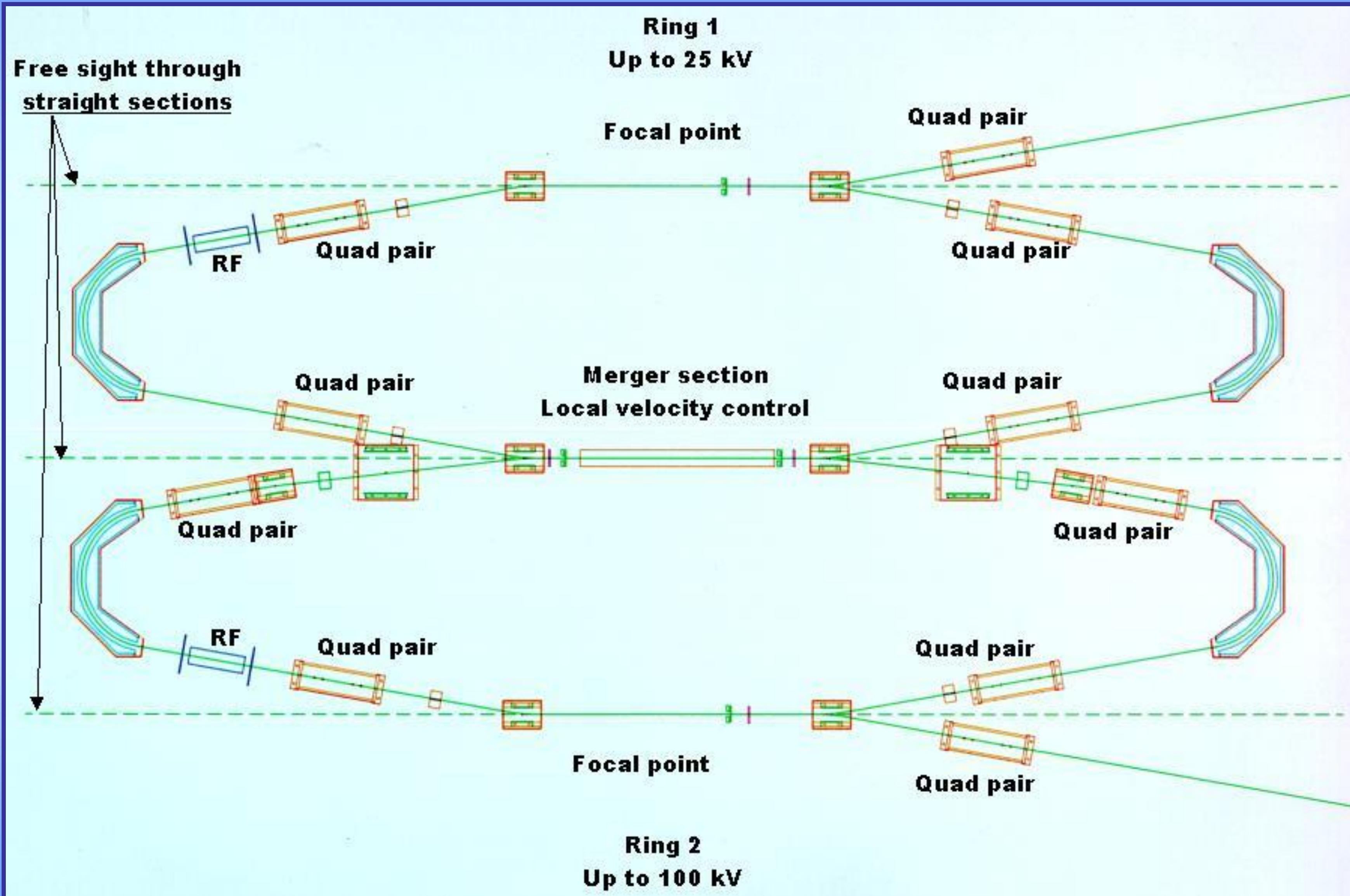

Ring 1
Up to 25 kV
Free sight through
straight sections
Focal point
Quad pair
Quad pair
RF
Quad pair
Quad pair
Merger section
Local velocity control
Quad pair
Quad pair
Quad pair
RF
Quad pair
Quad pair
Focal point
Quad pair
Ring 2
Up to 100 kV

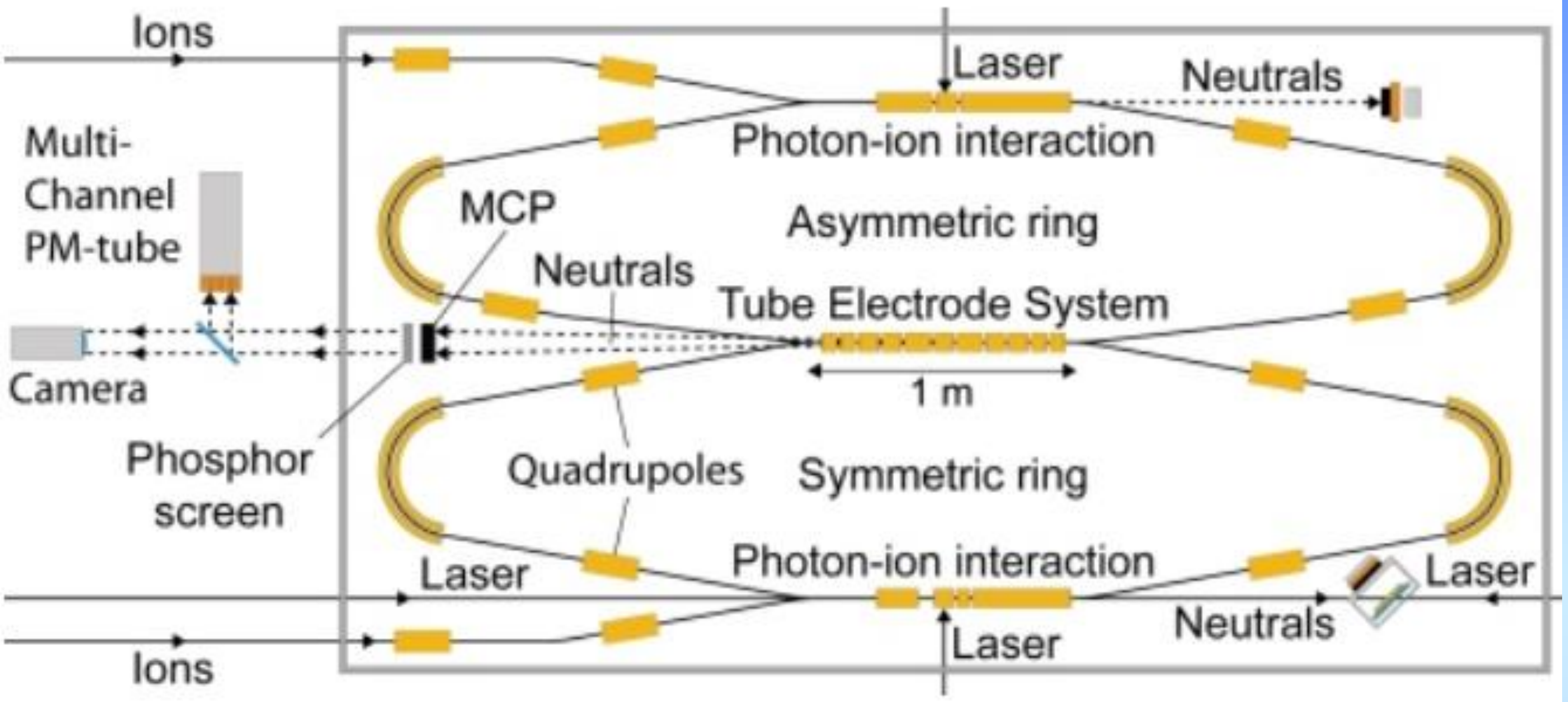

Desiree scheme

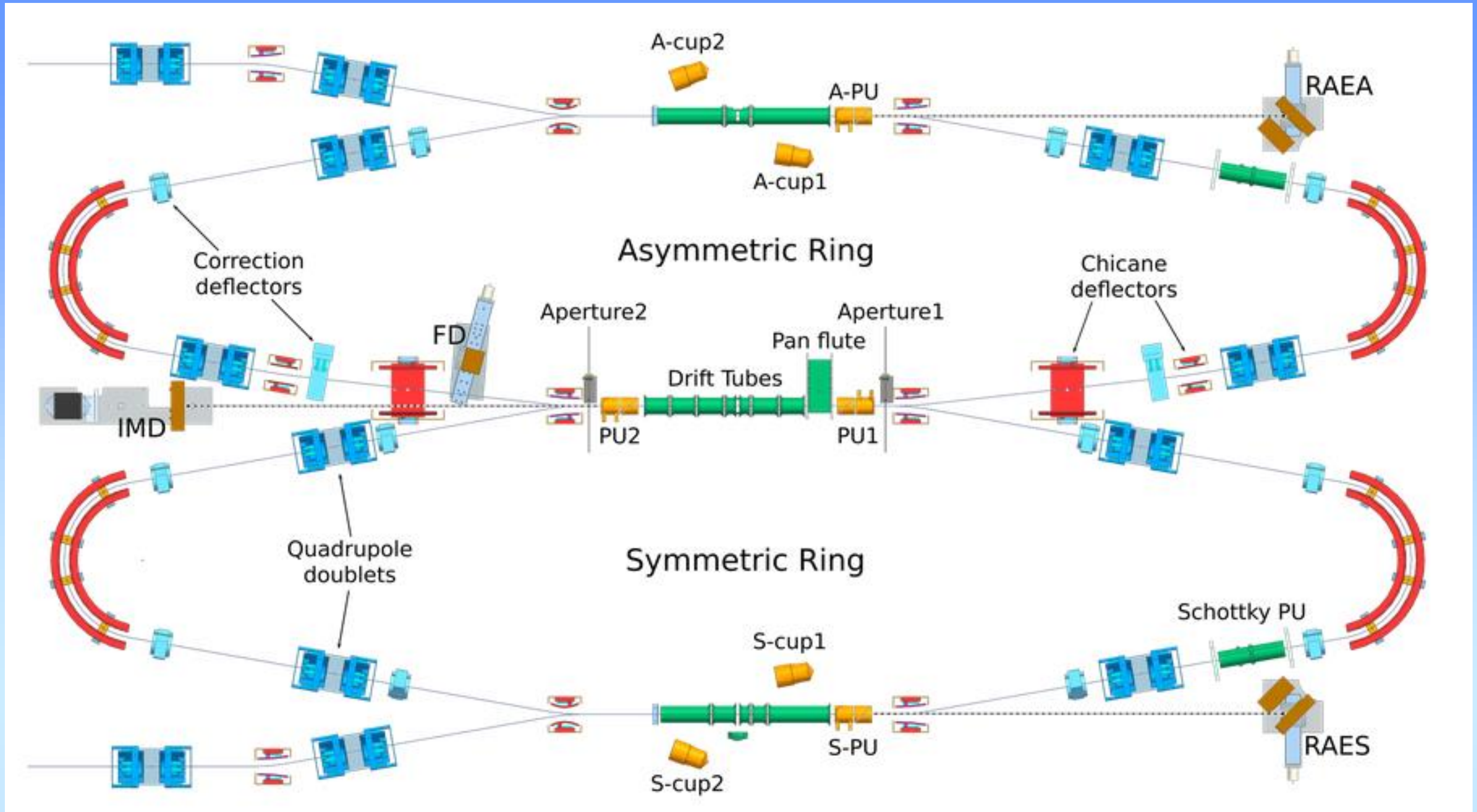

The DESIREE facility includes two storage rings with one common straight section. The symmetric ring has a four-fold symmetry while the asymmetric ring has a two-fold symmetry. The symmetric ring contains four 10° deflectors, two 160° cylindrical deflectors and four quadruple doublets. Ion beam with kinetic energy up to 35 keV can be stored in symmetric ring. The asymmetric ring has two common deflectors with the symmetric ring and can store ion beam with kinetic energy up to 100 keV. Depending on the beams' energies the angle before and after the common deflectors vary between 0.5° and 10°, this is then compensated with the chicane deflectors before and after the common section.

There are five ion-laser interaction pathways in total, three perpendicular interaction pathways in the centre of each injection section and the common section, and two co-linear pathways along the two injection sections through the RAES and RAEA detectors.

DESIREE storage ring

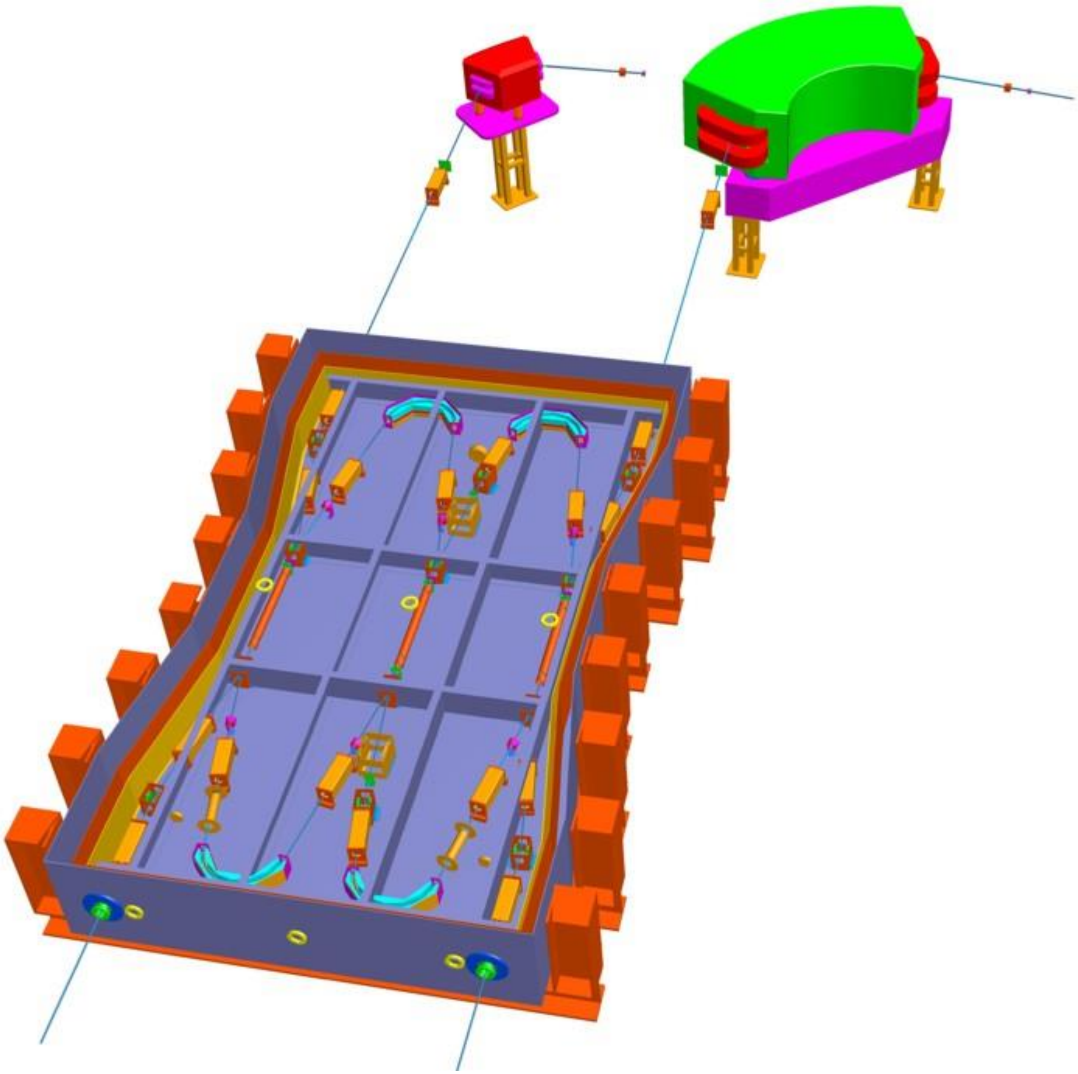

Double Electrostatic Ion Ring Experiment

The project is named DESIREE
(Double ElectroStatic Ion Ring ExpEriment)

The DESIREE storage rings in their cryogenic enclosure.

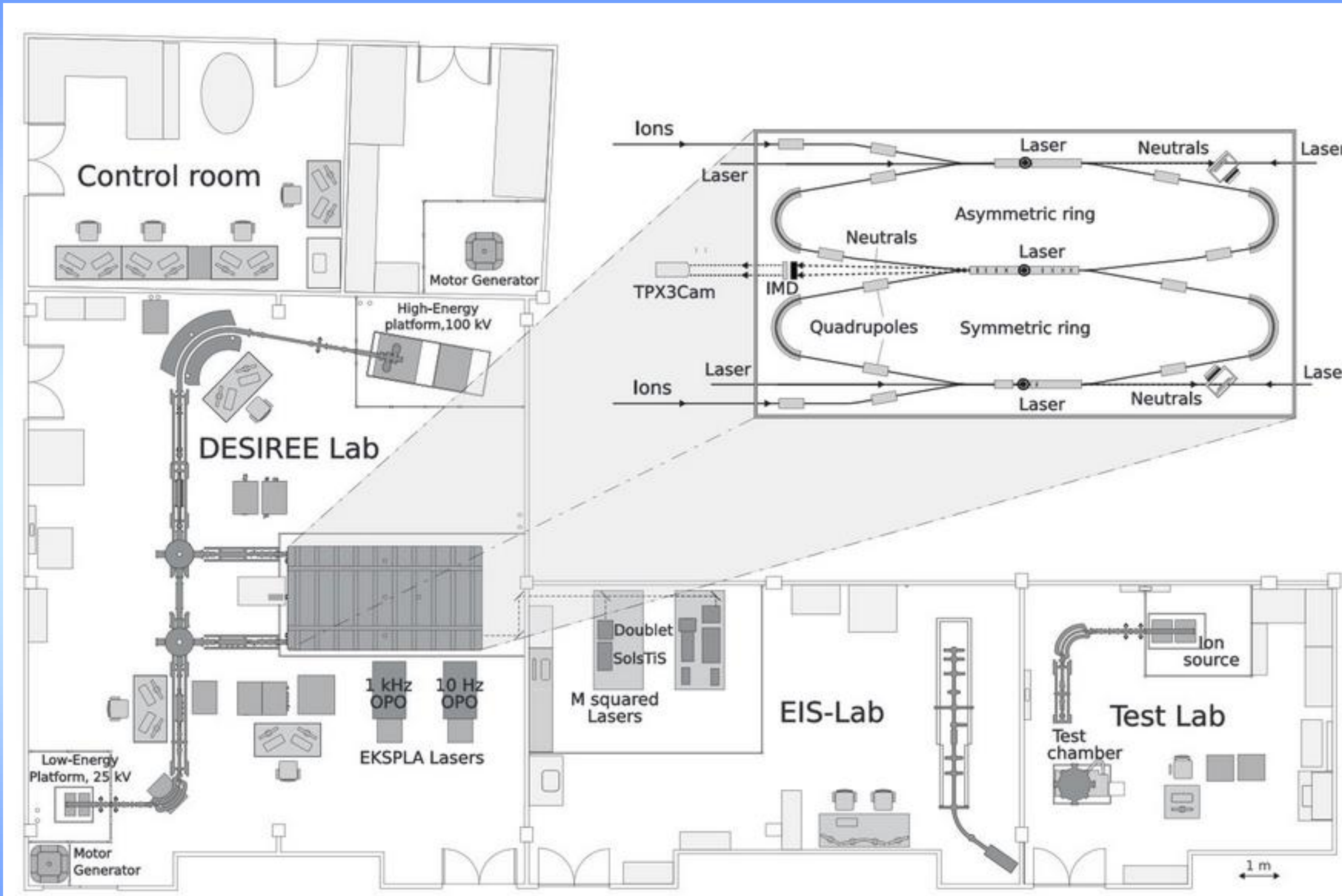

Control room
Motor Generator
High-Energy platform,100 kV
DESIREE Lab
Low-Energy Platform, 25 kV
Motor Generator
1 kHz OPO
10 Hz OPO
EKSPLA Lasers
Doublet
SolsTiS
M squared Lasers
EIS-Lab
Ion source
Test chamber
Test Lab
1 m
Ions
Laser
Laser
Neutrals
Laser
Asymmetric ring
Neutrals
Laser
TPX3Cam
IMD
Quadrupoles
Symmetric ring
Laser
Ions
Laser
Neutrals
Laser

astro

Ion List and Ion Sources

Ions on the following lists have been successfully produced and stored in DESIREE storage rings, a short description of each ion source is also attached below.

Atomic cations: H^+, He^+, Li^+, C^+, N^+, O^+, F^+, Ne^+, Na^+, Mg^+, Si^+, Ar^+, I^+, Xe^+, Ba^+

Atomic anions: H^-, D^-, O^-, $^{18}O^-$, Si^-, P^-, S^-, Cl^-, Ni^-, Cu^-, Ge^-, As^-, Se^-, Br^-, Rh^-, Pd^-, Ag^-, Sn^-, Sb^-, Te^-, I^-, Cs^-, La^-, Ir^-, W^-, Au^-

Molecular cations: O_2^+, N_2^+, I_2^+, NO^+, $HeNe^+$, HeH^+, HeD^+, H_3^+, D_3^+, H_3O^+

Molecular anions: CH^-, CD^-, CH_3^-, $^{13}C_4H^-$, $^{13}C_6H^-$, CO_2^-, CN^-, OH^-, OD^-, O_2^-, N_2O^-, LaO^-, SF_4^-, SF_5^-, SF_6^-, $^{16}O^{18}O^-$, $C_6H_4O_2^-$, HfF_5^-, WF_5^-, $C_6H_4O_2^-$(para-Benzoquinone).

Molecular dianions: C_7^{2-}, $^{13}C_7^{2-}$, C_9^{2-}, $^{13}C_9^{2-}$, C_{12}^{2-}, C_{60}^{2-}, $^6LiF_3^{2-}$.

Cluster anions: C_{2-15}^-, Cu_{2-21}^-, Si_2^-, Ag_{2-3}^-, Au_{2-15}^-

The battle ship enters the stage

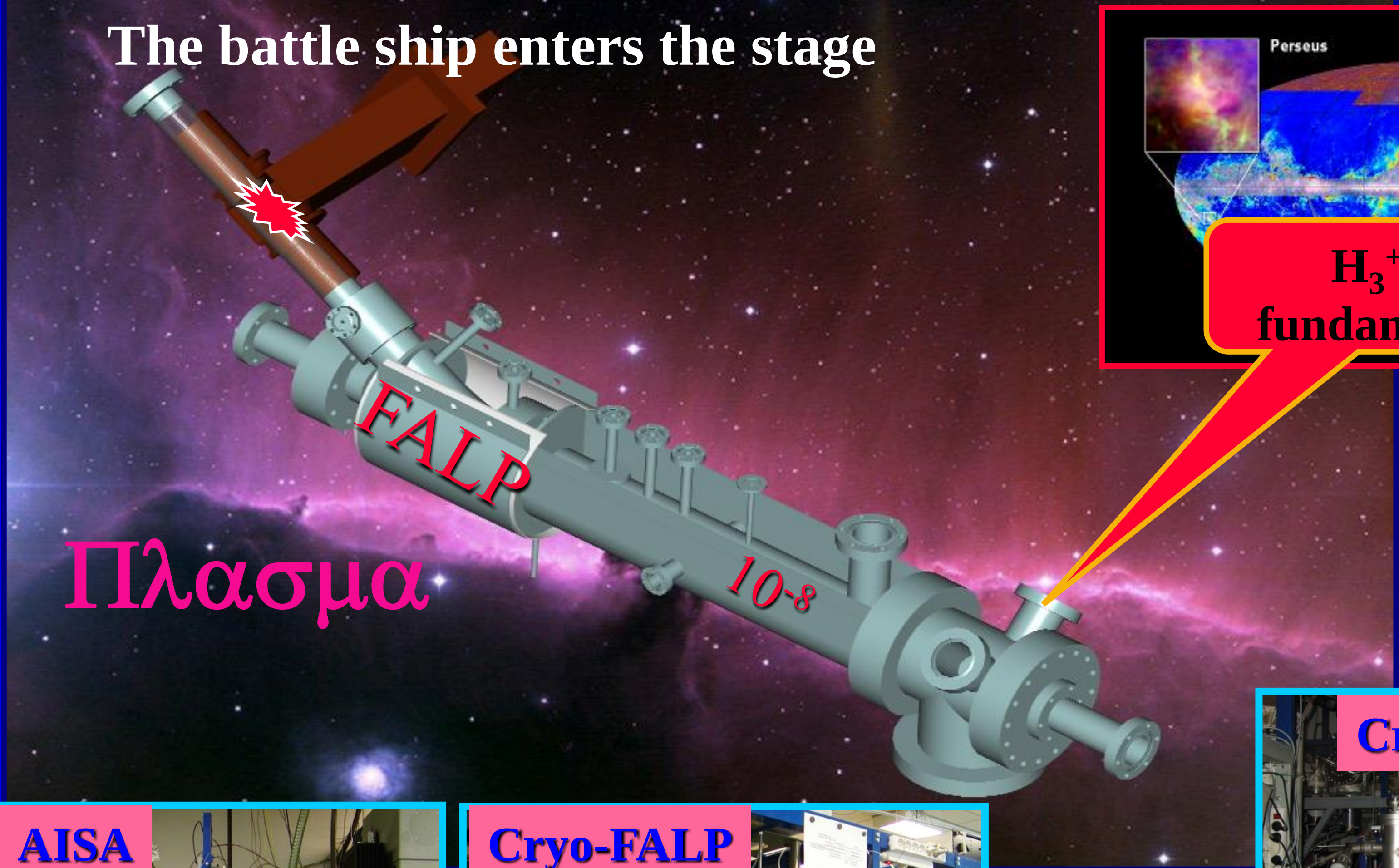

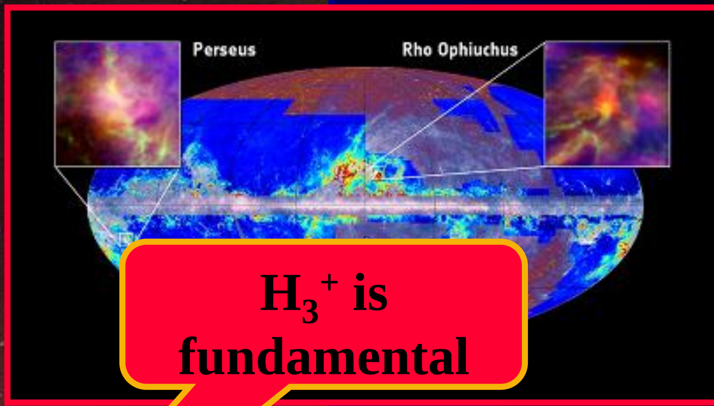

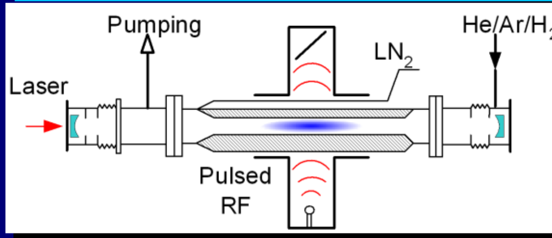

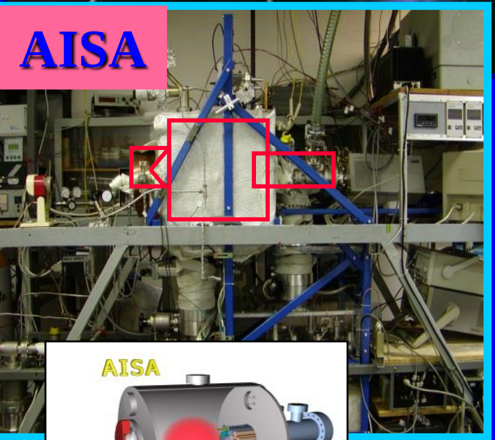

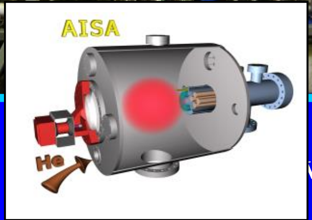

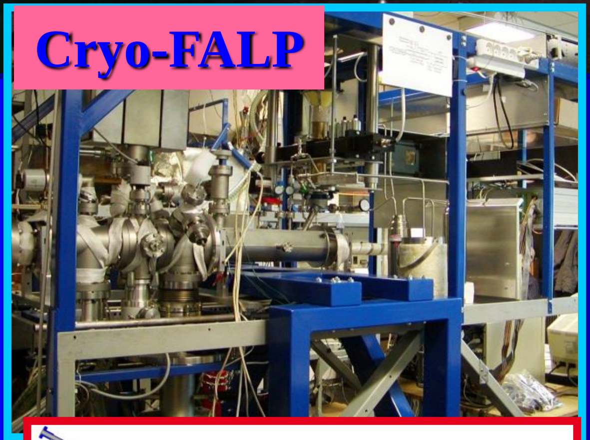

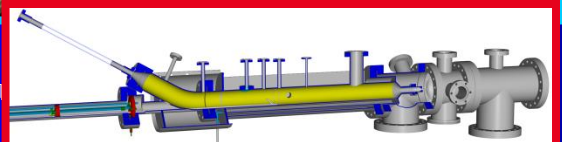

Different views
& different plasmas

H_3^+ and its interaction of with e^- is **FUNDAMENTAL**

If you understand hydrogen,
you understand all
that can be understood.
(*V. Weisskopf & G. Herzberg*).

$H_3^+ + e^-$

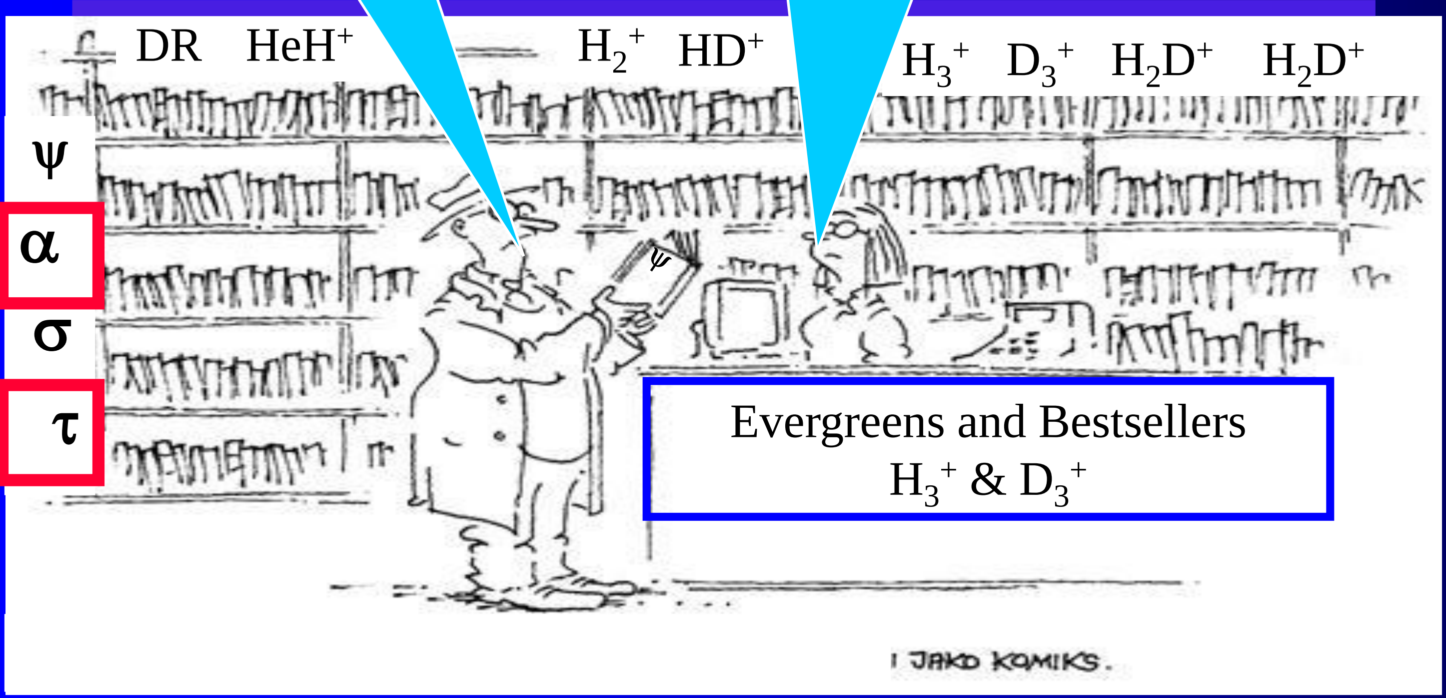

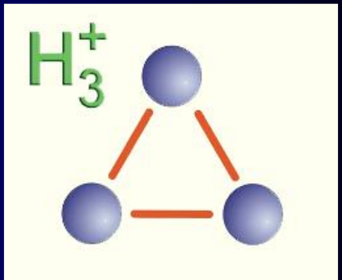

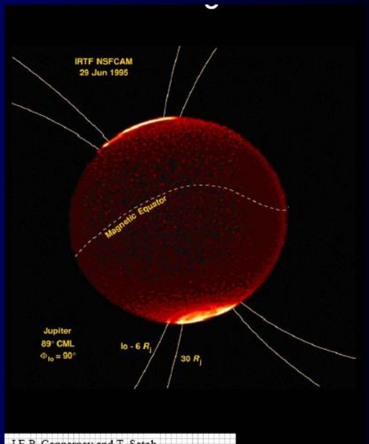

J.E.P. Connerney and T. Satoh,
Phil. Trans. R. Soc. Lond. A358, 2471 (2000)

VT - AISA

$dn_i/dt=-\alpha n_i n_e$

$He/Ar/H_2$

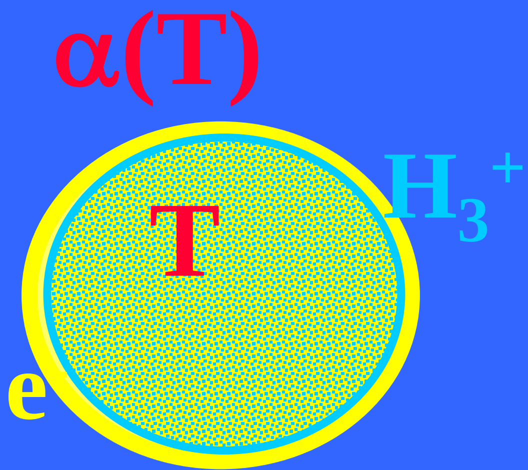

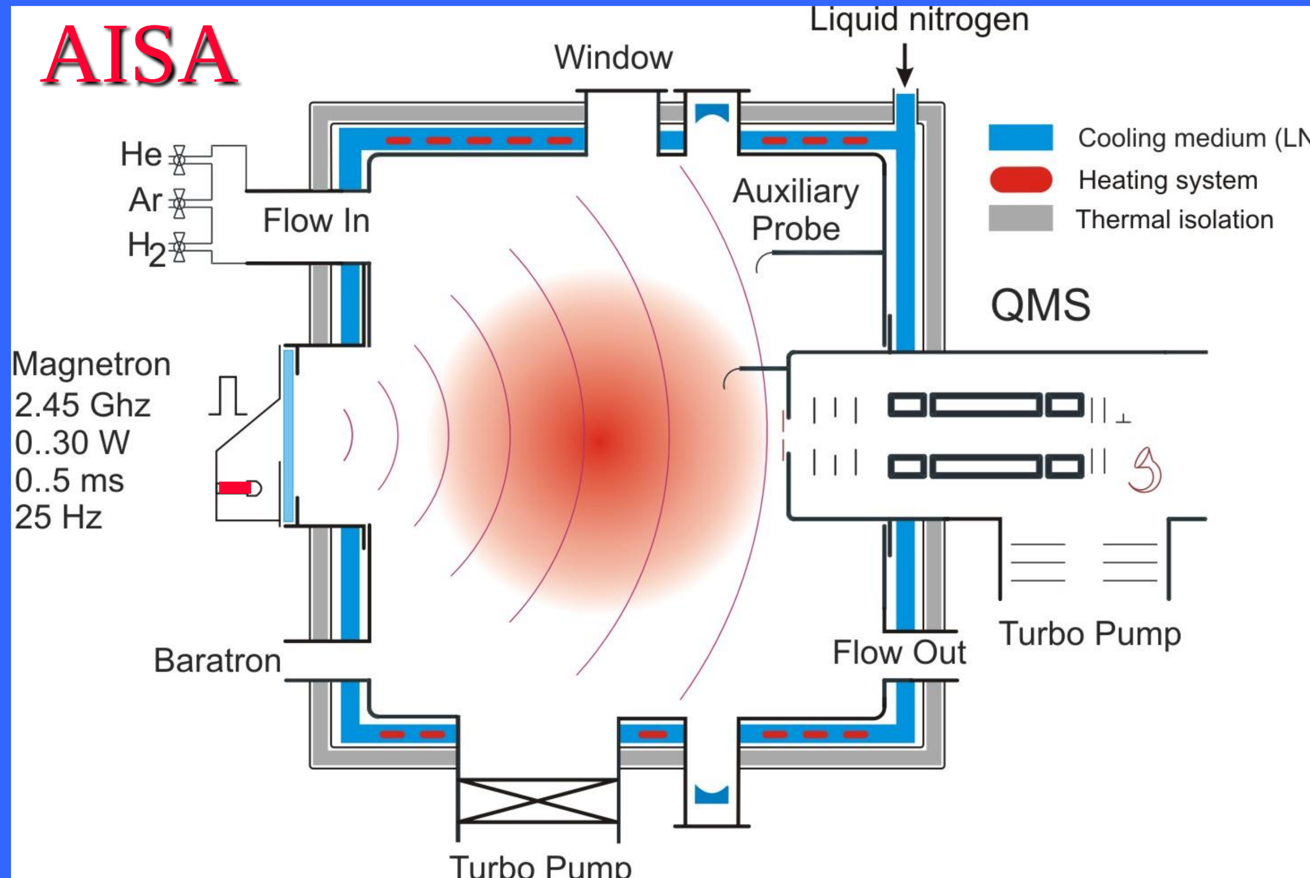

40 cm diameter
UHV - 10^{-9} Torr
External magnetron
2 Torr of $He/Ar/H_2$

PULSED STATIONARY AFTERGLOW

20-100ms decay

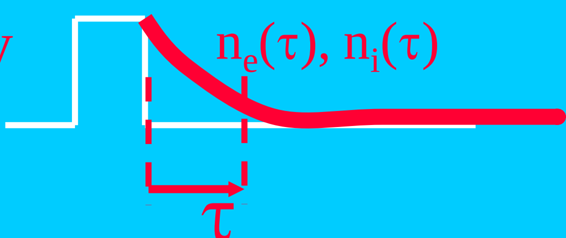

Formation of H_3^+ in He/Ar/H_2

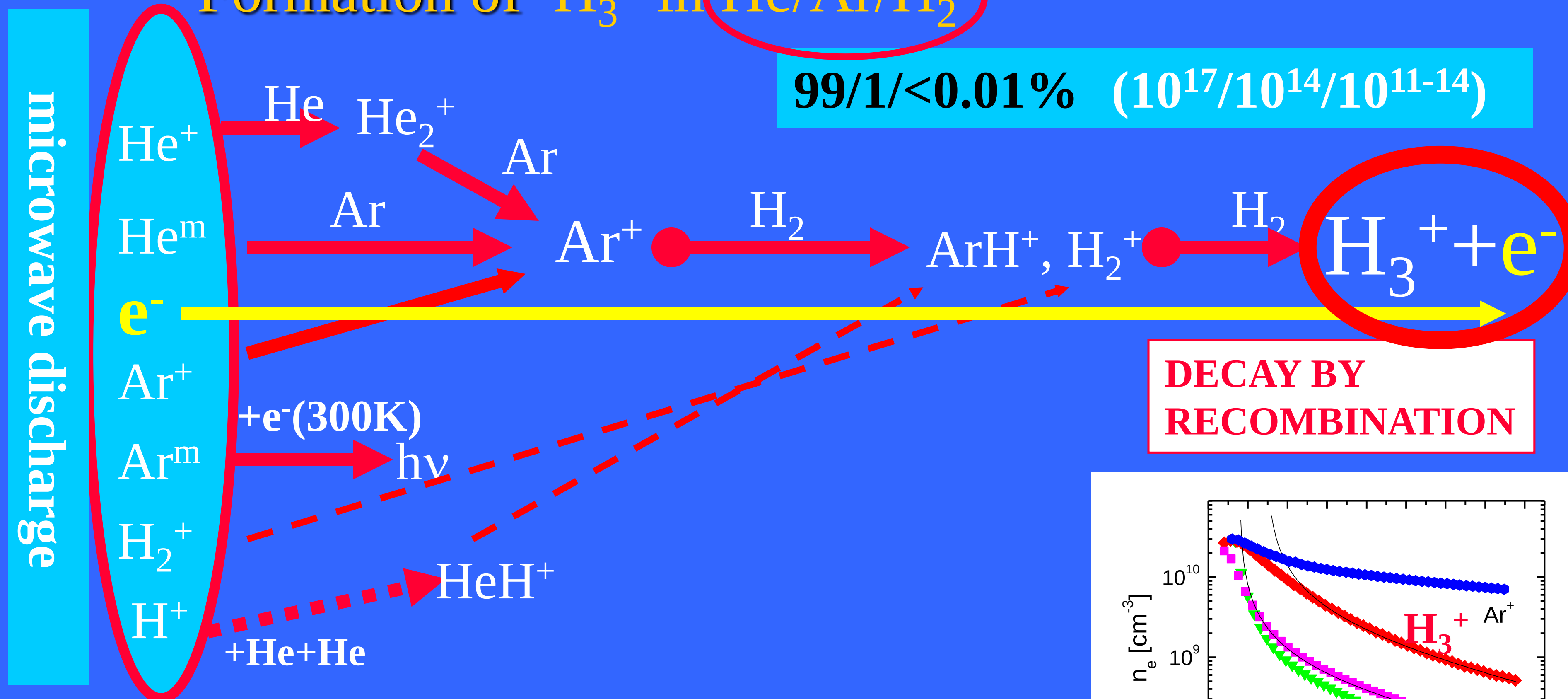

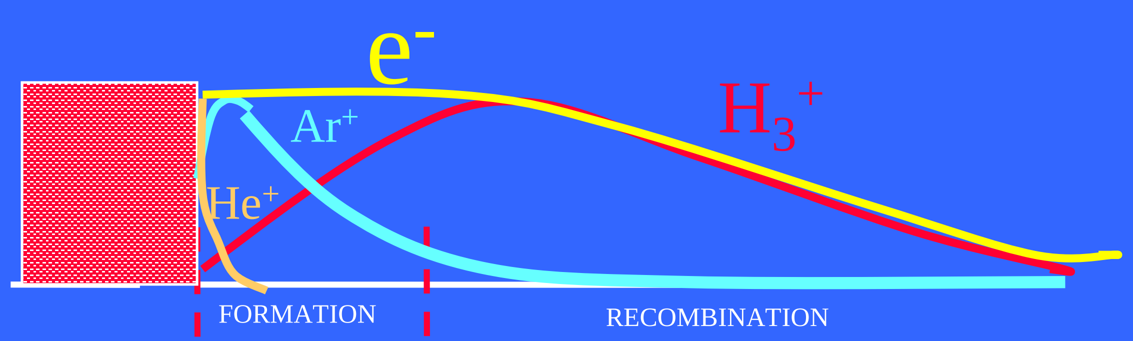

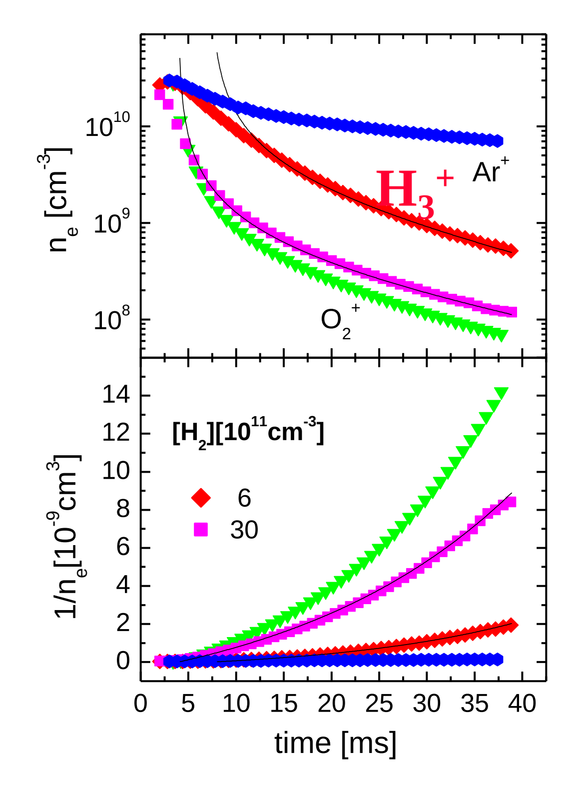

Time resolved mass spectra

FALP – Flowing Afterglow Langmuir Probe

Formation of H_3^+ in He/Ar/H_2 mixture (10 Torr)

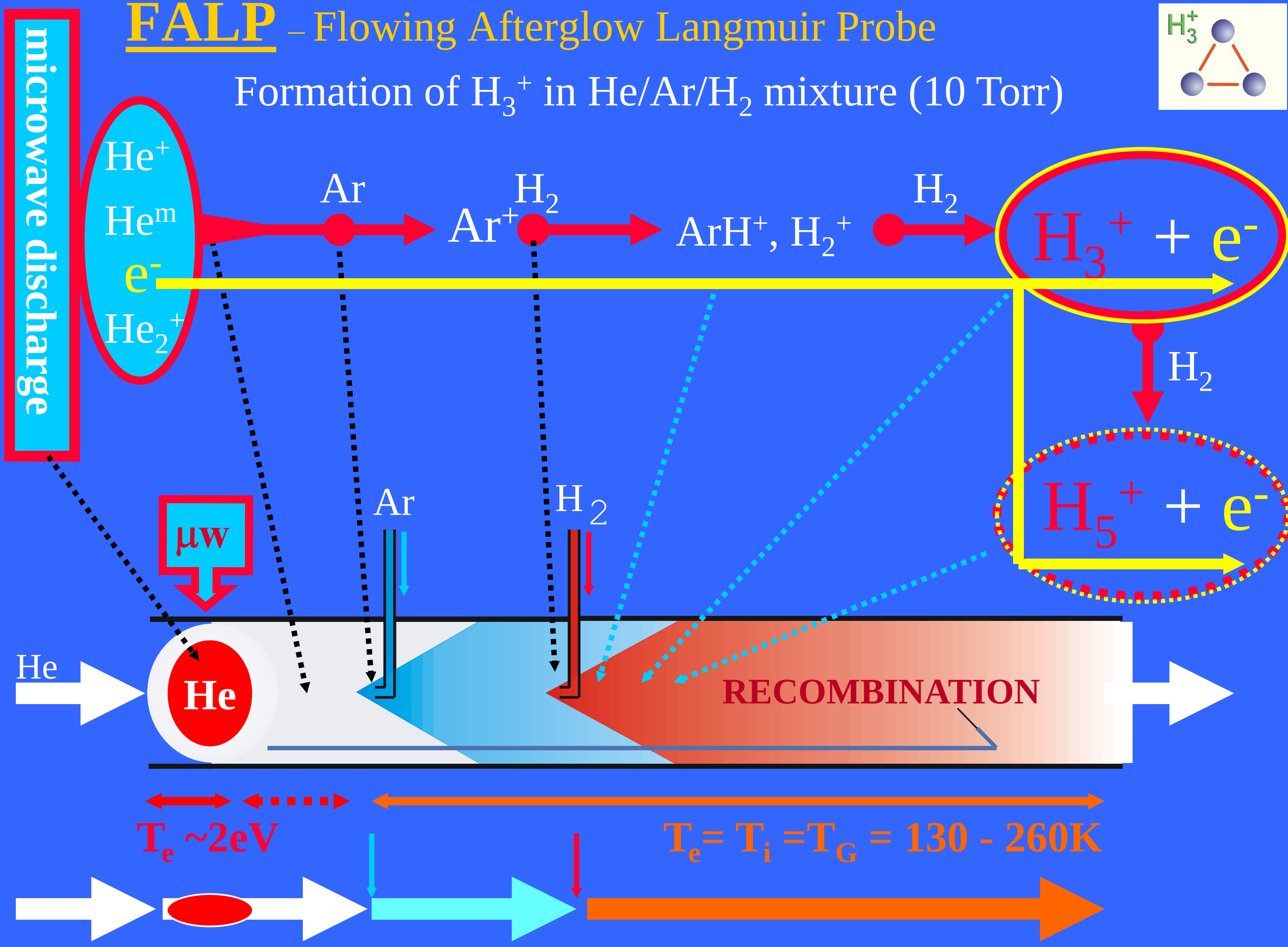

Nuclear spin dependence of H_3^+ recombination

H_3^+

B. J. McCall, et al. *Physical Review A* (2004)

H. Kreckel, J. Glosik, et al. Phys. Rev. Lett. 2005,

….2008, new improved calculations

Astronomy & Astrophysics October 13, 2008

L. Pagani[1], C. Vastel[2], E. Hugo[3], V. Kokoouline[4], Chris H. Greene[5], A. Bacmann[6], E. Bayet[7], C. Ceccarelli[6], R. Peng[8], and S. Schlemmer[3]

M. Larsson, B.J. McCall, A.E. Orel (2008)

J. Glosik, R. Plasil, et al. *Phys. Rev. A*, 2009.

H. Kreckel, O. Novotny, et al., Phys. Rev. A（2010）.

K. N. Crabtree, N. Indriolo, et al., Astrophys. J. (2011)

J. Varju, M. Hejduk, J. Glosik, et al. *Phys. Rev. Lett.*, 2011.

P. Dohnal, M. Hejduk, J. Glosik, et al. *J. Chem. Phys.*, 2012.

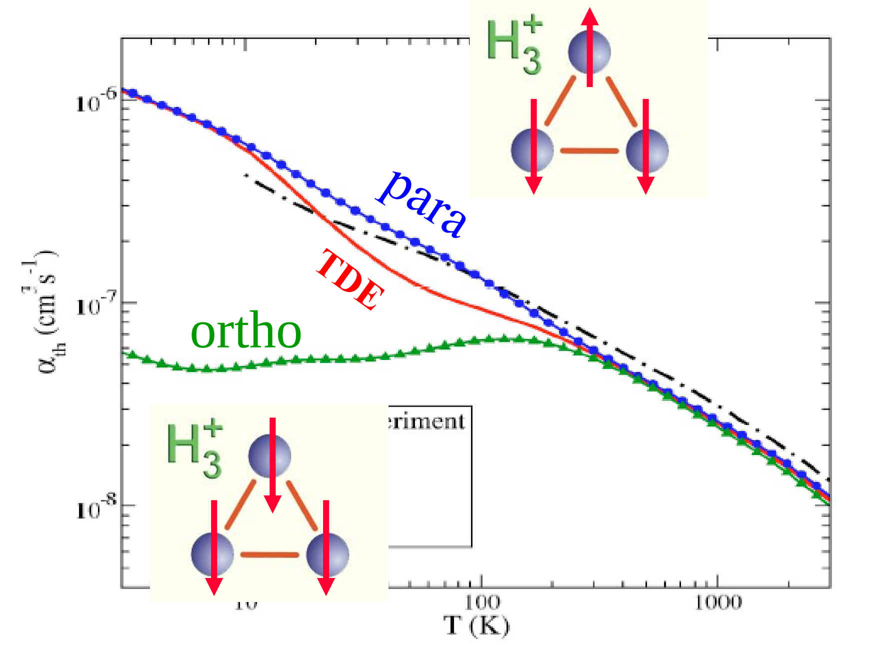

FIG. 5. (Color online) The present theoretical thermal rate coefficient for dissociative recombination of H_3^+ is compared with the experimental rate coefficient deduced from the storage ring experiment of McCall and co-workers (Refs. 9 and 10).

Doubts 2011

"Presently no rate coefficient measurement with a confirmed temperature below 300 K exists".

Petrignani *et al.* Phys. Rev. A (2011)

. Unfortunately the experiments on storage rings were stopped …. ☹ … ☹…

State of the art in 2013???

The dissociative recombination of H_3^+ – a saga coming to an end?

'Yes, the saga is coming to an end; but slowly.'

M. Larsson, B.J. McCall, A.E. Orel (2008)

….. Presently no reliable recombination rate coefficient for H3+ measured with storage rings below 300 K exists. …..

H. Kreckel, O. Novotny, K. N. Crabtree, et al., Phys. Rev. A (2010).
A. Petrignani, S. Altevogt, M. H. Berg, et al., Phys. Rev. A (2011).

The recent observations made towards several diffuse molecular clouds showed large difference between excitation temperatures T10(H2) and T(H3+), for details see ref. [cra11].

These observations lead to conclusion that in reliable chemical models the nuclear spin dependences of the reactions, including recombination of para- and ortho-H3+, have to be considered.
The dependences on spin, rotational excitation and temperature have to be measured.

K. N. Crabtree, N. Indriolo, H. Kreckel, B. A. Tom, and B. J. McCall, Astrophys. J. (2011)

Help! Theory for H_3^+ Recombination Still Needed
…. We still badly need theory …

Takeshi Oka, DR2013

…. It is time to present some recent results from afterglow experiments … ☺

$H_3^+ + e^- \rightarrow H + H_2; 3H$

Cross section

Single collision

v_r

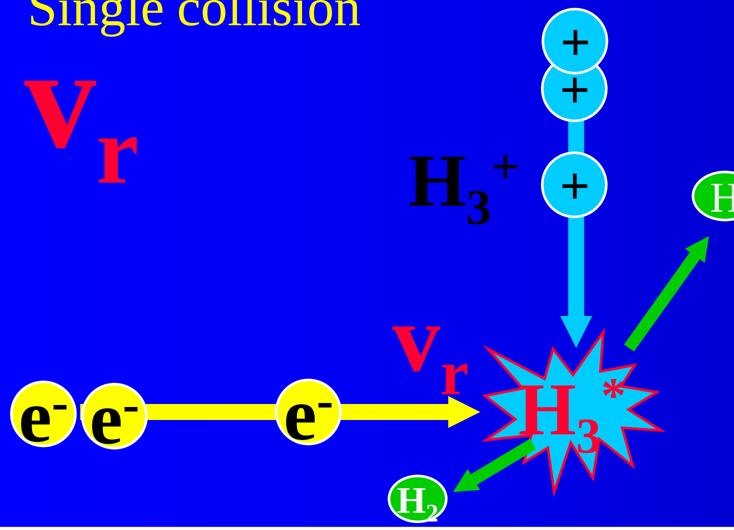

$\sigma(v_r)$

$\alpha(T)=\langle v\sigma\rangle$

$\alpha(T)$ Rate coefficient

T

Multiple collisions

He, H, H_2 $h\nu$…

$dn_e/dt = -\alpha n_i n_e = -\alpha n_e^2$

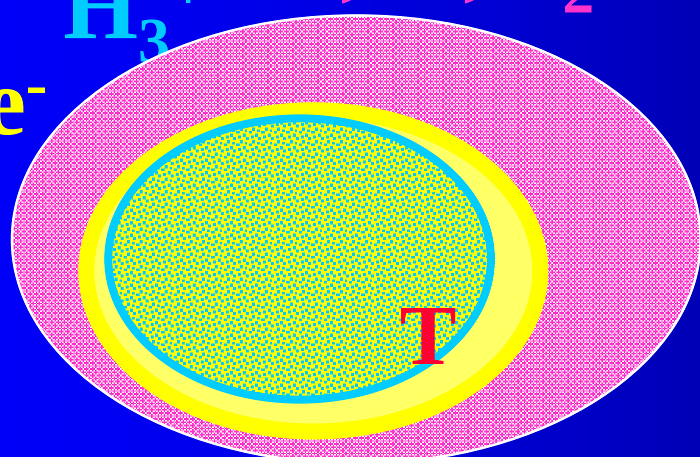

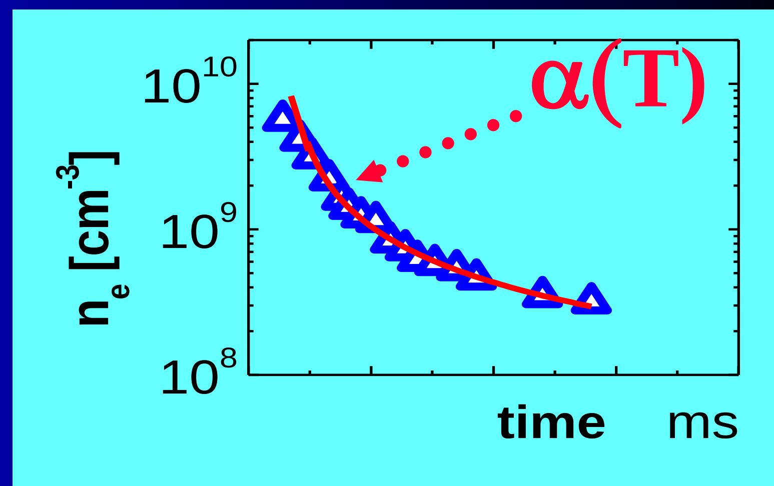

DR2007 - Dependence on He and H_2 pressure at 260 K

Afterglow in He/Ar/H_2 mixture

$a_{eff} = a_{eff}(T_e, T_i, n_e, [He], [H_2], {}^{o/p}f_2, {}^{o/p}f_3)$

$a_{eff} = a_{eff}(T, [He])$

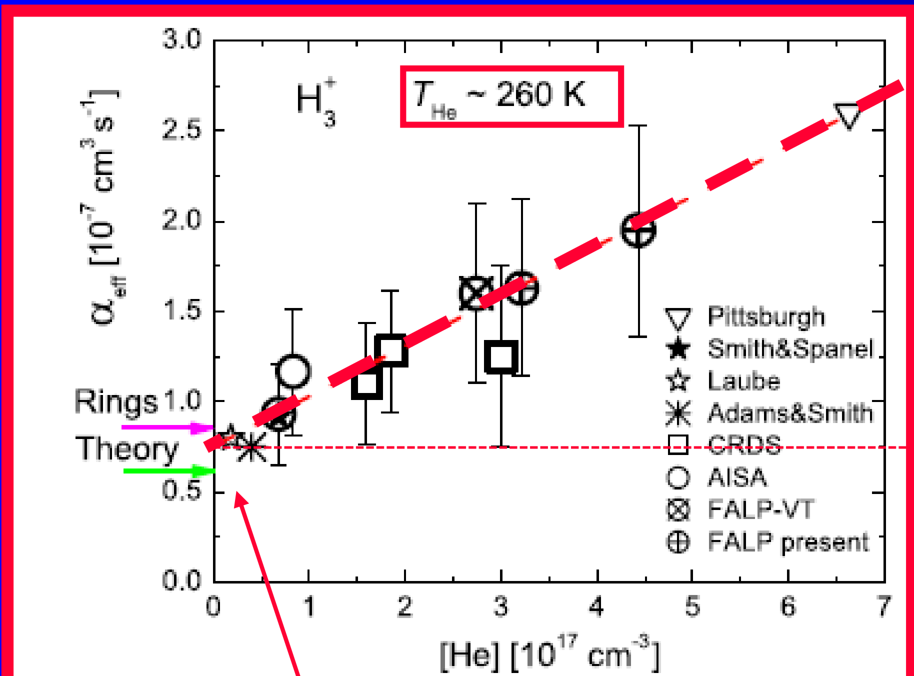

$$\alpha_{eff} = \alpha_{bin} + K_{He}.[He]$$

$$H_3^+ + e \underset{\leftarrow}{\overset{\alpha^*}{\rightleftarrows}} H_3^* \rightarrow products$$

He,

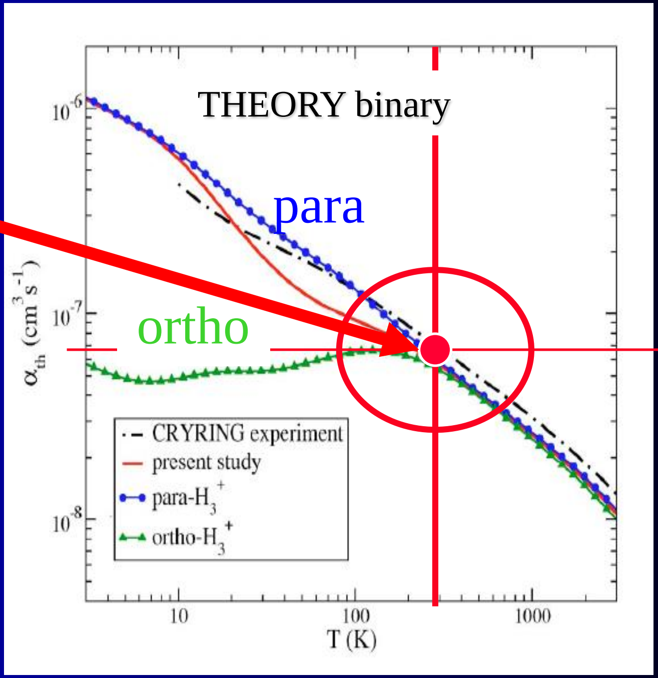

J. Phys. B: At. Mol. Opt. Phys. 41 (2008) 191001 (6pp)

Binary + He assisted ternary recombination

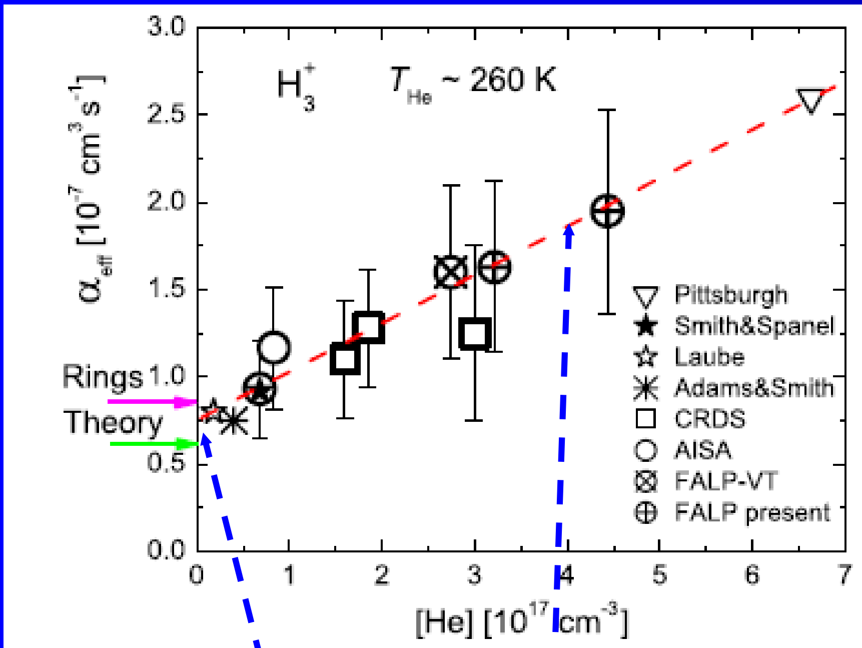

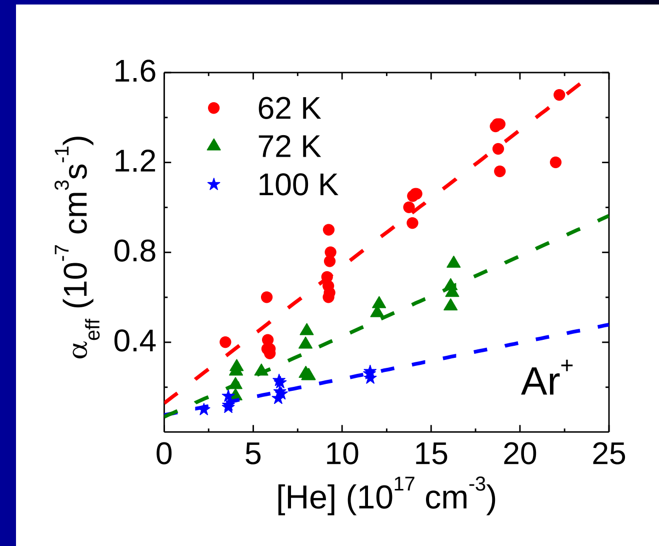

$$\alpha_{eff} = \alpha_{bin} + K_{He}.[He]$$

$$H_3^+ + e^- \xrightarrow{\alpha_{Bin}} H_2 + H, .H + H + H$$

$$H_3^+ + e^- \underset{\tau_a}{\overset{\alpha_F}{\rightleftarrows}} H_3^{\#} \xrightarrow[+He \ldots ks_{He}]{} \text{neutrals}$$

H_3^+ PLASMA EXPERIMENT $\alpha_{bin}(260K) = 7.5x10^{-8} cm^3 s^{-1}$

J. Phys. B: At. Mol. Opt. Phys. 41 (2008) 191001 (6pp)

$$\alpha_{eff} = \alpha_{eff}(T_e, T_i, n_e, [He], [H_2], {}^{o/p}f_3)$$

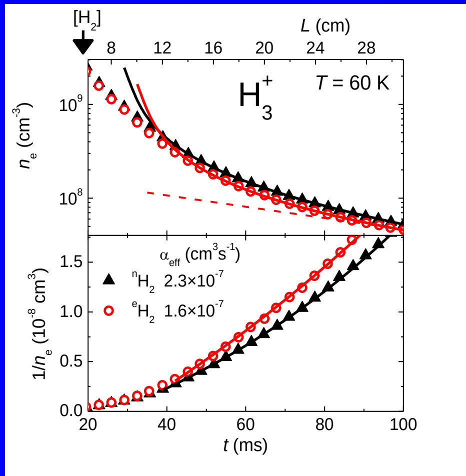

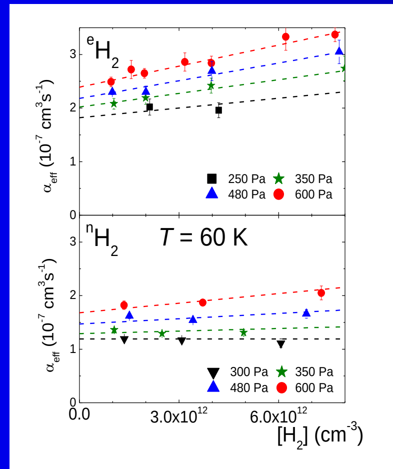

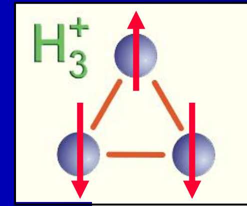

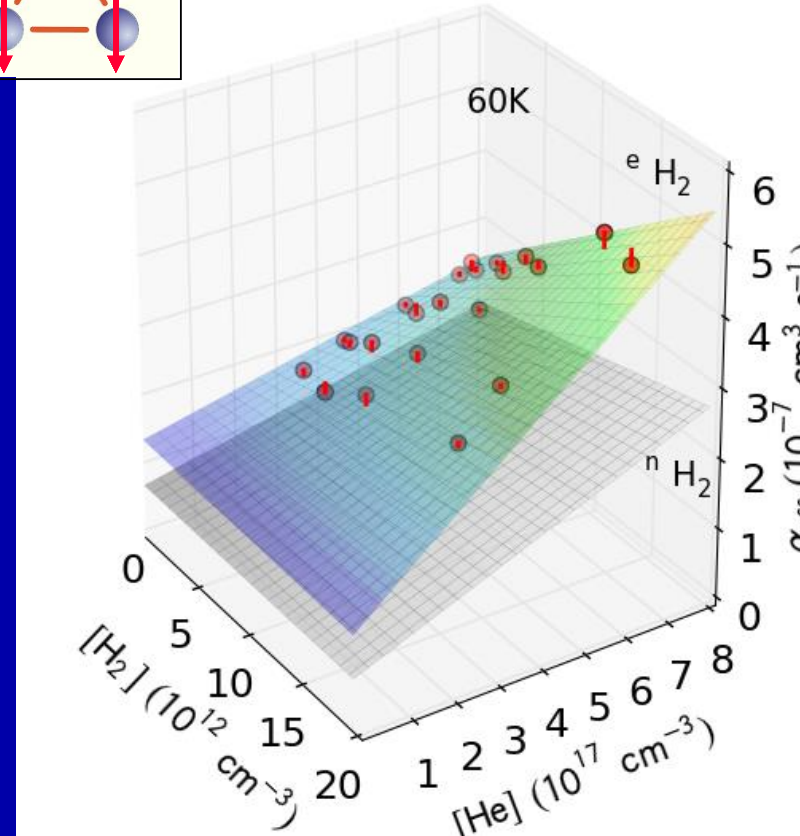

$$T = T_{wall} = T_{He} = T_e = T_{rot} = T_{kin\text{-}ion}$$

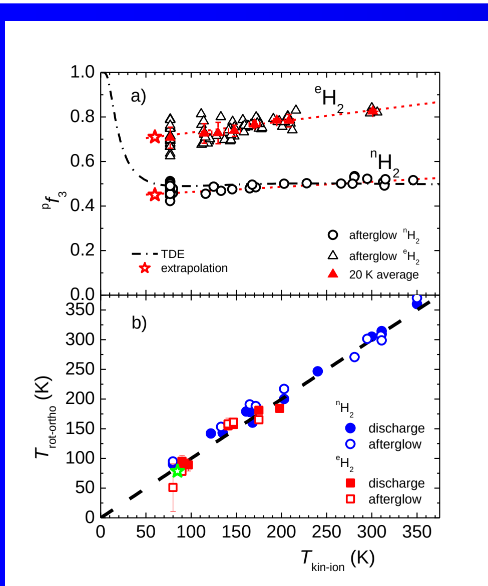

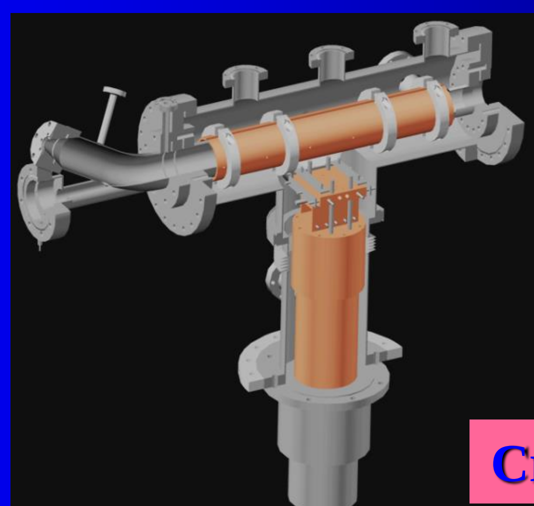

Cryo-FALP II

Calculated life time from Slava

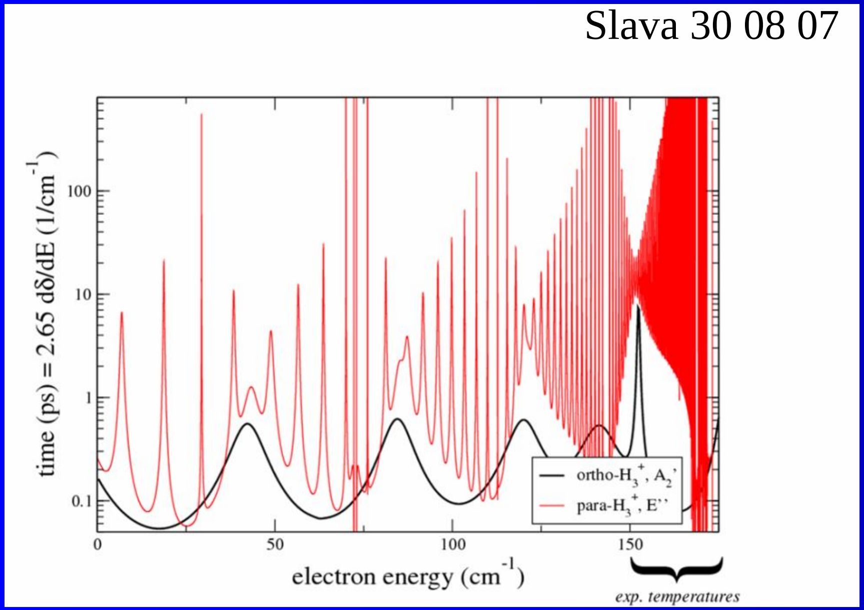

$$H_3^+ + e \rightarrow H_3^*$$

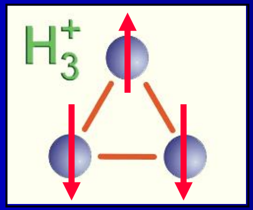

para

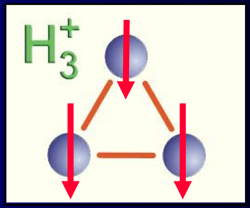

ortho

$$H_3^+ + e \Leftrightarrow H_3^* \rightarrow$$

Note enormous difference between para and ortho H_3^+

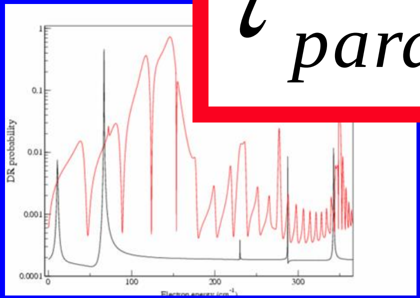

$$\tau_{para} \sim 100\,ps$$

$$\tau_{ortho} < 1\,ps$$

nding you t

probabilities for two different symmetries (red and black curves). The red curve corresponds to the rotational autoionization region. Fro this figure you can have an idea about the widths of the resonances. With best wishes, Slava

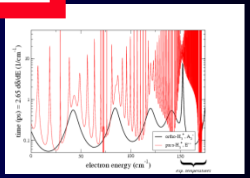

Model

$\alpha_{eff} = \alpha_{eff}(T_e, T_i, n_e, [He], [H_2], {}^{o/p}f_3)$

$$H_3^+ + e^- \xrightarrow{\alpha_{Bin}} H_2 + H, H + H + H$$

]

$$\xrightarrow{\alpha_F} H_3^{\#} \xrightarrow{H_2 \ldots k_{SH2}} \text{neutrals}$$

$$\xleftarrow{\tau_a} \qquad \xrightarrow[He \ldots k_{SHe}]{}$$

By solving the set of balance equations we obtain:

(He/Ar/H_2 mixture)

$$\frac{\partial n_e}{\partial t} = -(\alpha_{bin} - \alpha_F \frac{k_{SHe}[He] + k_{SH_2}[H_2]}{\frac{1}{\tau_a} + k_{SHe}[He] + k_{SH_2}[H_2]})[H_3^+]n_e$$

$$K_{He} = \alpha_F k_{SHe} \tau_a \qquad K_{H2} = \alpha_F k_{SH2} \tau_a$$

$$\alpha_{eff} = \alpha_{bin} + \alpha_F \frac{K_{He}[He] + K_{H2}[H_2]}{\alpha_F + K_{He}[He] + K_{H2}[H_2]}$$

In the low density limit ([He] and $[H_2] \rightarrow 0$), linear approximation

$$\alpha_{eff} = \alpha_{bin} + K_{He}[He] + K_{H2}[H_2]$$

Experiments - State of the art in 2015

$$H_3^+ + e + He \rightarrow \ldots\ldots + He$$
$$H_3^+ + e + H_2 \rightarrow \ldots\ldots + H_2$$

$$H_3^+ + e + He \rightarrow \ldots\ldots + He$$

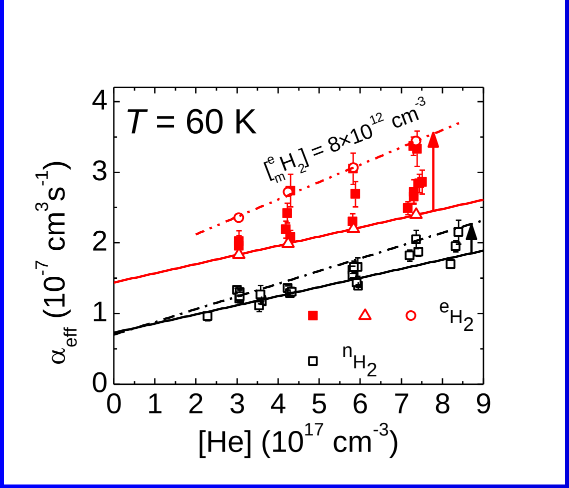

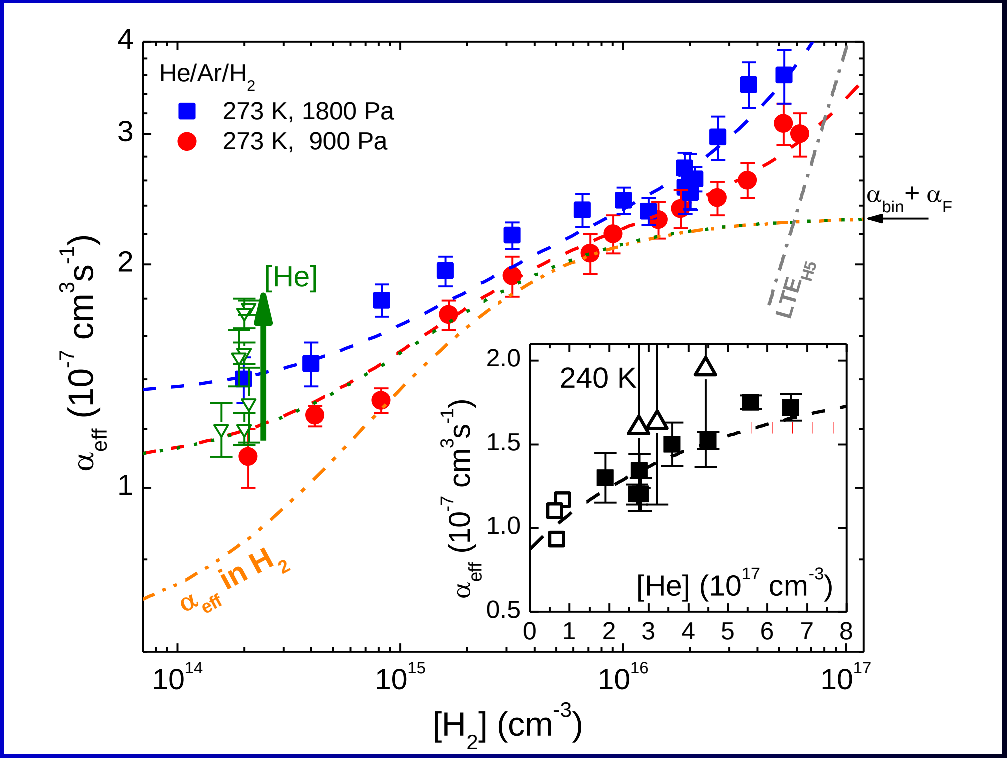

$$\alpha_{\mathrm{eff}} = \alpha_{\mathrm{bin}} + \alpha_{\mathrm{F}} \frac{K_{\mathrm{He}}[\mathrm{He}] + K_{\mathrm{H2}}[\mathrm{H}_2]}{\alpha_{\mathrm{F}} + K_{\mathrm{He}}[\mathrm{He}] + K_{\mathrm{H2}}[\mathrm{H}_2]}$$

CRR

$$H_3^+ + e + e \rightarrow \ldots\ldots + e$$

Rate coefficient binary

para-H_3^+ and orto-H_3^+

$$H_3^+ + e^- \xrightarrow{\alpha_{Bin}} H_2 + H, . H + H + H$$

$$H_3^+ + e^- \underset{\tau a}{\overset{\alpha_F}{\rightleftarrows}} H_3^{\#} \xrightarrow[He....ks_{He}]{H_2....ks_{H2}} \text{neutrals}$$

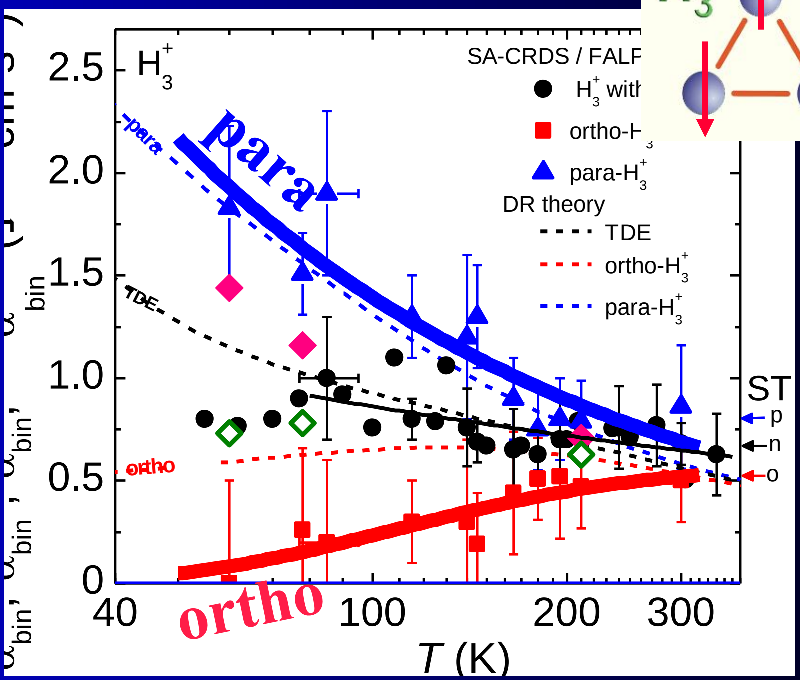

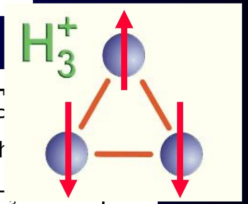

(He/Ar/H_2 mixture)

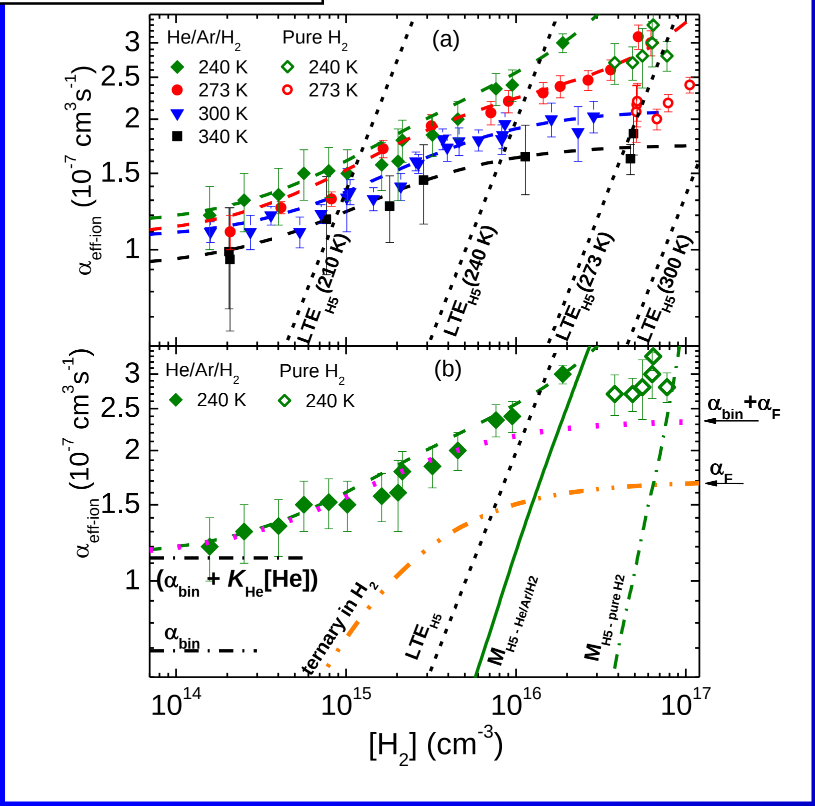

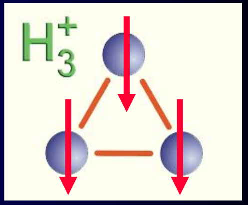

$$H_3^+ + e^- \xrightarrow{\alpha_{Bin}} H_2 + H, .H + H + H$$

$$H_3^+ + e^- \underset{\tau_a}{\overset{\alpha_F}{\rightleftarrows}} H_3^{\#} \xrightarrow[He \ldots ks_{He}]{H_2 \ldots ks_{H2}} \text{neutrals}$$

para-H_3^+ and orto-H_3^+

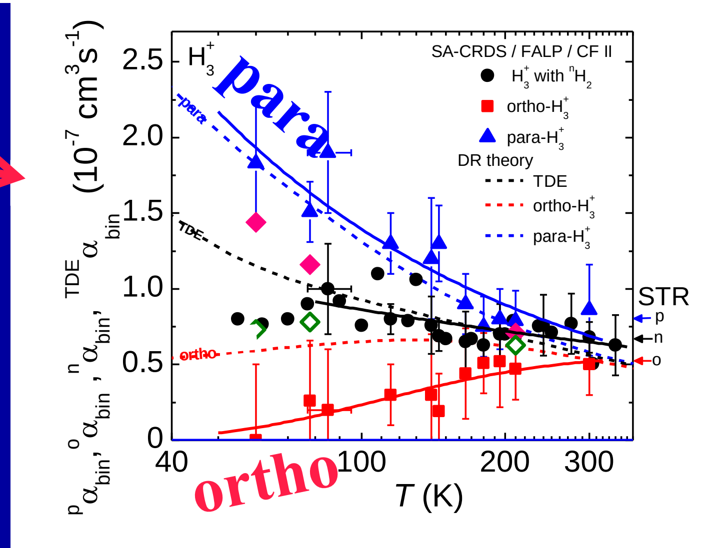

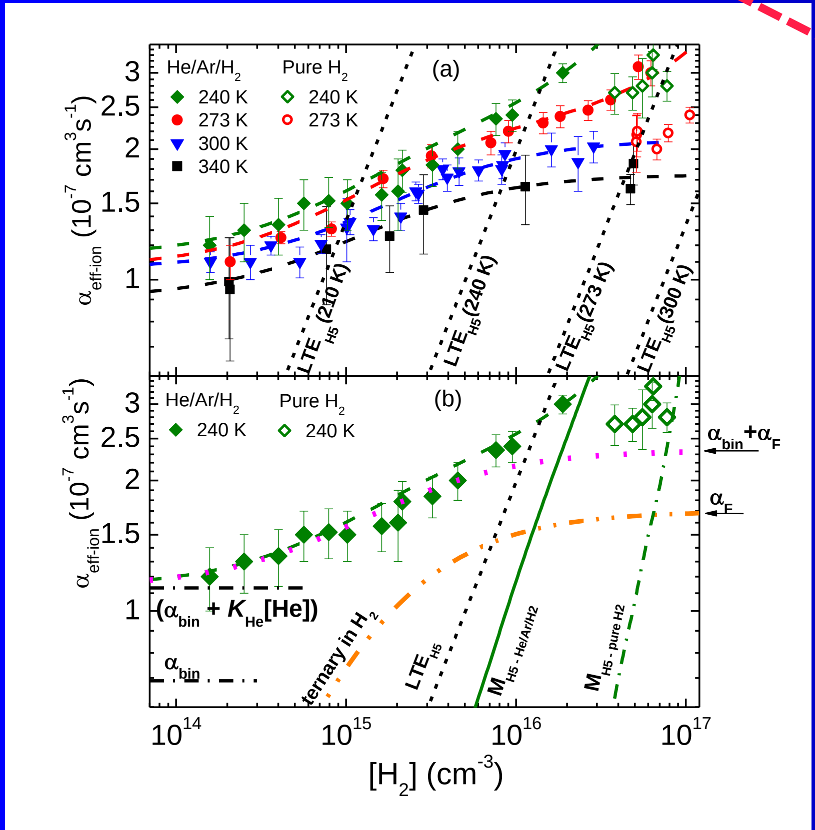

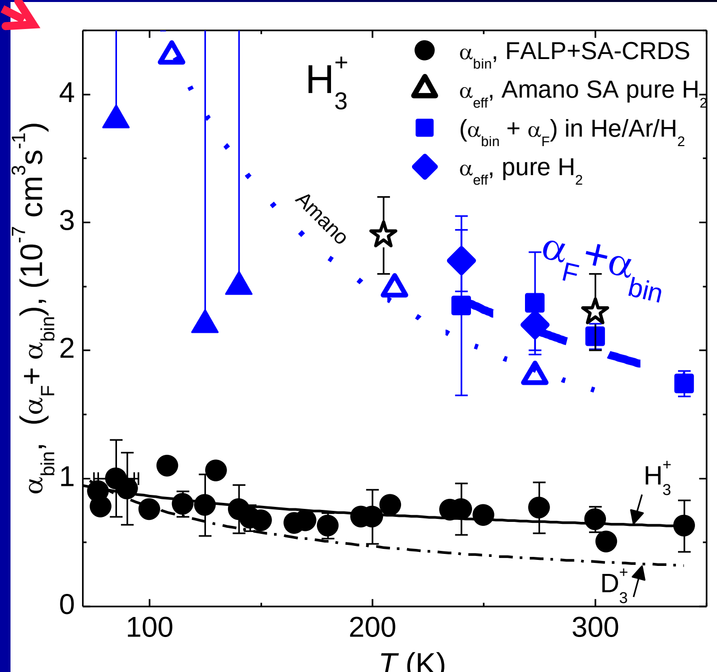

$$H_3^+ + e^- \xrightarrow{\alpha_{Bin}} H_2 + H, .H + H + H$$

$$H_3^+ + e^- \underset{\tau a}{\overset{\alpha_F}{\rightleftarrows}} H_3^\# \begin{array}{c} \xrightarrow{H_2 ....ks_{H2}} \\ \xrightarrow[He....ks_{He}]{} \end{array} \text{neutrals}$$

$$K_{He} = \alpha_F \, k_{SHe} \, \tau_a \qquad K_{H2} = \alpha_F \, k_{SH2} \, \tau_a$$

$$\alpha_{eff} = \alpha_{bin} + \alpha_F \frac{K_{He}[He] + K_{H2}[H_2]}{\alpha_F + K_{He}[He] + K_{H2}[H_2]}$$

K_{He} K_{H2}

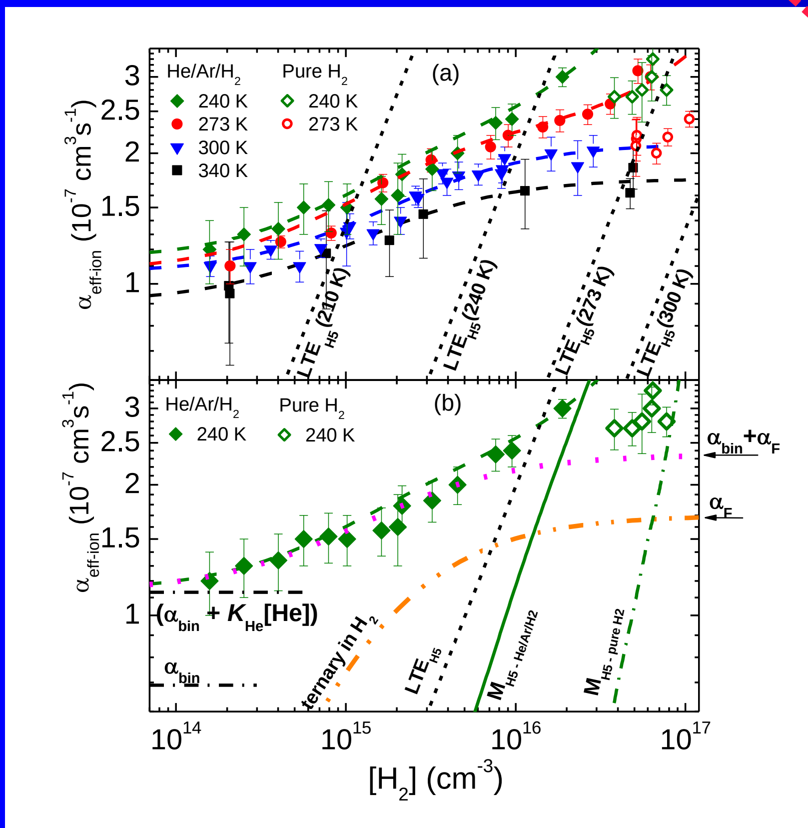

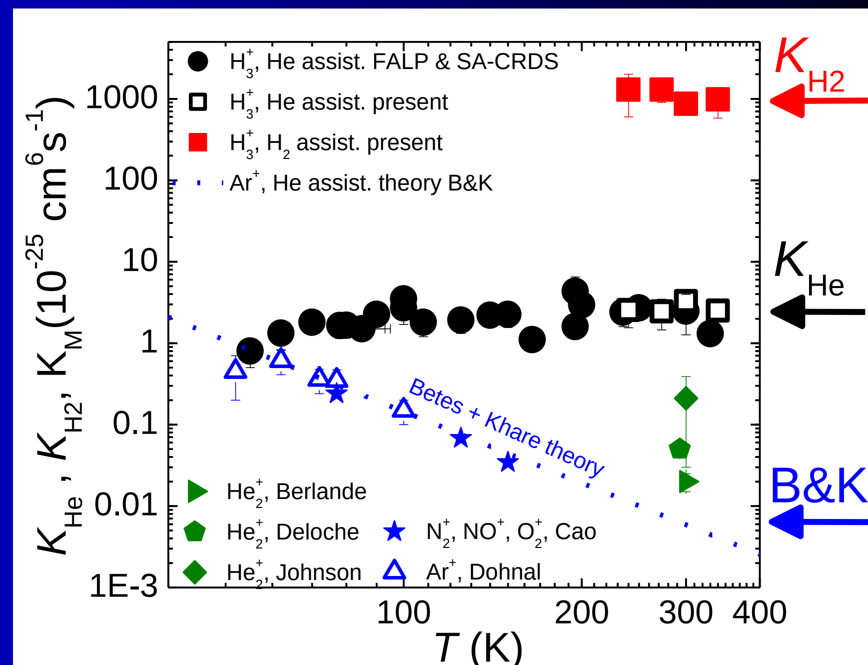

IOP Publishing Plasma Sources Science and Technology
Plasma Sources Sci. Technol. 24 (2015) 065017 (10pp) doi:10.1088/0963-0252/24/6/065017

Recombination of H_3^+ ions with electrons in He/H_2 ambient gas at temperatures from 240 K to 340 K

J Glosík[1], P Dohnal[1], P Rubovič[1], Á Kálosi[1], R Plašil[1], Š Roučka[1] and R Johnsen[2]

$$K_{He} = \alpha_F \, k_{SHe} \, \tau_a \qquad K_{H2} = \alpha_F \, k_{SH2} \, \tau_a$$

$$H_3^+ + e + H_2 \rightarrow \ldots\ldots + H_2$$

$$H_3^+ + e + He \rightarrow \ldots\ldots + He$$

$$Ar^+ + e + He \rightarrow \ldots\ldots + He$$

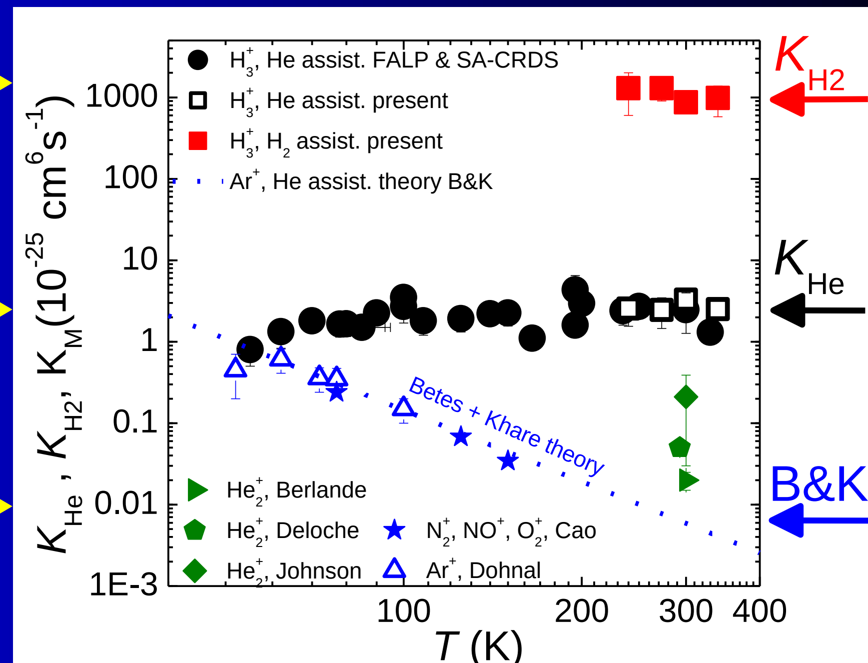

astro

H_3^+/e^- plasma in He/Ar/H_2 gas mixture

$$H_3^+ + e^- \Rightarrow H + H_2, 3H$$

α(T=300 K)

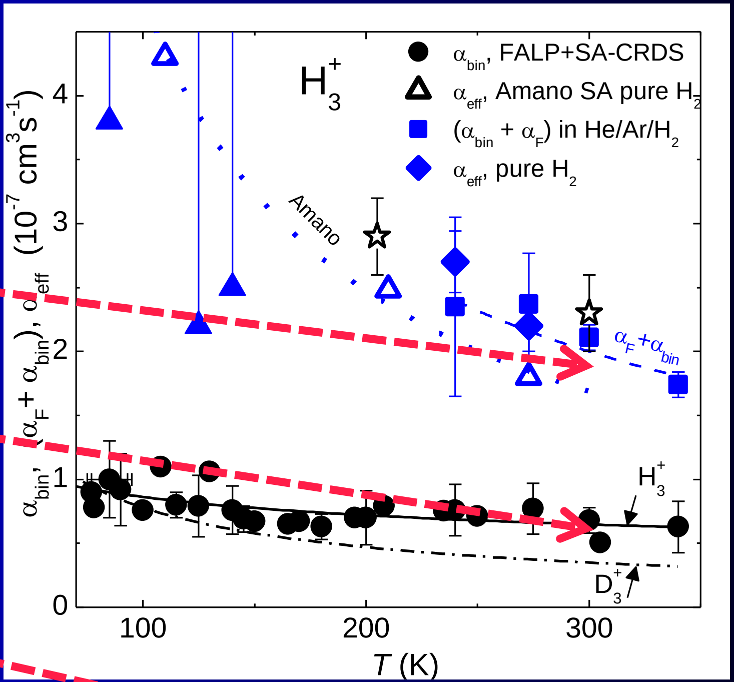

$$\alpha_{eff} = \alpha_{bin} + \alpha_F \frac{K_{He}[He] + K_{H2}[H_2]}{\alpha_F + K_{He}[He] + K_{H2}[H_2]}$$

$$H_3^+ + e + H_2 \rightarrow ...... + H_2$$

$$H_3^+ + e + He \rightarrow ...... + He$$

$$Ar^+ + e + He \rightarrow ...... + He$$

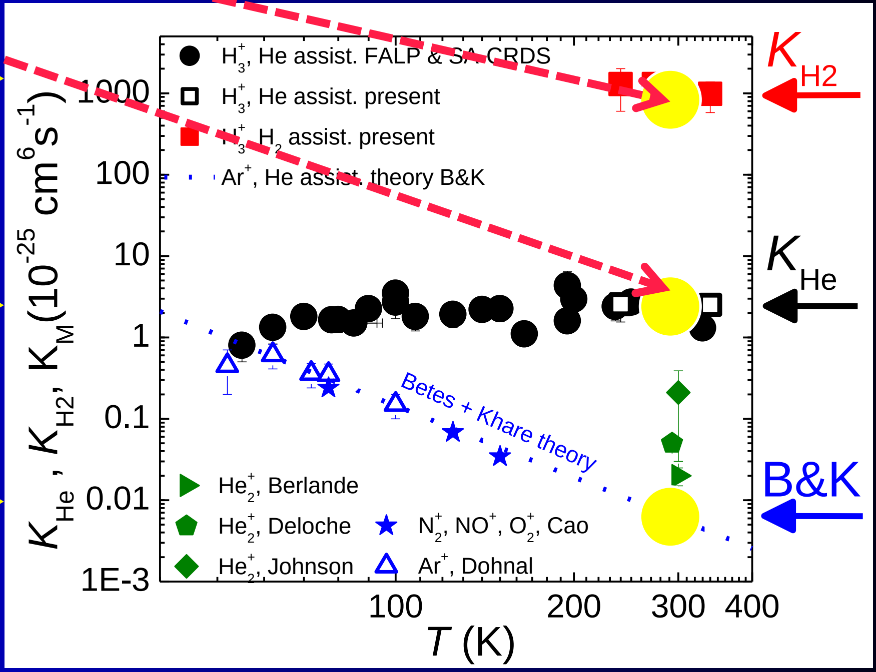

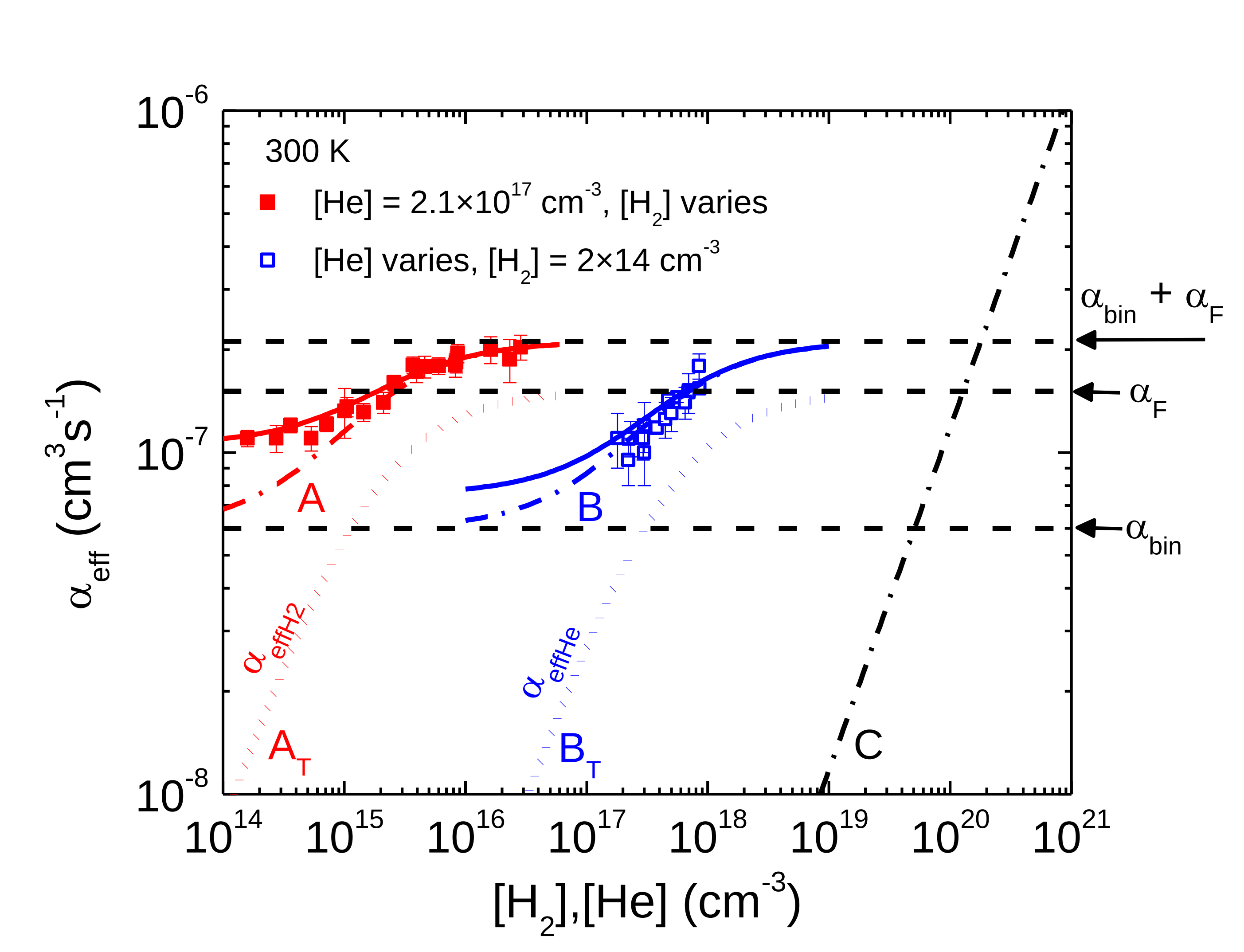

300 K
[He] = 2.1×10^17 cm^-3, [H_2] varies
[He] varies, [H_2] = 2×14 cm^-3
α_bin + α_F
α_F
α_bin
A
B
C
A_T
B_T
α_effH2
α_effHe
α_eff (cm^3 s^-1)
[H_2],[He] (cm^-3)
10^-6
10^-7
10^-8
10^14
10^15
10^16
10^17
10^18
10^19
10^20
10^21

Quo vadis ???

Motivation: ☺ Just for pleasure

"Intelligent play with simple, natural phenomena, the joys of discovery of unexpected experiences, are much better ways of learning to think than any teaching by rote."

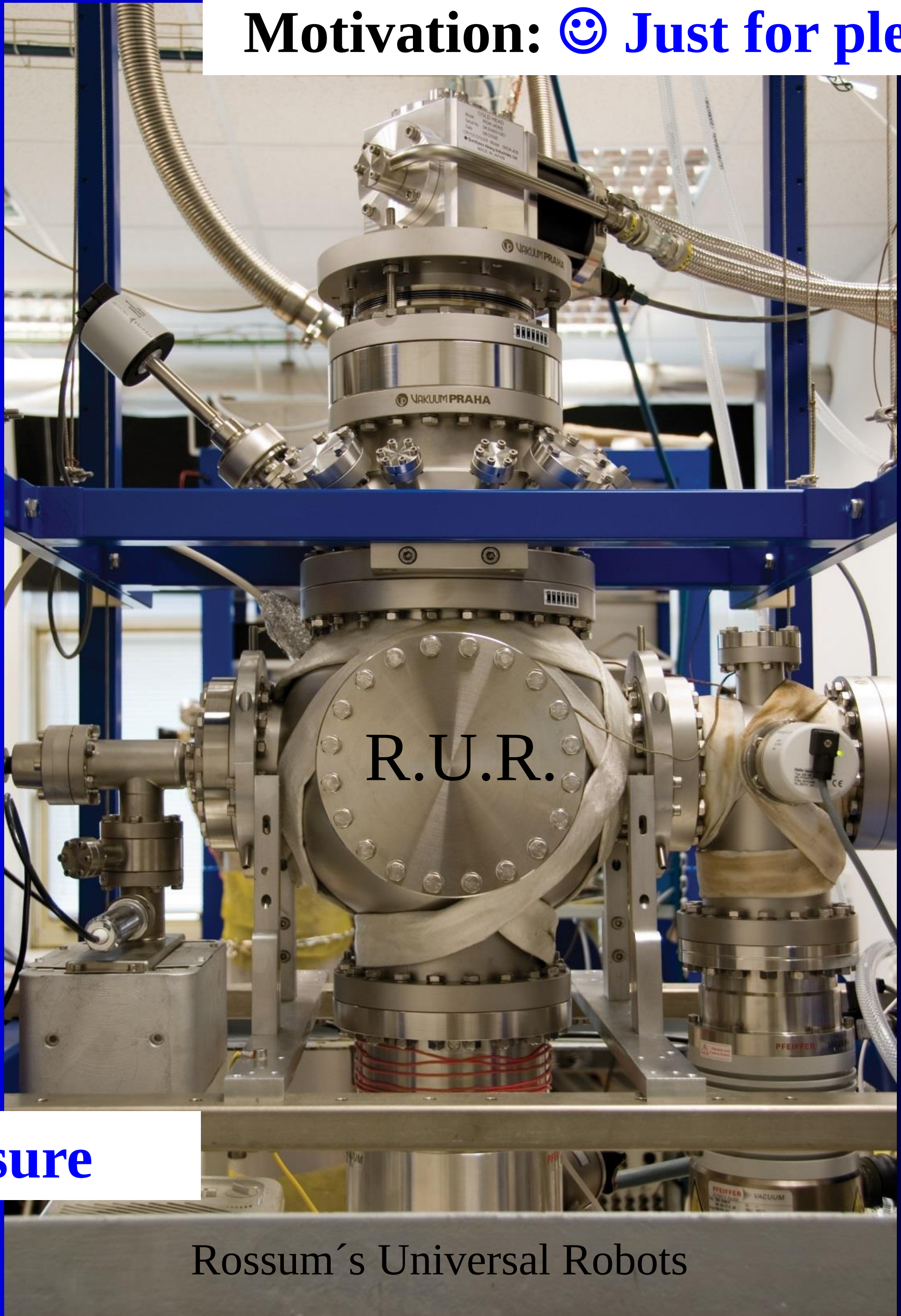

30 K ☺ Just for pleasure

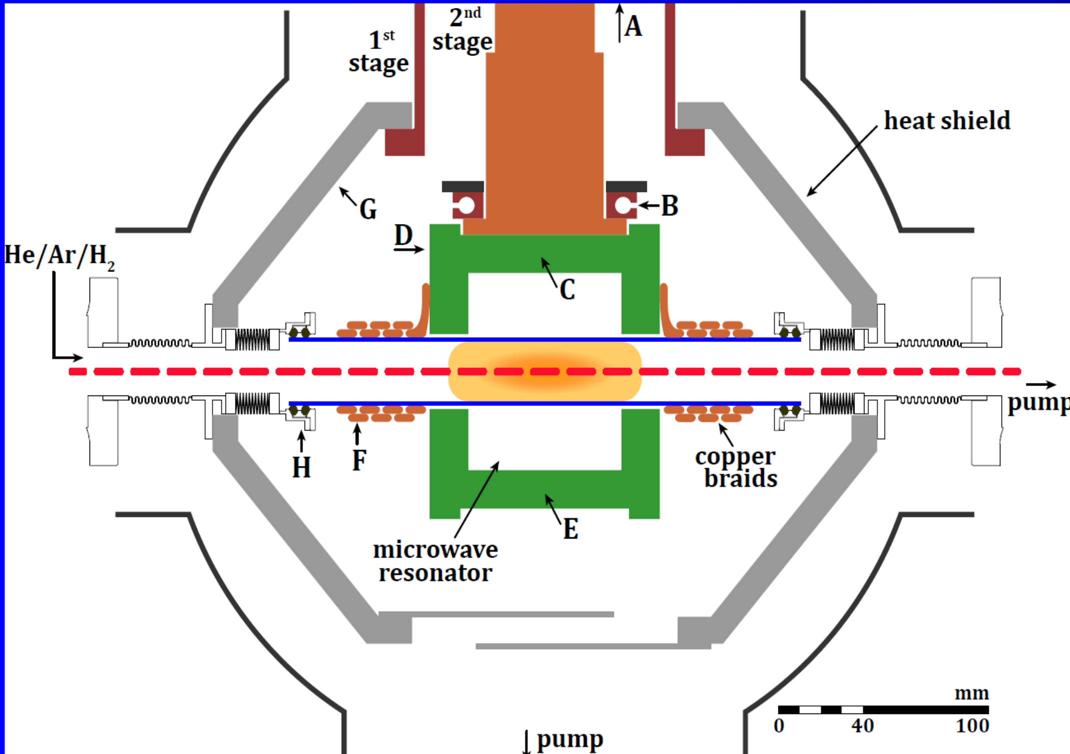
1st stage
2nd stage
A
heat shield
G
B
D
C
He/Ar/H2
pump
H
F
copper braids
E
microwave resonator
pump
mm
0
40
100

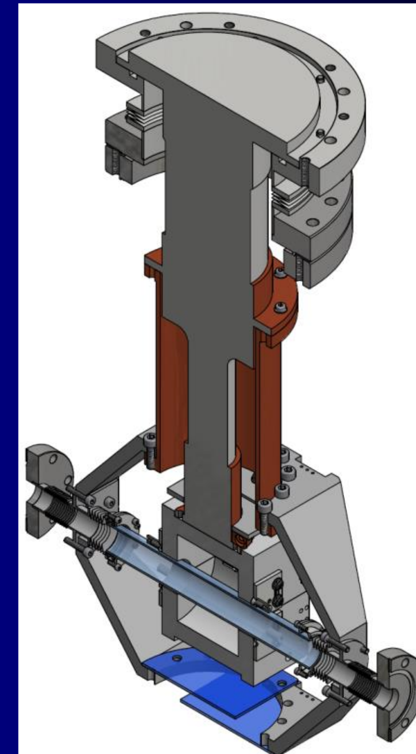

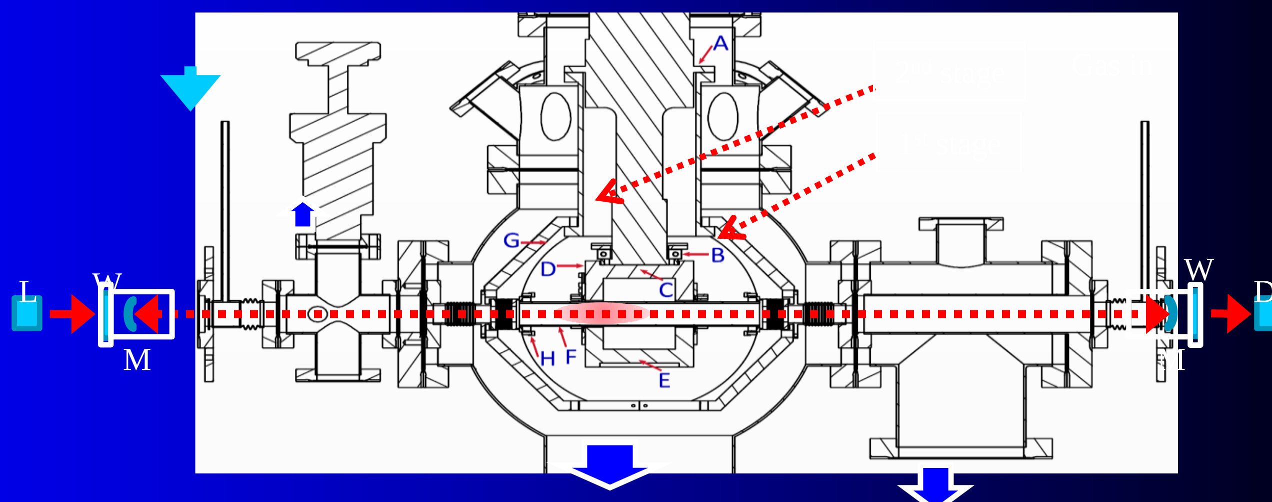
A
G
B
D
C
H
F
E
L
W
M
W
D

Recombination

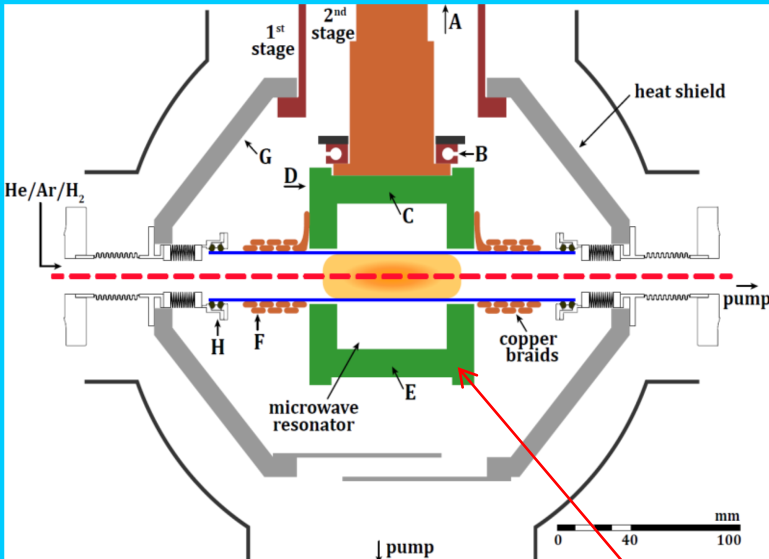

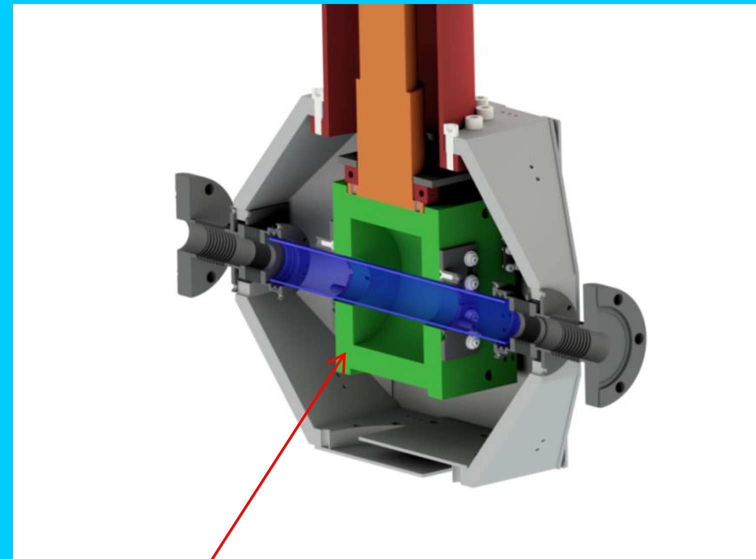

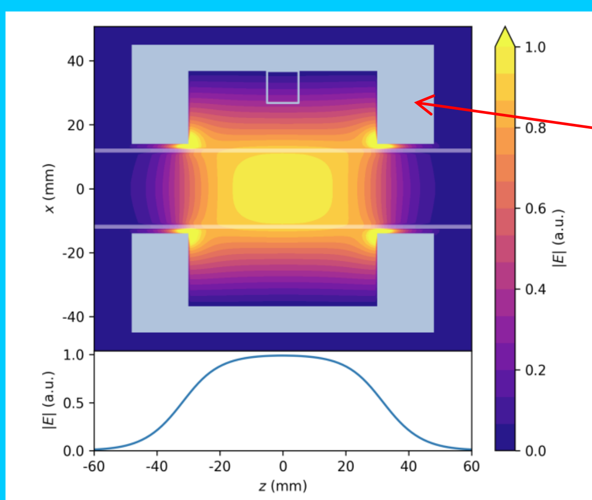

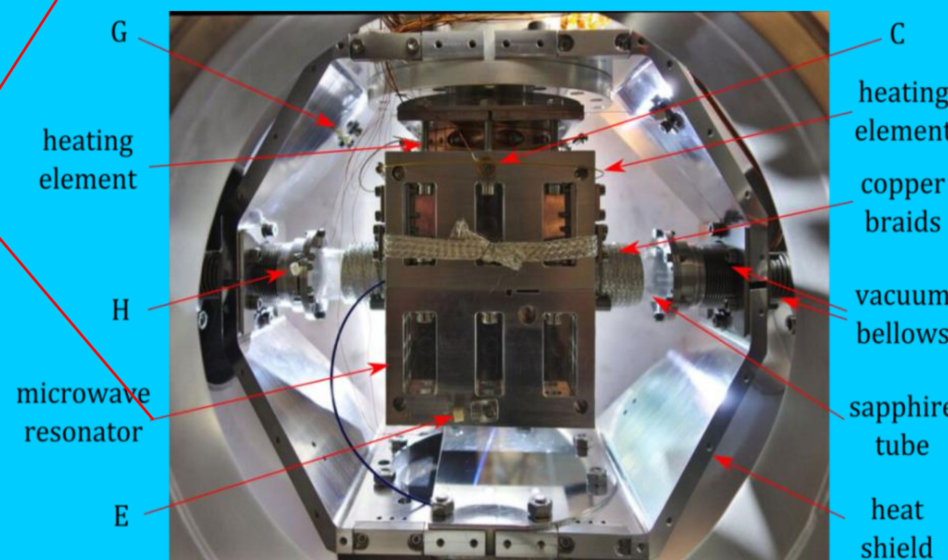

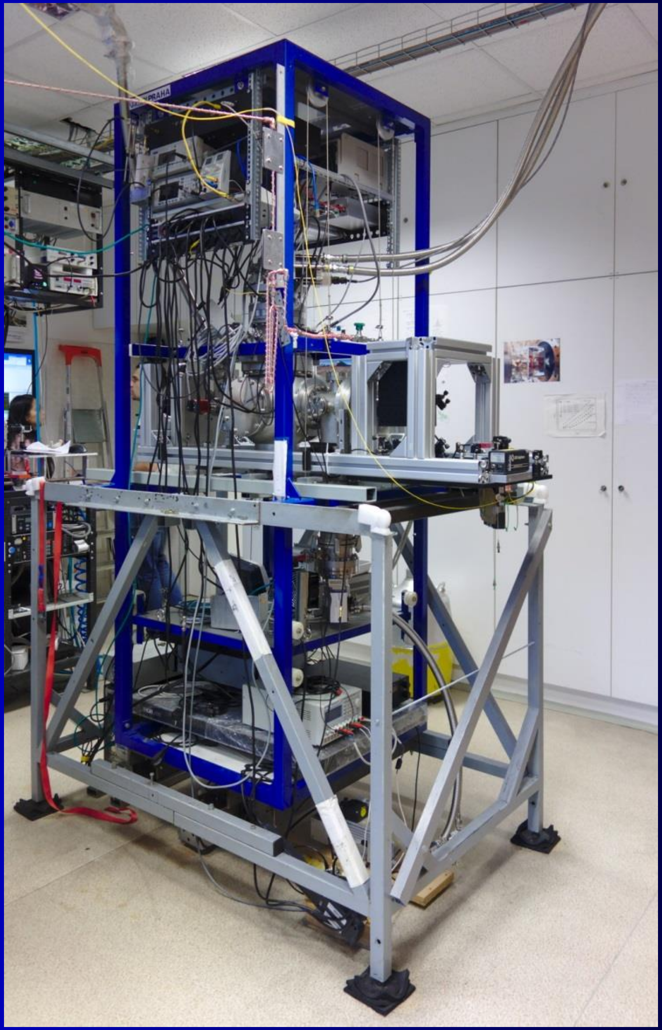

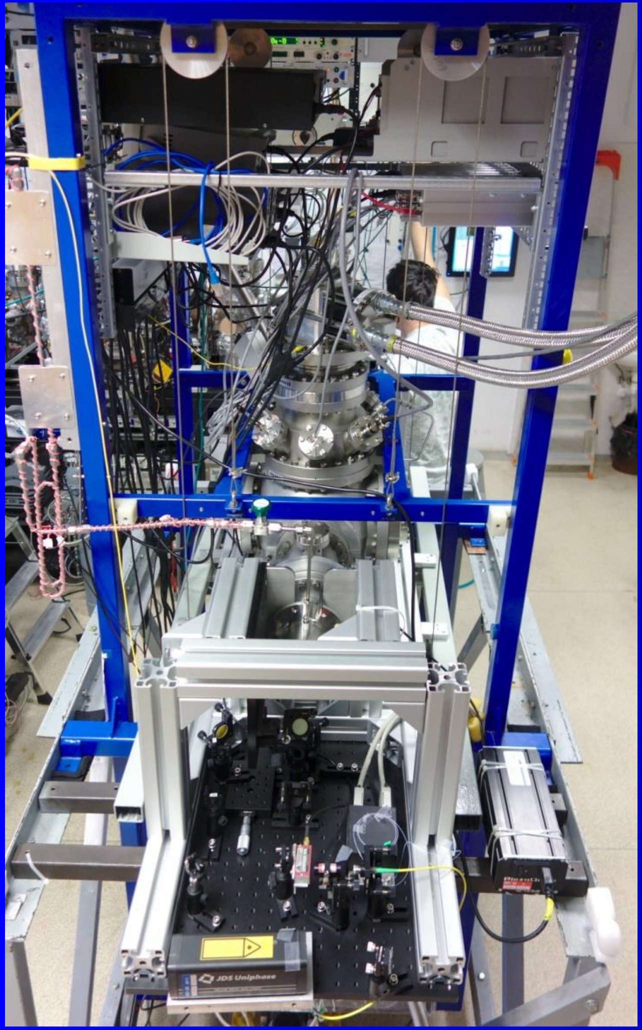
JDS Uniphase

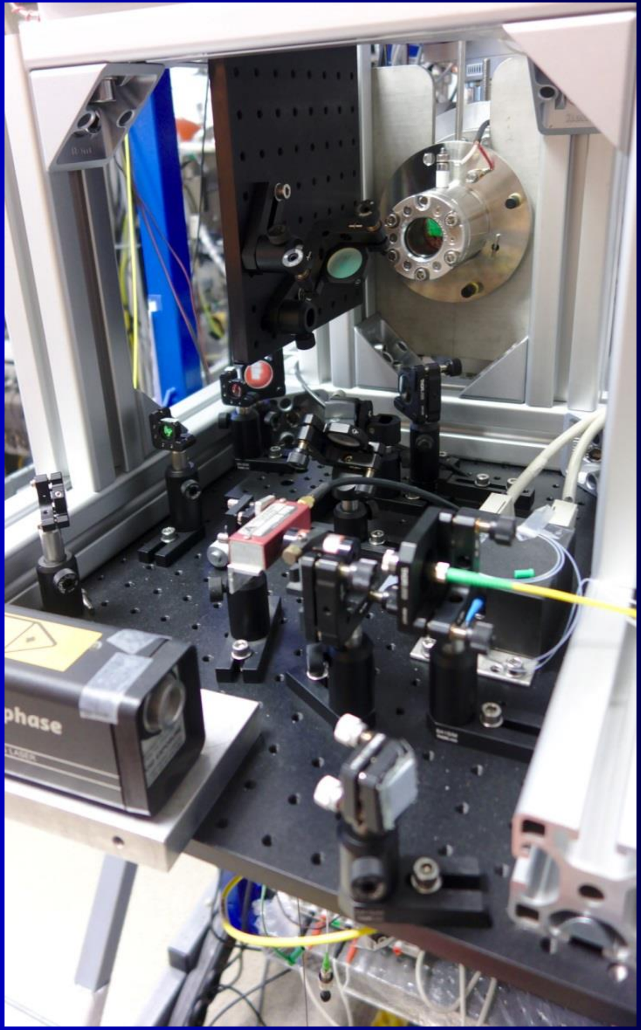
phase

Ionic composition of H_2/D_2 plasma

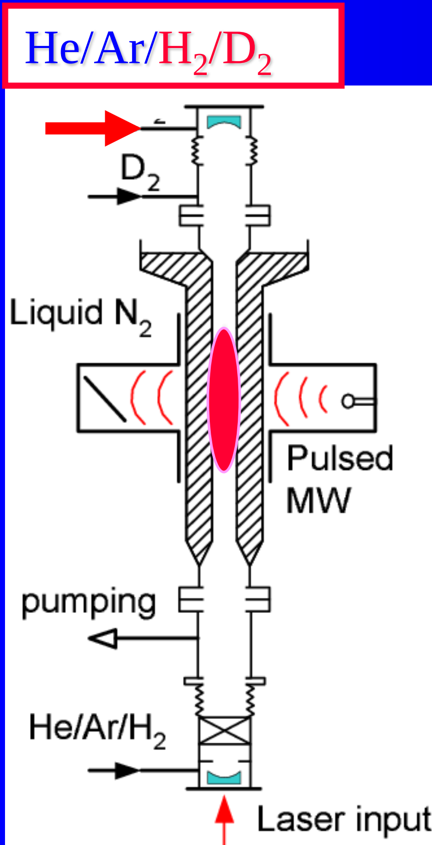

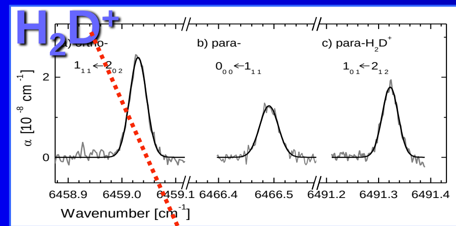

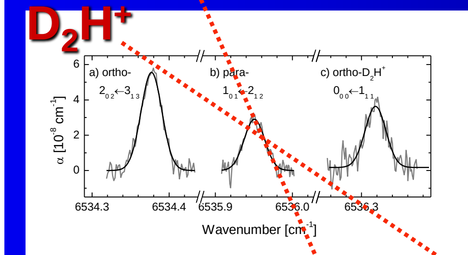

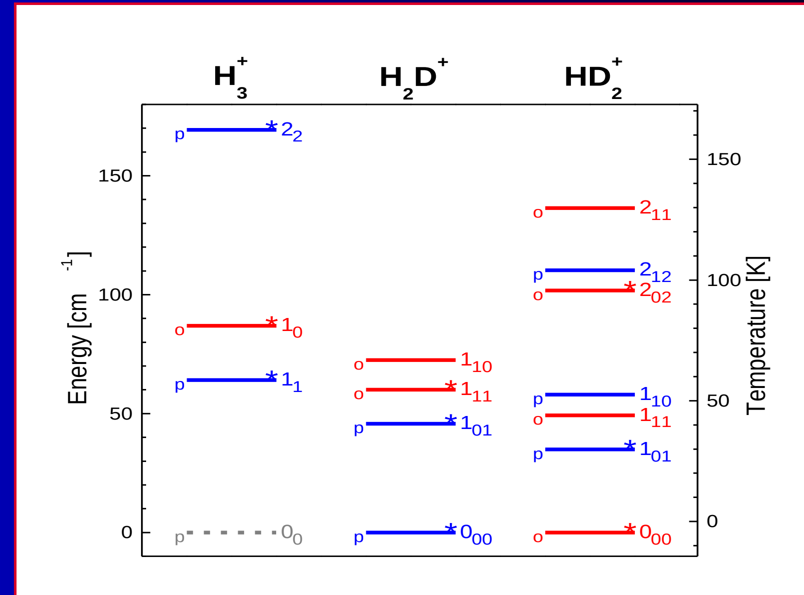

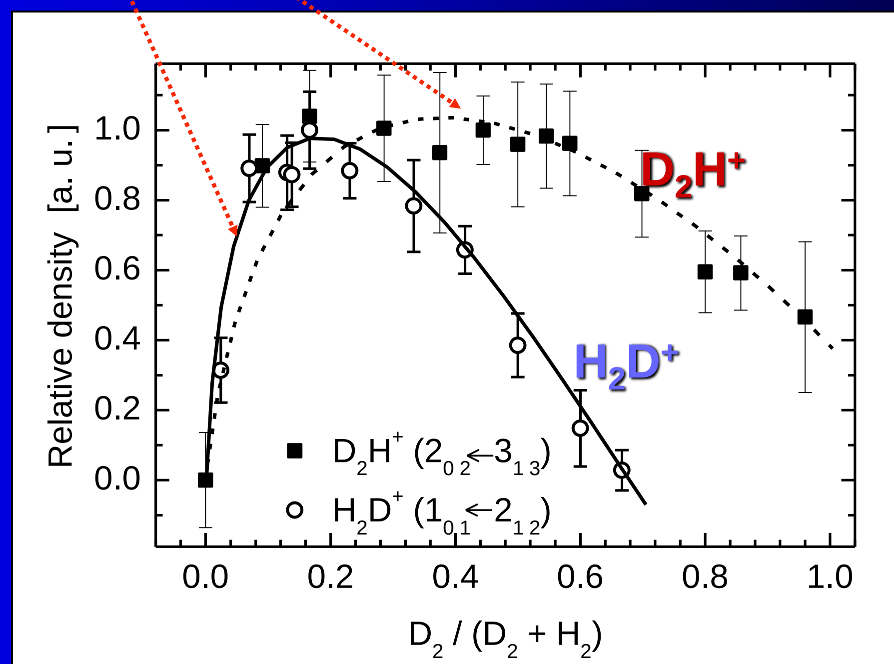

Ternary electron assisted recombination

Ternary electron assisted recombination

$$Ar^+ + e + e \rightarrow Ar + e$$

$$\frac{dn_e}{dt} = \frac{d[Ar^+]}{dt} = -K_e[Ar^+]n_e^{\,2} = -\alpha_{eff}[Ar^+]n_e$$

Collisional Radiative Recombination

CRR

K_{CRR} [cm^{6}s^{-1}]

$$\alpha_{eff} = K_e n_e$$

Ternary neutral assisted recombination

$$Ar^+ + e + He \rightarrow Ar + He$$

$$\frac{dn_e}{dt} = \frac{d[Ar^+]}{dt} = -K_M[Ar^+]n_e[He] = -\alpha_{eff}[Ar^+]n_e$$

K_M [cm^{6}s^{-1}]

$$\alpha_{eff} = K_M[He]$$

Stevefelt [*Stevefelt et al.*, 1975] derived analytical formula for apparent binary rate coefficient of CRR:

$$\alpha_{\mathrm{CRR}} = 3.8\times10^{-9} T_{\mathrm{e}}^{-4.5} n_{\mathrm{e}} + 1.55\times10^{-10} T_{\mathrm{e}}^{-0.63} + 6\times10^{-9} T_{\mathrm{e}}^{-2.18} n_{\mathrm{e}}^{0.37}\ [\mathrm{cm^3 s^{-1}}], \tag{4}$$

where T_e is electron temperature given in K and n_e is electron number density in cm^{-3}. The first term in

$$\alpha_{\mathrm{CRR}} = K_{\mathrm{CRR}} n_{\mathrm{e}}$$

For quasineutral plasma the differential equation describing the overall losses of charged particles in plasma due to above mentioned processes described by equations (1), (2) and (3) is:

$$\frac{\mathrm{d}n_{\mathrm{e}}}{\mathrm{d}t} = \frac{\mathrm{d}[\mathrm{A}^+]}{\mathrm{d}t} = -\alpha_{\mathrm{BIN}}[\mathrm{A}^+]n_{\mathrm{e}} - K_{\mathrm{M}}[\mathrm{M}][\mathrm{A}^+]n_{\mathrm{e}} - K_{\mathrm{CRR}}[\mathrm{A}^+]n_{\mathrm{e}}^2 - \frac{n_{\mathrm{e}}}{\tau_{\mathrm{D}}} = -\alpha_{\mathrm{eff}} n_{\mathrm{e}}^2 - \frac{n_{\mathrm{e}}}{\tau_{\mathrm{D}}} \tag{6}$$

where $[A^+] = n_e$ is the number density of ions, [M] is the number density of particles of buffer gas and τ_D describes the diffusion losses. We introduced the effective recombination rate coefficient α_{eff}:

$$\alpha_{\mathrm{eff}} = \alpha_{\mathrm{BIN}} + K_{\mathrm{CRR}} n_{\mathrm{e}} + K_{\mathrm{He}}[\mathrm{He}] \tag{7}$$

Theoretical calculations of rate coefficient of electron – ion ternary recombination (assisted by the particle of buffer gas) [*Thomson*, 1924; *Pitaevskii*, 1962; *Bates et al.*, 1965; *Bates*, 1980; *Flannery*, 1991] propose less pronounced temperature dependence of this process ($\alpha \approx T^{-2.5}$) than in case of CRR and also that the recombination coefficient should be lower for heavy ions than for light ions. Flannery [*Flannery*, 1991] derived following formula for helium assisted ternary recombination:

$$K_{\mathrm{He}} = 2.3\times10^{-27}(300/T_e)^{2.5}\ \mathrm{cm^6 s^{-1}}. \tag{8}$$

$Ar^+ + e^- + e^-$

$H^+ + e^- + e^-$

Anti hydrogen formation

Colisional Radiative Recombination -CRR

$$\frac{dn_e}{dt} = -K_{CRR}\ [Ar^+]n_e^2 - \frac{n_e}{\tau_D} = -K_{CRR}\ \ n_e^3 - \frac{n_e}{\tau_D}$$

$$\alpha_{CRR} = K_{CRR}\ n_e$$

$H^+ + e^- + e^- \rightarrow H + e^-$

PRL **98,** 133201 (2007) PHYSICAL REVIEW LETTERS week ending 30 MARCH 2007

Three-Body Recombination of Atomic Ions with Slow Electrons **2007**

S. X. Hu

Laboratory for Laser Energetics, University of Rochester, 250 East River Road, Rochester, New York 14623, USA

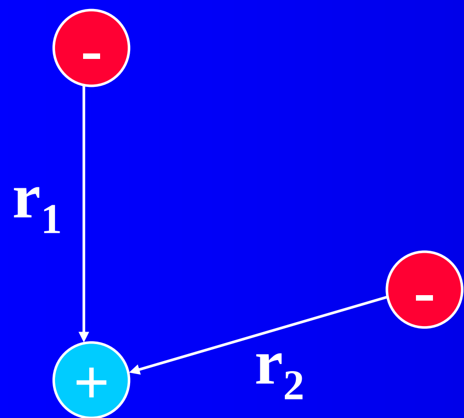

We consider the simplest TBR in the case of hydrogen formation, in which two free electrons interact with a proton. To investigate the three-body interaction dynamics, we numerically solve the six-dimensional (6D) time-dependent Schrödinger equation, which has the following form (atomic units are used throughout):

$$i\frac{\partial}{\partial t}\Phi(\mathbf{r}_1,\mathbf{r}_2,t) = \left[-\frac{1}{2}(\Delta_{\mathbf{r}_1}+\Delta_{\mathbf{r}_2}) - \frac{1}{r_1} - \frac{1}{r_2} + \frac{1}{|\mathbf{r}_1-\mathbf{r}_2|}\right]\Phi(\mathbf{r}_1,\mathbf{r}_2,t), \quad (1)$$

where $\mathbf{r}_1$ and $\mathbf{r}_2$ are the position vectors of each electron, with respect to the proton. We obtain a more tractable

with respect to the proton. We obtain a more tractable
solution by using the close-coupling recipe [12]: expanding the 6D wave function $\Phi(\mathbf{r}_1,\mathbf{r}_2|t)$ in terms of bipolar spherical harmonics $Y^{LS}_{l_1 l_2}(\Omega_1,\Omega_2)$, $\Phi(\mathbf{r}_1,\mathbf{r}_2|t) = \sum_{LS}\sum_{l_1 l_2}[\Psi^{(LS)}_{l_1 l_2}(r_1,r_2|t)/r_1 r_2]Y^{LS}_{l_1 l_2}(\Omega_1,\Omega_2)$, for a specific symmetry (LS). We can also expand the Coulomb repulsion term $1/|\mathbf{r}_1-\mathbf{r}_2|$ in terms of spherical harmonics. Substituting these expansions into the above Schrödinger Eq. (1) and integrating over the angles Ω_1 and Ω_2 yields a set of coupled partial differential equations with only two radial variables r_1 and r_2 left:

$$i\frac{\partial}{\partial t}\Psi_j(r_1,r_2|t) = [\hat{T}_1+\hat{T}_2+\hat{V}_c]\Psi_j(r_1,r_2|t) + \sum_k \hat{V}^I_{j,k}(r_1,r_2|t)\Psi_k(r_1,r_2|t), \quad (2)$$

where the partial-wave index j runs from 1 to the total number N of partial waves used for expansion. In Eq. (2),

$H^+ + e^- + e^- \rightarrow H + e^-$

$$i\frac{\partial}{\partial t}\Psi_j(r_1, r_2|t) = [\hat{T}_1 + \hat{T}_2 + \hat{V}_c]\Psi_j(r_1, r_2|t) + \sum_k \hat{V}^I_{j,k}(r_1, r_2|t)\Psi_k(r_1, r_2|t), \quad (2)$$

$$P_{nl}(E_2) = 2\sum_{LS}\sum_{l_2}\left|\int dr_1 \int dr_2 \phi^*_{nl}(r_1)\phi^*_{k_2 l_2}(r_2)\Psi^{(LS)}_{ll_2}(r_1, r_2, t = t_f)\right|^2,$$

K_E=0.1 eV

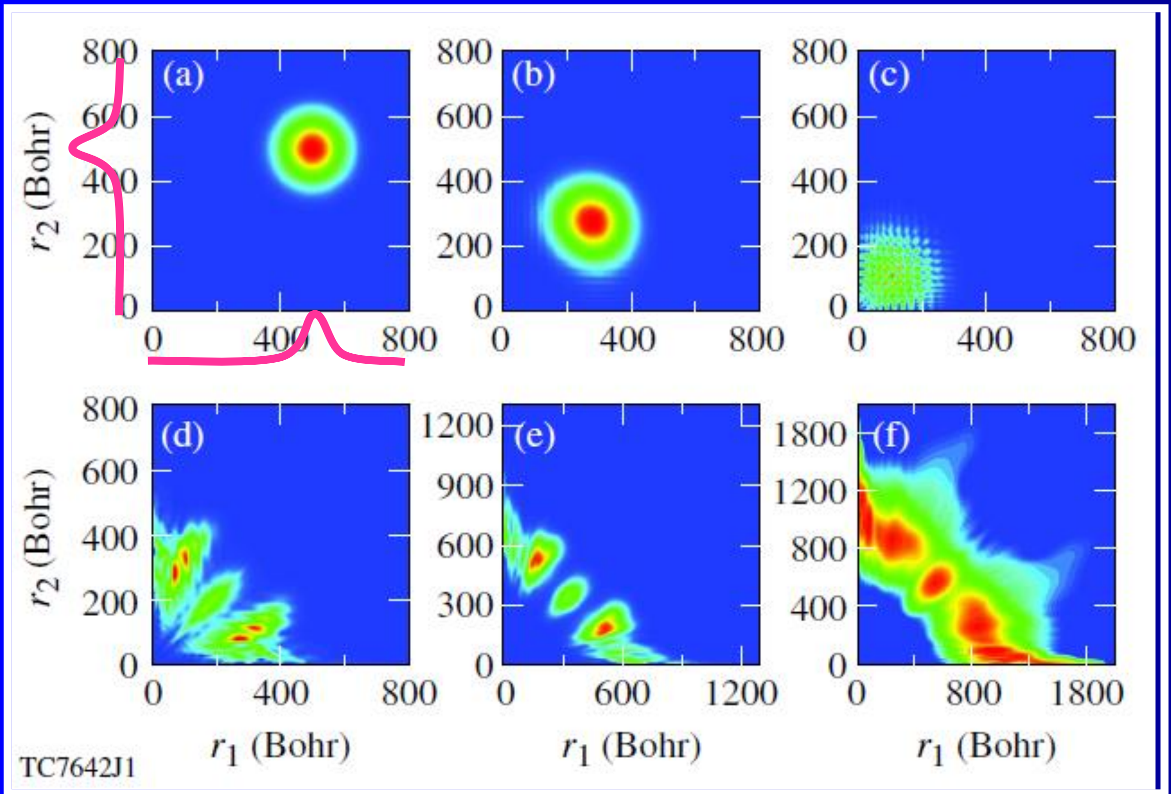

FIG. 1 (color online). Snapshots of electron probability distribution on the plane spanned by the radial coordinates r_1 and r_2 for different times: (a) $t = 0.0$ fs, (b) $t = 60$ fs, (c) $t = 100$ fs, (d) $t = 150$ fs, (e) $t = 194$ fs, and (f) (in log scale) $t = 260$ fs.

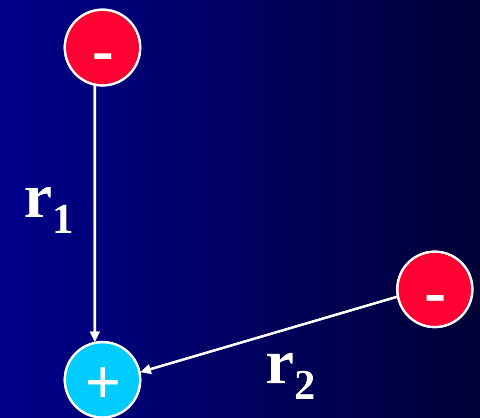

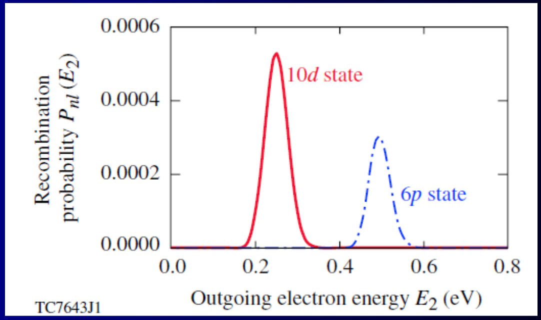

Thus, for the case of $K_E = 0.1$ eV considered in Figs. 1 and 2, the total system energy is about $E_{tot} \sim 0.12$ eV instead of $2K_E$. Hence, when one electron recombines to the 10d state ($|E_{10d}| \approx 0.136$ eV) of the H atom, the outgoing electron takes an initial total energy of 0.12 eV plus $|E_{10d}|$, thereby $P_{10d}(E_2)$ peaks at $E_2 \sim 0.256$ eV, as shown by the (red) solid line of Fig. 2. Similar energy conservation is also well satisfied for the recombination to the 6p state, as is illustrated by the (blue) dash-dotted line in Fig. 2. Our quantum calculations unambiguously reveal the essential feature of a TBR process.

$H^+ + e^- + e^- \rightarrow H + e^-$

K_E=0.1 eV

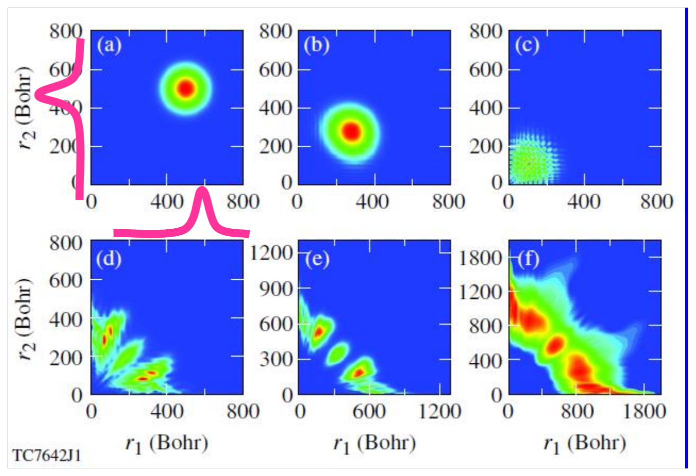

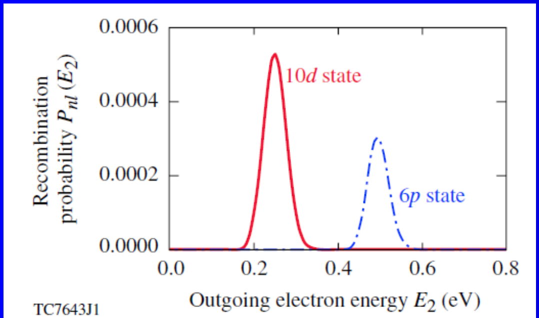

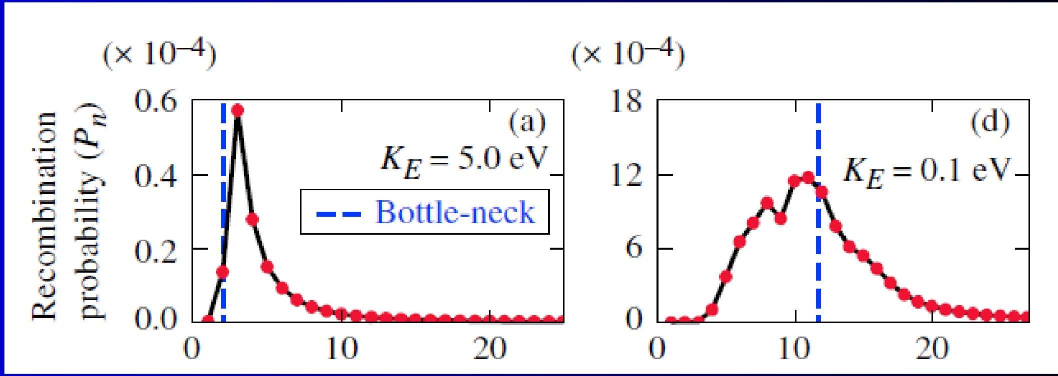

FIG. 3 (color online). The recombination probability P_n as a function of the energy level n, for different electron kinetic energies K_E marked in each panel.

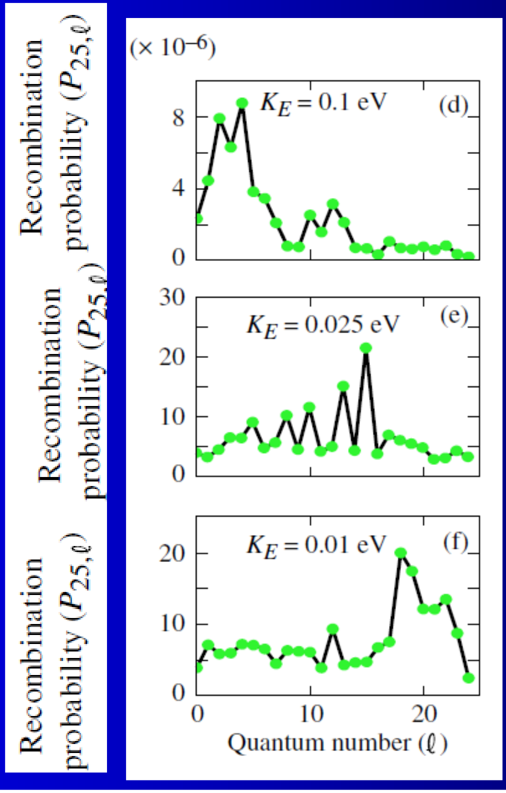

FIG. 4 (color online). The recombination probability $P_{n=25,l}$ as a function of the angular-momentum quantum number l, for different electron kinetic energies K_E marked in each panel.

$Ar^+ + e^- + e^-$

$H^+ + e^- + e^-$

Anti hydrogen formation

$$\frac{dn_e}{dt} = -K_{CRR}\ [Ar^+]n_e^2 - \frac{n_e}{\tau_D} = -K_{CRR}\ n_e^3 - \frac{n_e}{\tau_D}$$

$$\alpha_{\mathrm{CRR}} = 3.8\times10^{-9} T_e^{-4.5} n_e + 1.55\times10^{-10} T_e^{-0.63} + 6\times10^{-9} T_e^{-2.18} n_e^{0.37}\,\mathrm{cm^3 s^{-1}}$$

$$\alpha_{CRR} = K_{CRR}\, n_e$$

$$K_{\mathrm{CRR}} = 3.8\times10^{-9} T_e^{-4.5}\,\mathrm{cm^6 s^{-1}}$$

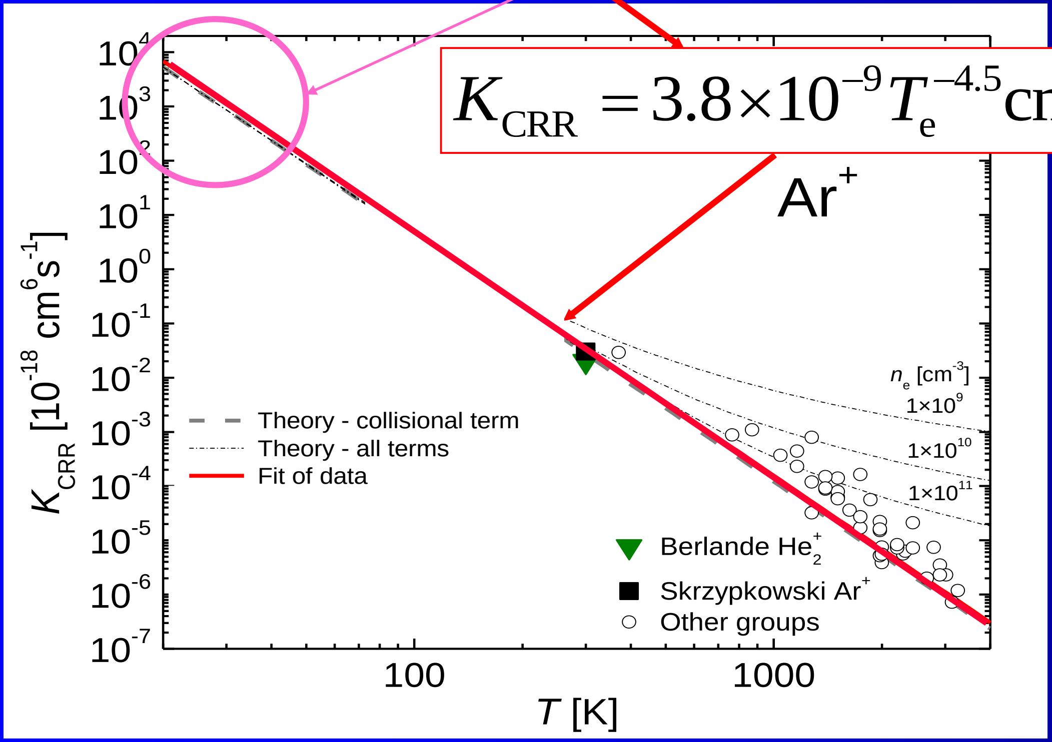

$Ar^+ + e^- + e^-$

$$\frac{dn_e}{dt} = -K_{CRR}\,[Ar^+]\,n_e^2 - \frac{n_e}{\tau_D} = -K_{CRR}\,n_e^3 - \frac{n_e}{\tau_D}$$

$$\alpha_{\mathrm{CRR}} = 3.8\times10^{-9}T_e^{-4.5}n_e + 1.55\times10^{-10}T_e^{-0.63} + 6\times10^{-9}T_e^{-2.18}n_e^{0.37}\,\mathrm{cm^3s^{-1}}$$

$$K_{\mathrm{CRR}} = 3.8\times10^{-9}T_e^{-4.5}\,\mathrm{cm^6s^{-1}}$$

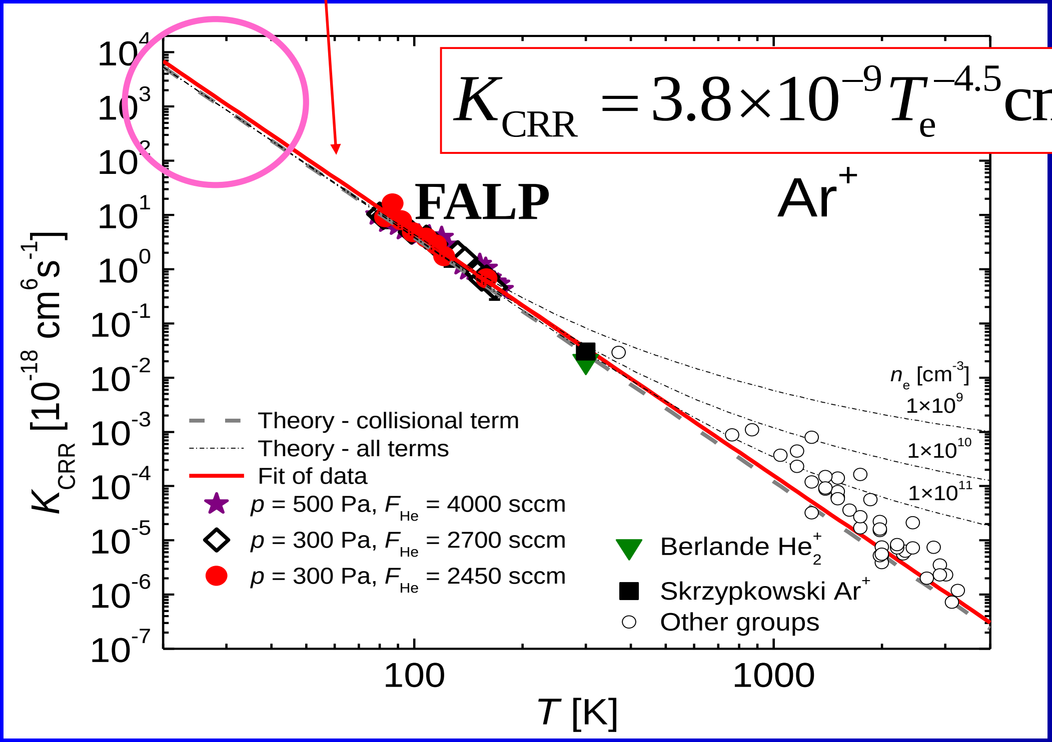

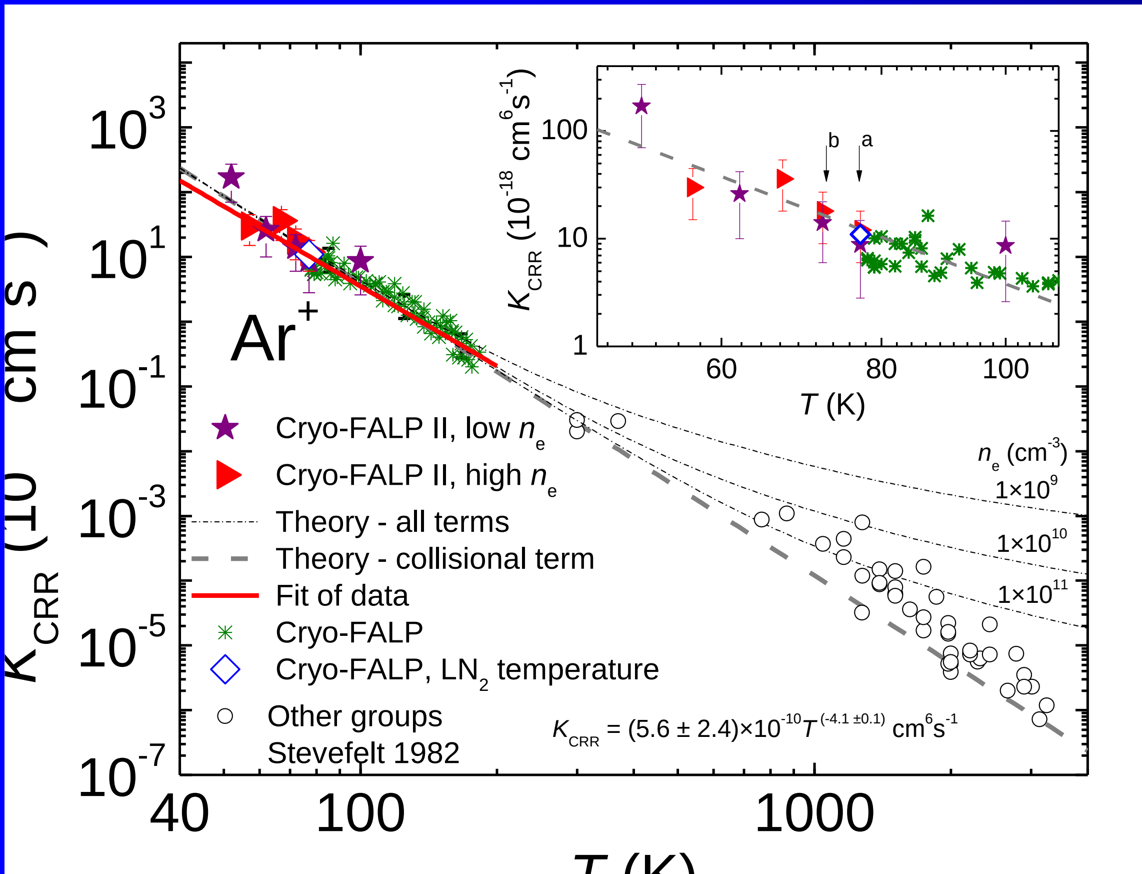

Ar+
Cryo-FALP II, low n_e
Cryo-FALP II, high n_e
Theory - all terms
Theory - collisional term
Fit of data
Cryo-FALP
Cryo-FALP, LN_2 temperature
Other groups
Stevefelt 1982
n_e (cm^{-3})
1×10^9
1×10^{10}
1×10^{11}
$K_{CRR} = (5.6 \pm 2.4)\times10^{-10} T^{(-4.1 \pm 0.1)}$ cm^{6}s^{-1}
K_{CRR} (10^{-18} cm^{6}s^{-1})
T (K)
b
a

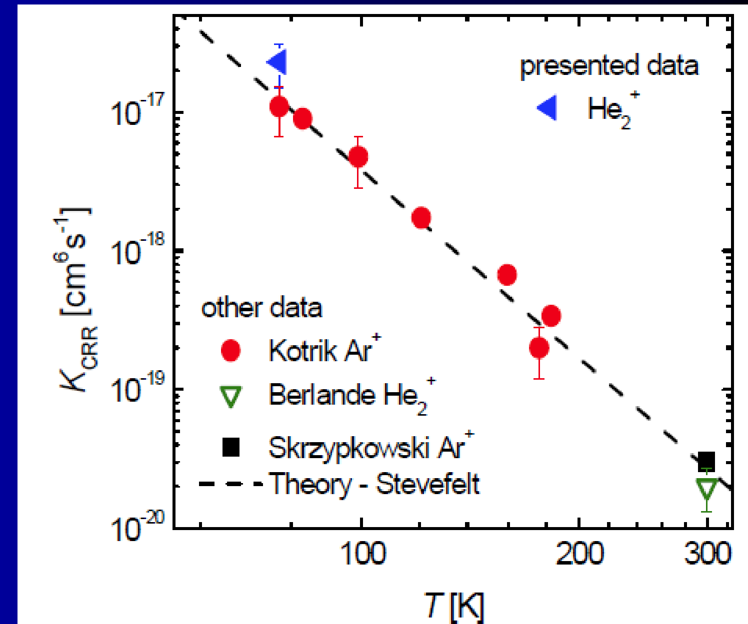

presented data
He$_2^+$
other data
Kotrik Ar$^+$
Berlande He$_2^+$
Skrzypkowski Ar$^+$
Theory - Stevefelt
K_{CRR} [cm^{6}s^{-1}]
T [K]

The temperature dependence of the ternary recombination rate coefficient of CRR (measured for several ions) is plotted in Figure 4. Our data for He_2^+ and Ar^+ [*Kotrik et al*, 2010] together with data measured in experiments of other groups [*Berlande et al.*, 1970; *Skrzypkowski et al.*, 2004] are in good agreement with theoretical calculations [Stevefelt et al., 1975].

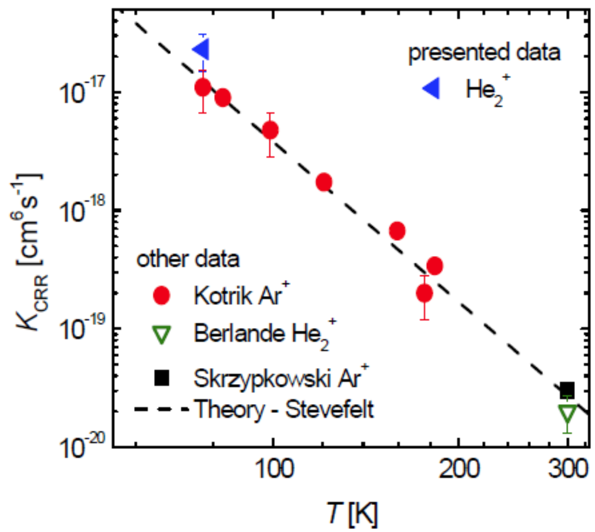

Figure 4. Ternary recombination rate coefficient of CRR as a function of gas temperature. Plotted are data of our group from measurements in Ar^+ [*Kotrik et al*, 2010] and He_2^+ dominated plasma and data obtained by Berlande [*Berlande et al.*, 1970] and Skrzypkowski [*Skrzypkowski et al.*, 2004] at 300 K. Theoretical dependence [*Stevefelt et al.*, 1975] is plotted by dashed line.

Coe et al (Ohio State univ., 1995) : $H_3O^+(H_2O)_n + OH^-(H_2O)_m$